Doctoral Dissertation

A Proposal of Designable Space of Diaphragm Made of Thin Stainless Steel for Electrical Assemblies Considering Clicking Behavior and Fatigue Life

（クリック特性と疲労寿命を考慮した電子機構部品用薄板ステンレス製ダイヤフラムの設計可能領域の提案）

XINGSHENG LI

July 2013

Graduate School of Engineering,
Osaka University

Contents

Chapter 1 Introduction

1.1 Role played by Momentary Push Button Switch

A switch is something refers to an electrical component designed to interrupt an electrical circuit or divert it from conductor to another. Standard switches, once activated, maintain function until deactivated, or switched off. A momentary push button switch works only temporarily, it works only the moment when it is pushed. Momentary push button switch is widely used in electric devices as computer, telephone etc. As the use of electric equipment in the home and commercial establishment's increases, there is a need to increase the number of electrical switches used for controlling or supplying electrical single to such equipment. Examples of application of toggle switch and momentary switch are shown in Fig. 1.1.

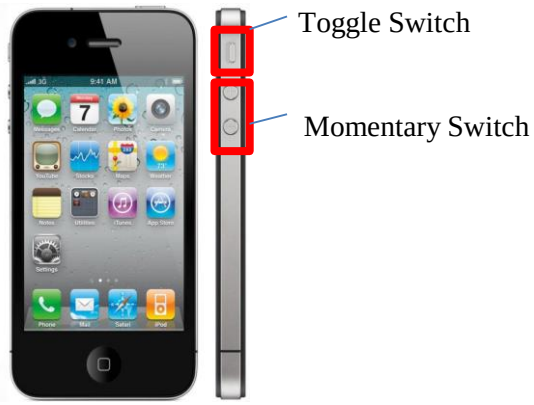

Fig. 1.1 Switches used in iPhone

With the developing of information technology electric devices are becoming inseparable from our daily life, as a result, it will be a big trouble when electric devices are broken down. Therefore, two basic factors are required in designing an electric device: the ability of right action and the service life. There are many electrical elements in electric devices, when a single one break down, the electric device are not able to work properly. As momentary push button switch endures cyclic loading frequently, it will fatigue at last.

The reliability of service of momentary push button switch is very important, although the proportion of the value of a single switch in the whole device are very small, for momentary push button switch is used to control the electric single supply, if

it is broken down the electric device will not be able to work. Therefore, in designing Momentary Push Button Switch, high service reliability and low unit costing is required.

1.2 Diaphragm used in Momentary Push Button Switch

Switches can be found in many types and configurations to fit different function and usage. A two-step operation switch module and a multi-function switch module are shown in Fig. 1.2 and 1.3 separately. Two-step sequential operation switch module is widely used in shutter of the camera. When the shutter button is pressed half-way, exposure and focus are locked as long as you hold it that position, then depress the shutter button all the way down to take the photo. The multi-function switch module has more than one diaphragm resembled in it. It is widely used in mobile phone, PDA, AV devices etc. Even though the function and configuration of the two switches are different, they are having the similar structure that the main part of movable contact piece used in switch is a metallic diaphragm made of stainless steel. Fig. 1.4 shows the structure image of momentary push button switch.

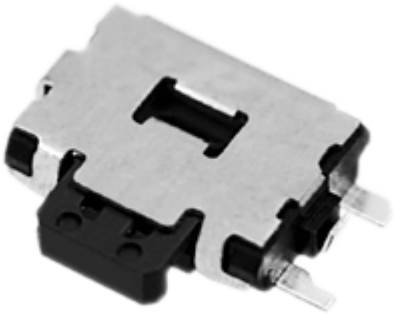

Fig.1.2 Two-step operation switch module [1]

Fig.1.3 Multi-function switch module [1]

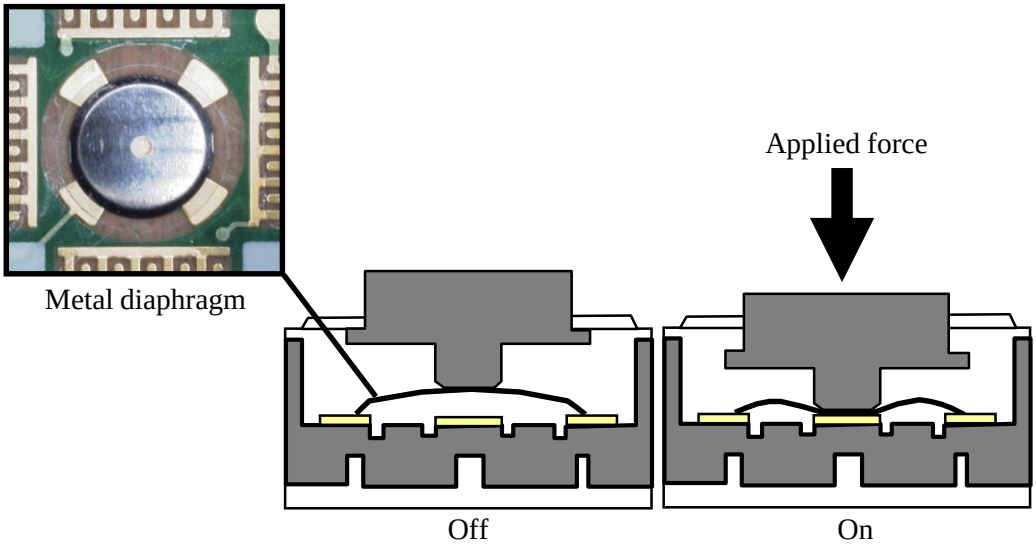

Fig.1.4 A metal diaphragm in switch module and its function

Diaphragm has a special characteristic that it can give user a positive tactile feedback when it is clicked, as a result, even without visual confirmation user can know whether or not diaphragm is touching the panel. The evaluation of click characteristics is very important in designing diaphragm. The click characteristics and touch feeling of diaphragm can be described as a feeling curve which means the relation between reaction and displacement of a diaphragm, as shown in Fig. 1.5. The force increases during clicking process. After the force reaches the maximum value, the buckling phenomena of diaphragm appears. The load (P2) means the state when diaphragm contacts with the ground. The click characteristic of diaphragm can be evaluated quantitatively as the parameters of 'click ratio' and 'load max'. The load max (P1) shows the biggest force in click process and the click ratio is defined as Eq. (1.1).

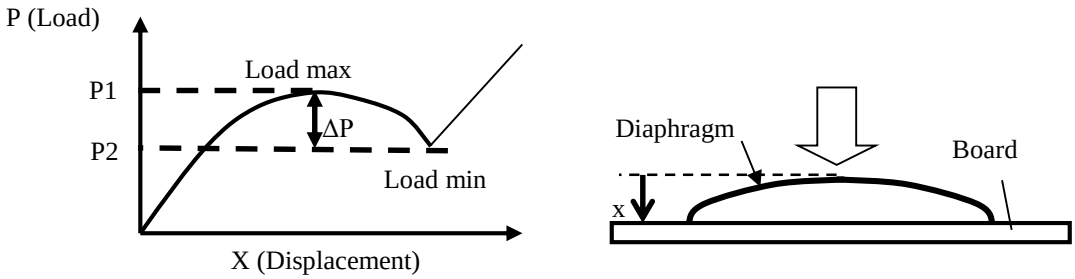

Fig. 1.5 Diaphragm and feeling curve

$$Click\_ratio = \frac{P1 - P2}{P1} \quad \text{(Eq.1.1)}$$

1.3 Problem of designing diaphragm

The diaphragm with high click ratio and high load max may induce the sharp touch-feeling and decrease the probability of miss operation. However, the requirement of click characteristics is various due to the culture, age, physique, etc. It is not important to find the optimum value of click characteristics, but it is important to catch the designable range of diaphragm which satisfies user requirements. Therefore, it is necessary to estimate the effects of design parameters on click characteristics of diaphragms. Making trial pieces based on experience is a common way for designing diaphragm with certain click characteristics, which is very time consuming and costly.

On the other hand, even required click characteristics can be obtained, whether the fatigue life is acceptable is a problem. Press experiment that simulates the working process is the only way to ensure the service life of diaphragm, which takes plenty of time. And experience depended designing often encounters difficulties to deal with new type diaphragm of different shape. In order to satisfy the requirement of short design period and design diversity, a simple efficient design method is needed.

1.4 Purpose of this research

To solve the problem mentioned before, the purpose of this research is propose a convenient approach for designing diaphragm considering both click characteristics and fatigue life.

There are many reports about the mechanical behavior of elastomeric keyboard rubber diaphragms [2] ~ [4]. Studies on the development of design system for keyboard rubber diaphragm using the database and nonlinear programming also have been reported [3], [4]. In the case of metallic diaphragms, the click characteristic is affected by the residual stress due to the manufacturing process of diaphragms [5]. The diameter of actuator also affects the click characteristics [6]. But the relationship between design parameter and click characteristics of diaphragm is still unknown. On the other hand, due to cyclic loading, estimation of the fatigue life of diaphragm is very important for designing diaphragm. Therefore, this paper aims to propose a convenient design method considering both operability and fatigue life at the same time in designing. This approach consists of three procedures. Residual stress distribution of metallic

diaphragm generated in the manufacture process is estimated based on elastoplastic finite element analysis, and then the functional design space of the relationship between the design parameter and click characteristics is obtained. The stress distribution of every point on diaphragm obtained from pressing simulation is calculated into couples of stress amplitude and mean stress which is used in the process of fatigue life evaluation. Finally, the design space of fatigue reliability of diaphragm can be obtained. By comparing the functional design space and fatigue reliability design space with the requirement of diaphragm, the designable design space considering failure probability can be obtained.

This paper contains 6 chapters. Chapter 1 is the preface. The application of momentary push button switch and the current situation of designing switch and the problem in designing switch are introduced.

Chapter 2 introduces the current situation of designing diaphragm, and against the situation the designable space method is proposed.

In chapter 3, the round type diaphragm is discussed. First, the simulation model is introduced, and then the mechanism behavior of pressing process is discussed. In order to find out how the residual stress affect the clicking characteristic, clicking analysis of the model without residual stress are carried out to compare with the model with residual stress. At last, the design space of round type diaphragm are presented and how to apply it are discussed.

In chapter 4, the oval type diaphragm is discussed. First, the stress distribution and the deformation mode of oval type diaphragm are discussed. From the simulation the click characteristics are lower than that of round type diaphragm. In order to improve the Load max and the clicking ratio, a renovated kind of diaphragm are proposed, and then the simulation results are discussed. At last the design space of the proposed diaphragm is presented.

In chapter 5, an example of fatigue reliability evaluation of oval type diaphragm is introduced. The designable space considering failure reliability of new oval type diaphragm is obtained by comparing the designable space with the design space of failure probability. The design parameter can be known When click characteristics and fatigue reliability is required by using designable space considering fatigue probability.

Chapter 6 is the final, which gives the summary of the paper.

At last, the scheme of this paper is shown as below.

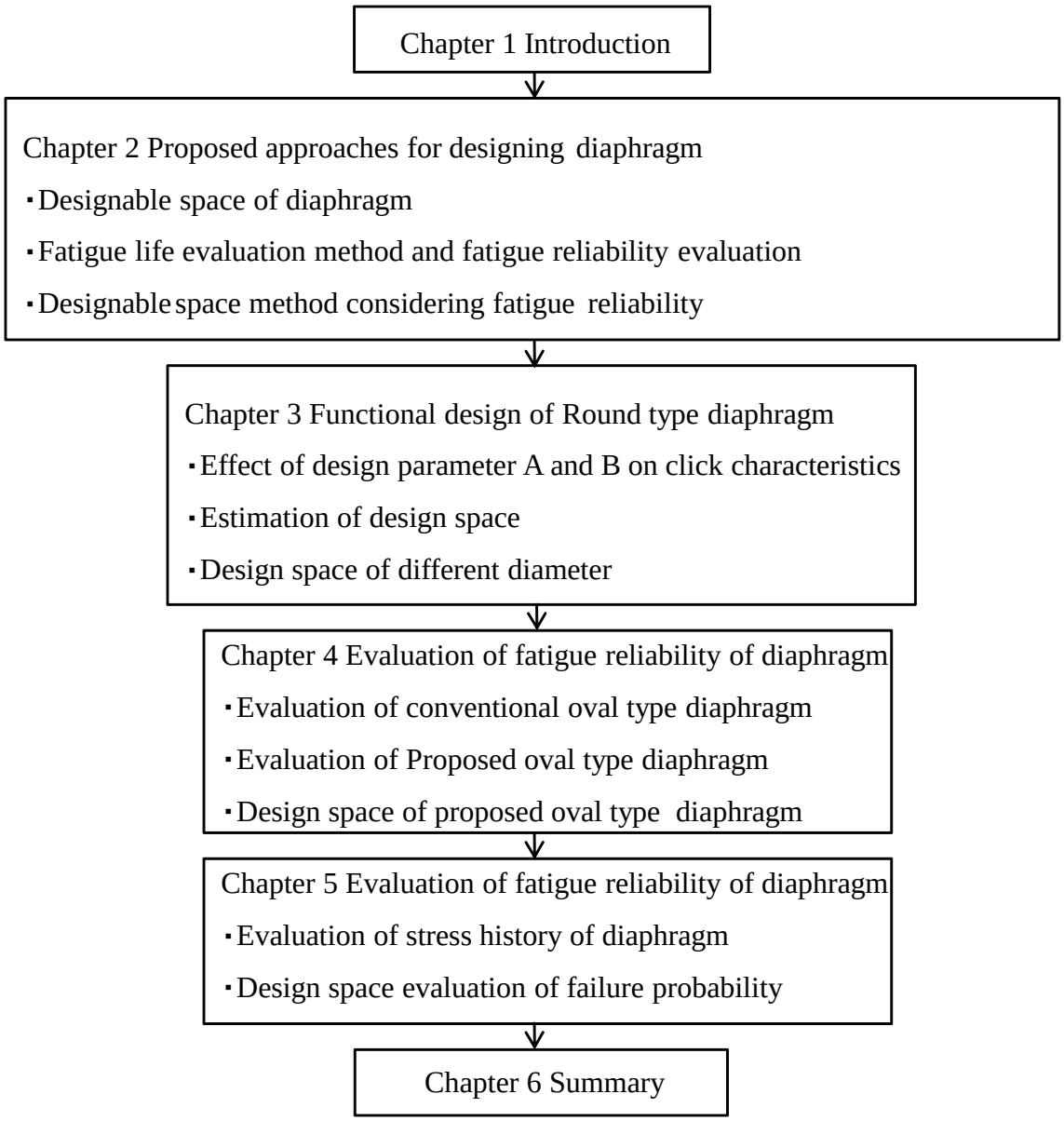

Fig. 1.6 Flow chart of this study

Chapter 2 Proposed approaches for designing diaphragm

2.1 Designable space of diaphragm

The process of making diaphragm is shown in Fig. 2.1. To make a diaphragm first shape the stainless sheet steel by punching and pressing, next cut off the frame part, then form stainless sheet to designed shape. Assemble the diaphragm in the switch then the whole manufacturing process is done. The round type diaphragm shown in Fig. 2.1 is a typical type which is widely used.

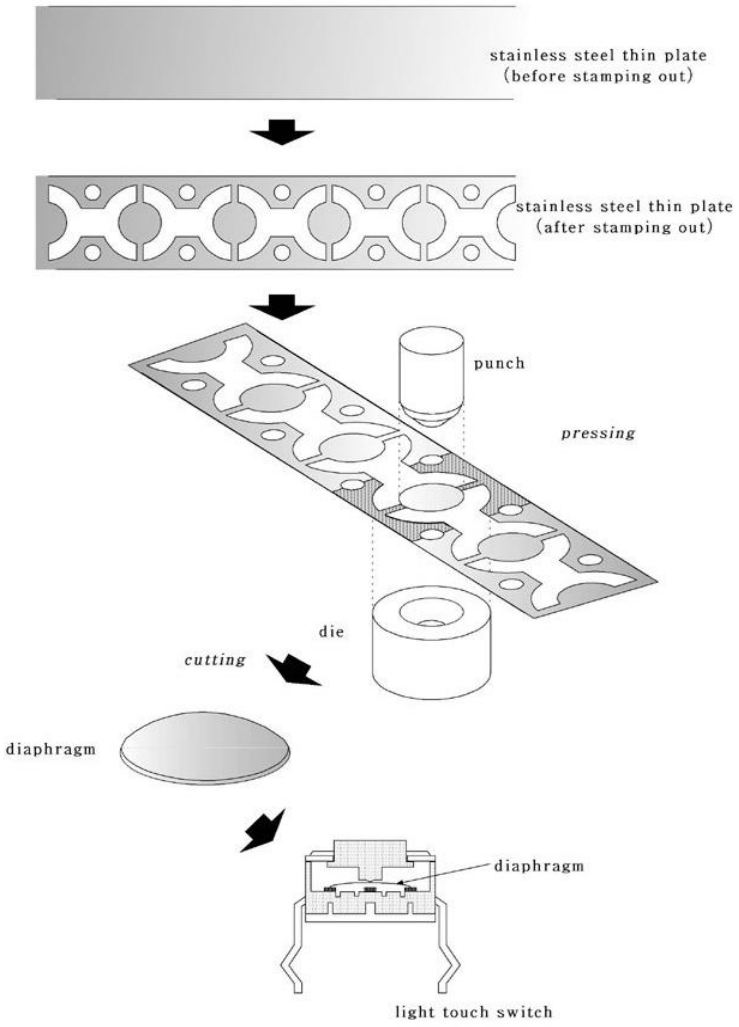

Fig. 2.1 Scheme of manufacturing process

The click characteristics and fatigue life of diaphragm are determined mainly by two factors: the material property of the stainless sheet and the geometry of diaphragm. Although the material property is a main factor determines the click characteristics, the thin stainless steel sheet can be used for diaphragm is limited. As a result, the geometry of diaphragm is where the designing focusing on. The image of the geometry of punch and die is shown in Fig. 2.2.

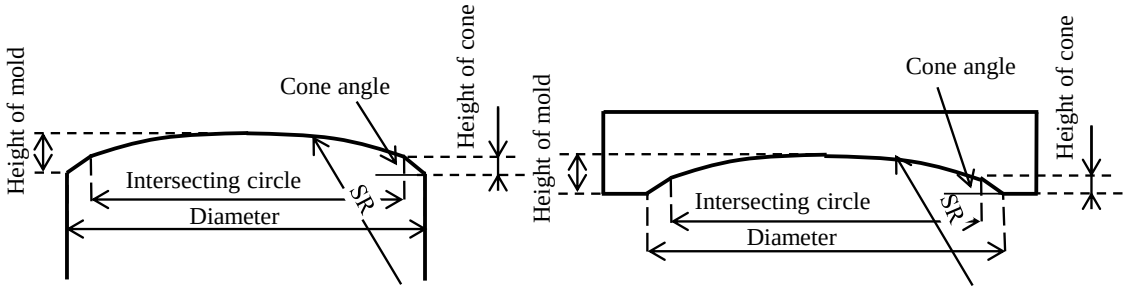

Fig. 2.2 Image of the geometry of punch and die for making diaphragm

As mentioned in chapter 1, the favorite click characteristics of diaphragm is various due to the culture, age, physique, etc. This is because diaphragm can give user a tactile feedback when it is pressed. The preferred press feeling (click characteristics) is different from people to people. To satisfy different customers, diaphragms with different click characteristics are needed. To design diaphragm that satisfies the requirement, prototypes are usually used. The geometry of punch and die is usually determined based on experience, which is usually take much times to get to the required click characteristics. Regarding to this problems, a convenient and efficient designing method is proposed in this study.

In this paper, finite element method is used to evaluate the mechanical behavior of click process in detail. The relationship of the design parameters (the height of diaphragm and the radius of the intersecting circle) and click characteristics is evaluated. Based on the numerical result, the design space is constructed. It will be very efficient to use a design space in designing diaphragm. If the design space of load max and click ratio are obtained by numerical simulation shown in Fig. 2.3. X and Y indicate the design parameters. The values in the image show the load max and click ration corresponding to the combination of X and Y. It will be easy to designing diaphragms with the click characteristics located in the design space. For example, if diaphragm with click characteristics of load max ranges from 1~1.1 and click ratio ranges from 0.5~0.6 are required. The designable space can be obtained by comparing the load max

design space with the click ratio design space, which is shown in Fig. 2.4. It is clearly that the red area satisfies the requirement which is defined as designable area. Diaphragm made by the combinations of design parameters in the red area are considered to satisfy the requirement. When click characteristics required is not located in design space shown in Fig. 2.3, it is considered to be impossible to make such diaphragm in the condition of changing the design parameter of X and Y. In this situation, other design parameters or other types of diaphragm should be considered. By using design space method, the designable space of diaphragm under certain design parameters can be known.

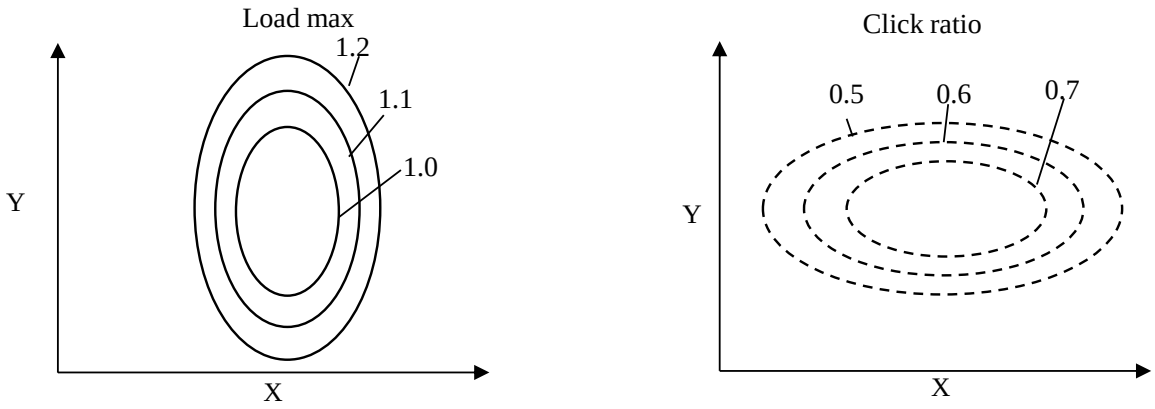

Fig. 2.3 Schematic plot of design space of Load max and Click ratio

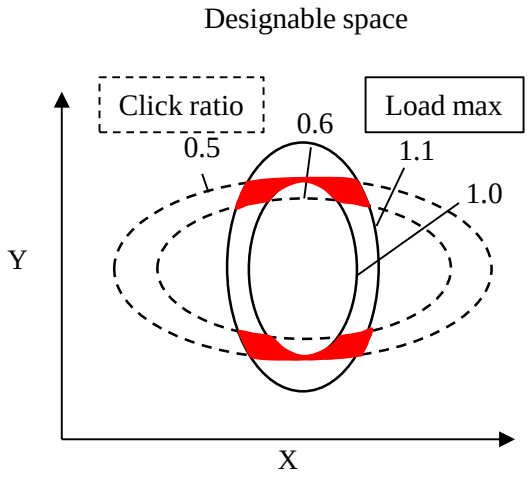

Fig. 2.4 Designable space satisfying requirement

2.2 Fatigue life evaluation method and fatigue reliability evaluation of diaphragm

2.2.1 Fatigue of structures and materials

It has often been said that the majority of mechanical failures in metallic structures occurs as a result of fatigue. The percentage of failures due to fatigue is even supposed to be in the order of 90% [7]. Rigorous definition of exactly what is meant by metal fatigue is difficult and not particularly helpful for its understanding. An early dictionary definition is: the condition of weakness in metal caused by repeated blows or long continued strain [8]. A more recent definition is: failure of a metal under a repeated or otherwise varying load which never reaches a level sufficient to cause failure in a single application [9]. August Wöhler performed many laboratory fatigue tests under repeated stresses, in Germany during the 1850s and 1860s. Thus, Wöhler has been called the "father" of systematic fatigue testing. Investigation of the mechanisms of metal fatigue started in earnest in the 1900s. He pointed out that for fatigue, the range of stress is more important than the maximum stress [10]. According to Ewing and Humphrey [11], metal fatigue damage in a plain specimen is a surface phenomenon. They showed that, in a ductile metallic material, bands of slip lines form on the surface of grains under fatigue loading. These slip lines eventually turn into cracks. In general only one crack develops to any considerable depth, and this crack propagates across the material until the section is so reduced that static failure takes place. Detailed investigation of the mechanisms of fatigue crack propagation in metals started in the 1960s [12] ~ [14].

Criteria for fatigue design have evolved from so-called infinite life to damage tolerance. Infinite-Life design is the oldest criterion. The criteria for fatigue design include usage of the four fatigue life models. It requires local stresses or strains to be essentially elastic and safely below the pertinent fatigue limit. Safe-Life design is to make the products to survive a specific design life with a chosen reserve. Fail-safe design requires that if one part of a structure fails, the system does not fail. Fail-safe design recognizes that fatigue cracks may occur, and structures are arranged so that cracks will not lead to failure of the structure before they are detected and repaired. Damage-tolerant design is refinement of the fail-safe philosophy. It assumes that cracks will exist, caused either by processing or by fatigue, and uses fracture mechanics analyses and tests to determine whether such cracks will grow large enough to produce failures before they are detected by periodic inspection.

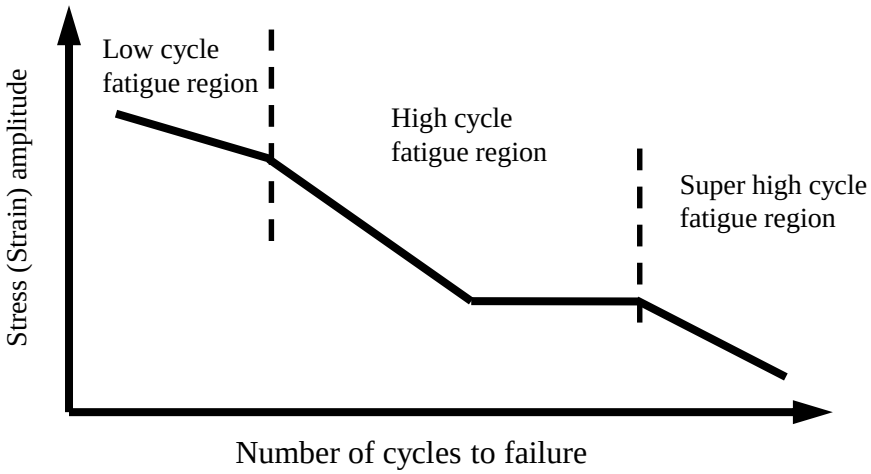

Fig. 2.5 Schematic S-N curve

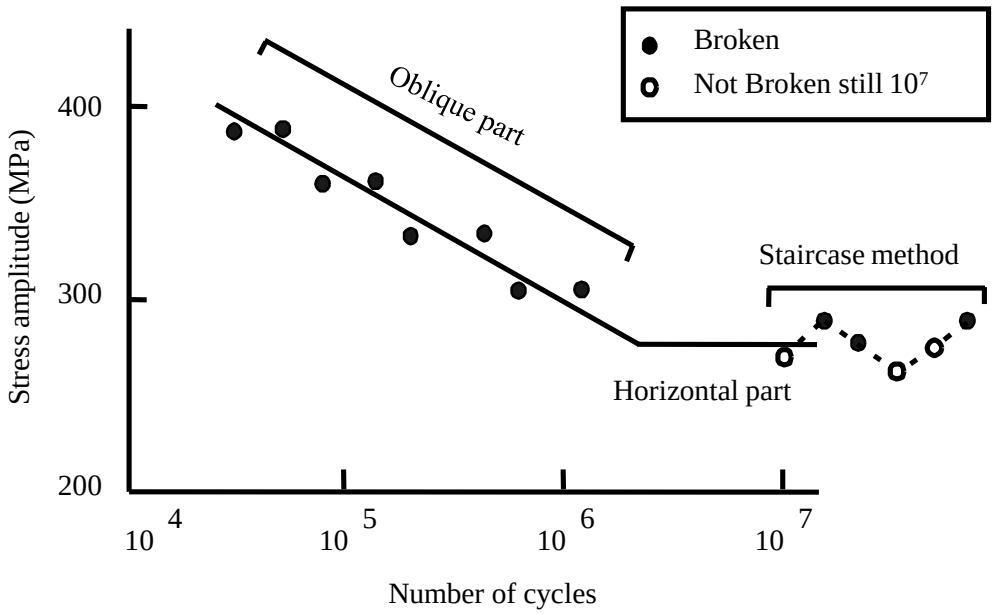

Fig. 2.6 Model of S-N diagram based on statistic method [23]

S-N curves are usually obtained by axial load or stress control test. Here S is the applied nominal stress, and N is the number of cycles or life to failure. A schematic S/N curves is shown in Fig. 2.5. The region where failure takes place in less than about 10^4 cycles is called low cycle fatigue, and the region for longer endurances high cycle fatigue. It was usually found for steels having tensile strengths up to about 700MPa that, if a specimen has not broken after 10^7 cycles, it was most unlikely to break if tests were continued to longer endurances, and suggested that the line through the points became horizontal. The tress corresponding to the horizontal line is called the fatigue limit. It

was implied that specimens tested at below the fatigue limit would never break no matter how many stress cycles were applied. It is now widely known that the S/N does not become quite horizontal and that failures can occur in the region of 10^9 cycles. The endurance above 10^7 cycles, especially, from 10^9 to 10^{10} cycles is called super cycle fatigue [15] ~ [17]. Fatigue life of diaphragm is considered in the range of high cycle fatigue.

Fatigue testing is very time consuming. For example, if a testing machine operates at 30Hz then 10^8 cycles takes more than a month [18], [19]. It is necessary to determine S-N curve by small samples. There are many regression model of S-N used for different material is reported [20]. Linear-Log and Log-Log scale is commonly used in general structural material. There are also models which consider the fatigue limits were proposed. Nishijima classify S-N curve with slop and linear line into four types: Weibull, Serensen, Bastenaire and Hyperbolic type [21]. Asymptotic regression and linear regression is used in the circumstance of Linear-Log and Log-Log scale by Sakai, the validity of which is verified by many fatigue test done by the committee of the Materials Research Society who make the fatigue strength database [22]. Fig. 2.6 shows the schematic plot of the experimentation of making S-N ruled by JSME.

2.2.2 S-N curve considering distribution of fatigue strength and fatigue life

By the very nature, metal fatigue is a random process, and the consequent scatter of results, even in carefully controlled experiments, complicates both the analysis of experimental data and their subsequent application to practical problems. The amount of scatter in data is greater than can be accounted for by experimental error. The experimental circumstance, the geometry of the sample, the difference in material component, residual stress due to matching etc. are often considered being the reason. It is difficult to confirm the reason. The determination of an S/N curve involves subjective judgments when fitting a curve to the individual data points. The ASME Code fatigue design curves have been obtained from the best–fit curves by first adjusting for the effects of mean stress on fatigue life and then reducing the fatigue life at each point on the adjusted curve by a factor of 2 on strain (or stress) or 20 on cycles, whichever is more conservative. However, this is not appropriate for all the materials, and it may be too conservative for same materials. Hence, it is necessary to consider the scatter characteristics in reliability design.

If a number of nominally identical fatigue specimens are tested at the same stress amplitude and the lives tabulated, a histogram may be plotted by dividing lives into

groups, of a fixed width, distributed about the mean value. If a large enough number of specimens is tested, the groups may be made sufficiently narrow for the histogram to be represented by a smooth curve. Gaussian distribution is found to give an adequate fit certain data. If batches of specimens of a particular metallic material are tested at different stress levers, S-N curves for different probabilities of failure can be drawn. 50 percent probability corresponds to the median that is the middlemost life, and is the conventional S-N curve. Fig. 2.7 shows the schematic P-S-N diagram for three probabilities of failure and log Normal distributions of lives. Distributions of fatigue lives of metallic specimens do not conform to the Normal distribution, but it has been shown that, in many cases, the Normal distribution is a good approximation to the distribution of the logarithms of lives of metallic specimens [24], [25]. Other distributions are sometimes used in modern work, for example in Murakami [26] and Schijve [27]. Large numbers of specimens have sometimes been tested in attempts to find the precise form of the probability density function in given circumstances. A quantity evaluation of low fatigue probability design rule for determinate S-N with little experimental results is proposed by Zako et al. in consideration of practicality[28]~[31]. For this research, considering the high reliability and economics requirements of diaphragm, the method of determinate S-N proposed by Zako et al. is used.

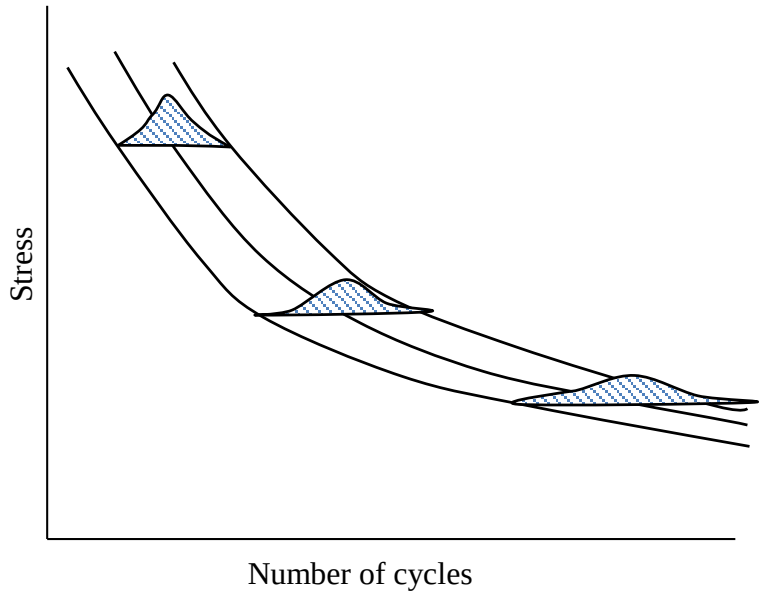

Fig. 2.7 Schematic P-S-N diagram

2.2.3 Fatigue design method based on reliability

2.2.3.1 Assumptions of fatigue design method based on reliability

In order to estimate the distribution of fatigue lives, assumptions have been made as follows:

(1) The S-N curve can be indicated with a straight line when the vertical axis of S-N diagram has an antilogarithmic or logarithmic scale.

(2) The distribution of fatigue life follows Log-normal or Weibull distribution.

(3) Types of distribution of fatigue life are approximately identical.

The scheme of S-N based on these assumptions is shown in Fig. 2.8.

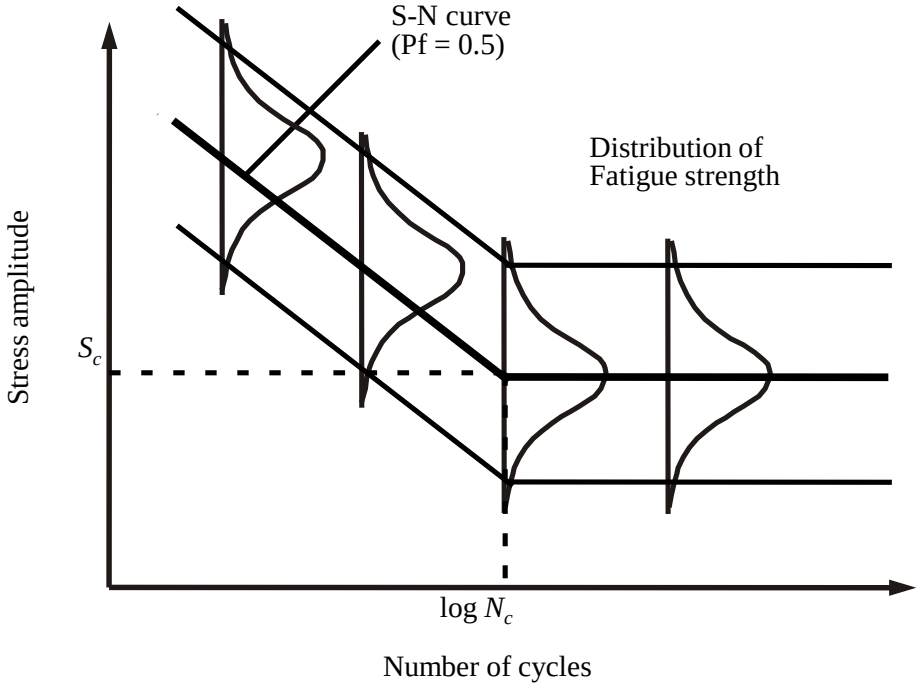

Fig. 2.8 Scheme of S-N model

2.2.3.2 S-N regression model

According to the assumption (1), the S-N model can be written as follows.

(a) In the case of Log-log

$$\begin{aligned} &\log S + m_0 \log N_f = \log D_0 && (N_f \le N_c) \\ &S = S_c && (N_f > N_c) \end{aligned} \qquad \text{(Eq.2.1)}$$

(b) In the case of linear-log

$$S + m_0 \log N_f = D_0 \qquad (N_f \le N_c)$$
$$S = S_c \qquad (N_f > N_c) \qquad \text{(Eq.2.2)}$$

D0 is the constant for static strength, and m0 is the constant for reduction of stress level to logarithm of fatigue life. Nc and Sc is the endurance and stress amplitude of fatigue limit.

2.2.3.3 Normalized stress

In order to estimate S-N curve using a small amount of experiment data, a notion of normalized stress is introduced. As shown in Fig. 2.9, the stress strength of the point converted into endurance Nc based on the assumption (2) is called normalized stress. The calculation of Normalized stress is shown as bellow.

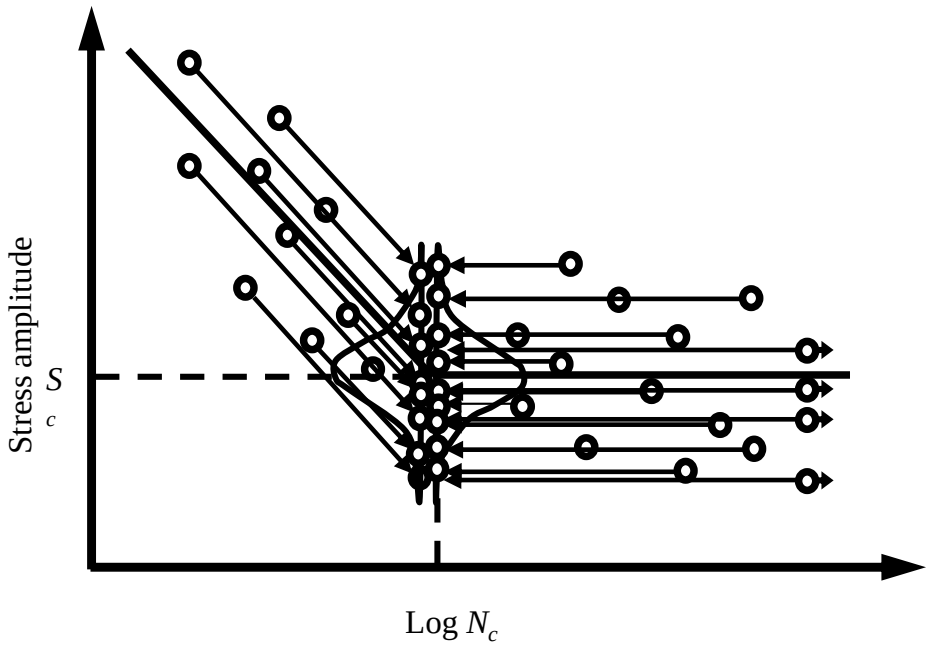

Fig. 2.9 Scheme of normalized stress

(a) In the case of Log-log

$$S^* = S \times \left(\frac{N_f}{N_c} \right)^{m_0} \qquad (N_f \le N_c)$$
$$S^* = S \qquad (N_f > N_c) \qquad \text{(Eq.2.3)}$$

(b) In the case of linear-log

$$S^* = S - m_0 (\log N_c - \log N_f) \quad (N_f \le N_c)$$
$$S^* = S \qquad (N_f > N_c) \qquad \text{(Eq.2.4)}$$

2.2.3.4 Determination of S-N

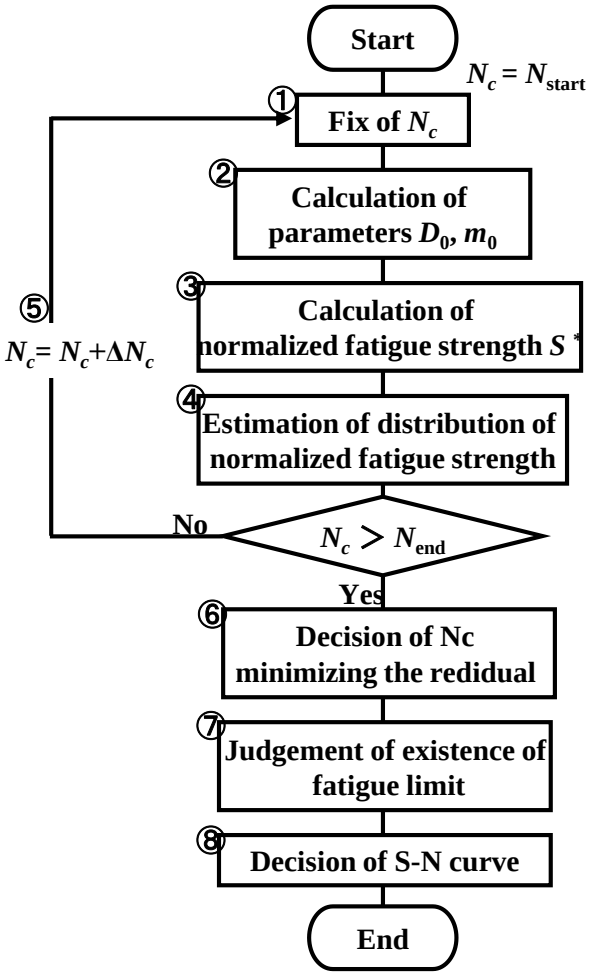

Fig. 2.10 Flowchart of decision of the S-N curve

The process of determining S-N is as follows:

(1) Set the fatigue limit of Nc

(2) Calculate parameters of D0 and m0 in (Eq.2.1) and (Eq.2.2) based on least squares method.

(3) Calculate Normalized stress

(4) Calculate the parameter of distribution

(5) Change the Nc by small steps, repeat from step (1) to (4).

(6) Nc is fixed when the sum of squares error of the distribution is the smallest.

(7) Estimate whether fatigue limits is exit by comparing the error when all data is considered belonging to slop.

(8) Determination of S-N and fatigue strength distribution.

Fig. 2.10 shows the flowchart of decision of the S-N curve

2.2.4 Fatigue limit diagram considering failure probability

There are two limitations to the S-N curve. One is the inability to predict life at stress ratios different from those under which the curve was developed; the other is not capable of considering mean stress effect, the effect of which is widely studied[32]~[35]. Stress ratio is marked as R as shown in Eq.2.5, which is the minimum peak stress divided by the maximum peak stress. The relationship of mean stress σ_m, stress amplitude σ_a and stress ratio R can be presented as Eq. 2.6, 2.7, and 2.8.

$$R = \frac{\sigma_{\min}}{\sigma_{\max}} \qquad \text{(Eq.2.5)}$$

$$\sigma_a = \frac{\sigma_{\max} - \sigma_{\min}}{2} \qquad \text{(Eq.2.6)}$$

$$\sigma_m = \frac{\sigma_{\max} + \sigma_{\min}}{2} \qquad \text{(Eq.2.7)}$$

$$\sigma_m = \frac{1+R}{1-R}\sigma_a \qquad \text{(Eq.2.8)}$$

As the load structure and component endures is usually not the same with fatigue test that the stress ratio equals 0. Modified Goodman diagram and Gerber diagram etc. are used for predict life at any stress ratio and considering the mean stress effect. Substantial scatter exists, but the general trend indicating that tensile mean stresses are detrimental is quite evident. Typical fatigue limit diagram are shown in Fig. 2.11.

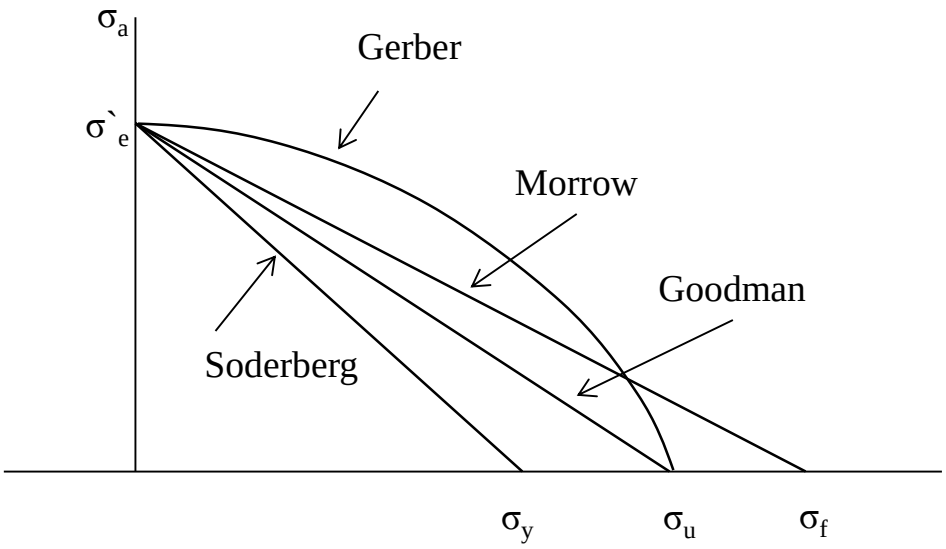

Fig. 2.11 Comparison of Mean Stress Equations

The $\sigma`_e$ is the effective alternating stress at failure for a lifetime of N_f cycles, and σ_u is the ultimate tensile strength. It appears that much of the data fall between the straight (Goodman line) and curved lines (Gerber parabola). As a result, Goodman diagram is used in this study. An additional popular relationship has been formulated by replacing σ_u with σ_f (Morrow line)or σ_y (Soderberg line), where σ_f is the true fracture strength and σ_y is the true fracture stress. The following equations represent these tensile mean stress effects for uniaxial state of stress:

Soderberg [36]: $$\frac{\sigma_a}{\sigma`_e} + \frac{\sigma_m}{\sigma_y} = 1 \quad \text{(Eq.2.9)}$$

Goodman [37]: $$\frac{\sigma_a}{\sigma`_e} + \frac{\sigma_m}{\sigma_u} = 1 \quad \text{(Eq.2.10)}$$

Gerber [38]: $$\frac{\sigma_a}{\sigma`_e} + \left(\frac{\sigma_m}{\sigma_u}\right)^2 = 1 \quad \text{(Eq.2.11)}$$

Morrow [39]: $$\frac{\sigma_a}{\sigma`_e} + \frac{\sigma_m}{\sigma_f} = 1 \quad \text{(Eq.2.12)}$$

This kind of diagram is all presenting the average value, but the fatigue probability is not considered. A method that can evaluate fatigue reliability of all circumstance is necessary. Fatigue limit diagram with fatigue strength distribution is shown in Fig. 2.12. Fatigue strength distribution in fatigue limit diagram is on certain line that the stress

ratio is the same. It is time consuming to make fatigue strength distribution of different stress ratio. It is necessary to evaluate fatigue strength distribution of all stress ratios from 1 or 2 kind of stress ratio.

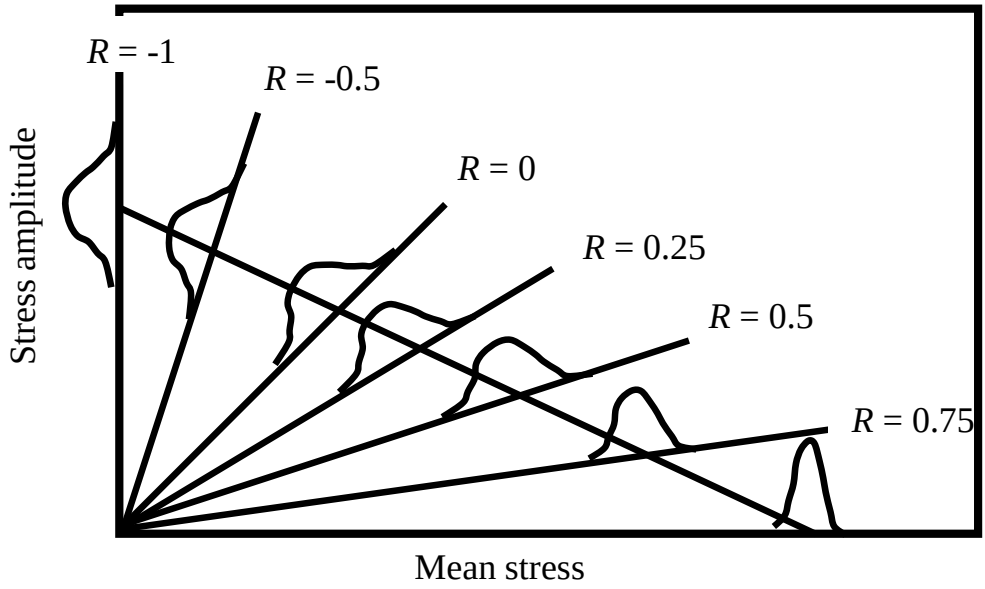

Fig. 2.12 Scatter of fatigue limit curve

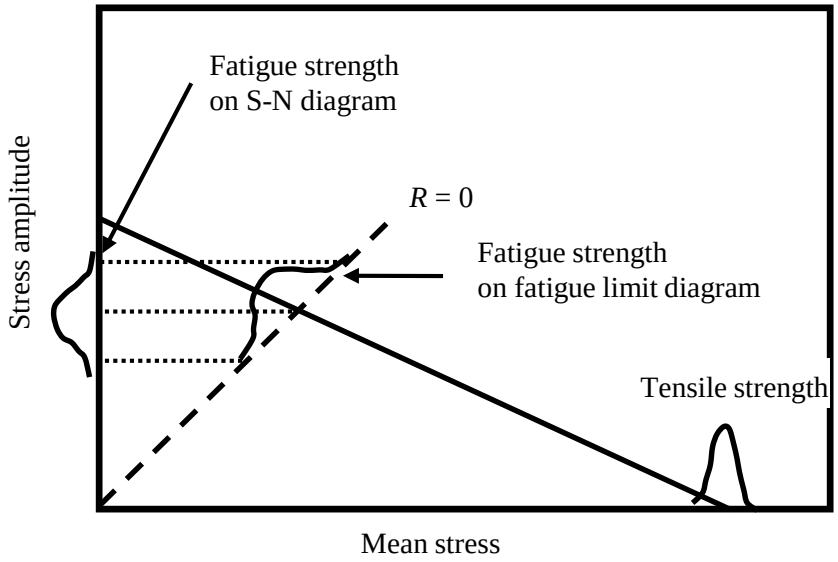

Fig. 2.13 Fatigue limit diagram considering fatigue strength distribution

It is obviously that the distribution of strength in fatigue limit diagram is equivalent of the strength distribution of S-N. Fig. 2.13 shows modified Goodman diagram and the fatigue strength distribution of stress ratio of R=0. The distribution of fatigue strength of

stress ration R=0 can be obtained by projecting the strength distribution of S-N on to fatigue limit diagram. Consequently, fatigue limit diagram considering strength distribution can be obtained by using this method.

2.2.5 Reliability evaluation considering fatigue probability

Different from fatigue test Structural components are frequently subjected to complex time histories of stress. The counting methods for load frequency are associated with three categories as follows [40].

Peak counting methods: The turning points in a load-time trace are administrated according to their load level.

Level crossing counting methods: This counts the number of times a load-time trace crosses a certain level, either in a positive or negative direction. Peak counting and level crossing counting are related: the number of positive level crossings is equal to the number of peaks above a level minus the number of troughs above that level. This implies that the result of a level crossing counting can be derived from a peak counting result. As the opposite is not true, level crossing counting is considered to be of a lower order than peak counting.

Rang counting methods: It appears logical to count load variations directly because fatigue damage accumulation comes from variations in load rather than from individual peaks and troughs. Ranges may be counted as either single ranges or as range pairs. The counting of single ranges, usually indicated as range count, is a straightforward counting of all subsequent load ranges in their order of occurrence. This principle splits up a loading trace at any occurrence of a load reversal. The rang-pair counting avoids this sensitivity. Rather than splitting up a loading trace, it searches for full-load cycles that are contained within main load variations.

Rain flow counting method also called range-pair-range counting method, have been accepted widely [41] ~ [44]. The image of frequency counting with rain flow method is shown in Fig. 2.14.

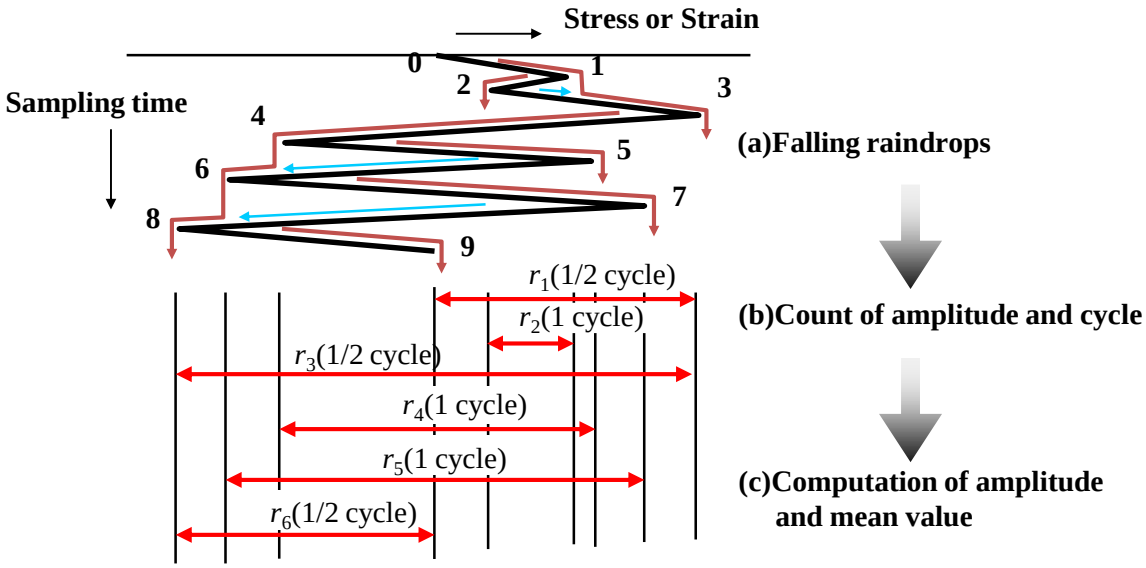

Fig. 2.14 Frequency count with rain flow method

The algorithm is as follows.

1. Reduce the time history to a sequence of (tensile) peaks and (compressive) troughs.
2. Imagine that the time history is a template for a rigid sheet (pagoda roof).
3. Turn the sheet clockwise 90° (earliest time to the top).
4. Each tensile peak is imagined as a source of water that "drips" down the pagoda.
5. Count the number of half-cycles by looking for terminations in the flow occurring when either:
   a. It reaches the end of the time history;
   b. It merges with a flow that started at an earlier tensile peak; or
   c. It flows opposite a tensile peak of greater magnitude.
6. Repeat step 5 for compressive troughs.
7. Assign a magnitude to each half-cycle equal to the stress difference between its start and termination.
8. Pair up half-cycles of identical magnitude (but opposite sense) to count the number of complete cycles. Typically, there are some residual half-cycles.

2.2.6 Miner`s law for cumulative damage

Langer [45] and Miner [46], suggested that fatigue damage at a given stress level could be considered to accumulate linearly with the number of stress cycles. By using the S-N data, number of cycles of S1 is found as N1 which would cause failure if no other

stresses were present. Operation at stress amplitude S1 for a number of cycles n1 smaller than N1 produces a smaller fraction of damage which can be termed as D1 and called as the damage fraction. As shown in S-N of Fig. 2.15, number of cycles of S1 is found as N1 which would cause failure if no other stresses were present. Operation at stress amplitude S1 for a number of cycles n1 smaller than N1 produces a smaller fraction of damage which can be termed as D1 and called as the damage fraction. Operation over a spectrum of different stress levels results in a damage fraction Di for each of the different stress levels Si in the spectrum. It is clear that, failure occurs if the fraction exceeds unity:

$$D1+D2+...+Di-1+Di\geq 1.0 \quad \text{(Eq.2.13)}$$

The damage fraction at stress level Si will be,

$$D_i = \frac{n_i}{N_i} \quad \text{(Eq.2.14)}$$

Then, a total damage can be defined as the sum of all the fractional damages over a total of k blocks,

$$D = \sum_{i=1}^{k} \frac{n_i}{N_i} \quad \text{(Eq.2.15)}$$

and the event of failure can be defined as

$$D \geq 1.0 \quad \text{(Eq.2.16)}$$

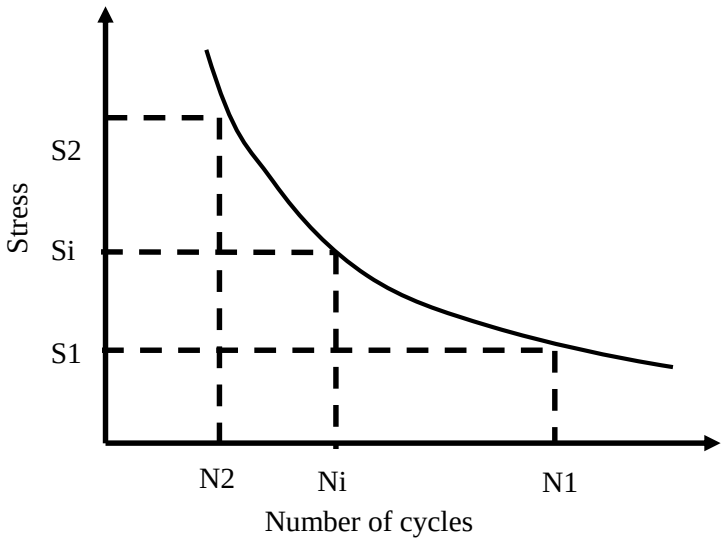

Fig. 2.15 Constant amplitude S-N curve

From rain flow counting analysis, the stress amplitude and mean stress can be obtained. As there are many couples of stress amplitude and mean stress. It is impossible to evaluate the fatigue life by S-N curve, fatigue limit diagram considering strength distribution mentioned above is used to evaluate the cumulative damage under certain failure probability. The process of fatigue evaluation is introduced as follows.

Firstly, fatigue limit diagram considering strength distribution can be made based on the fatigue test result and static strength distribution. Secondly, analysis the load frequency using rain flow counting method, and then compare the couples of stress amplitude and mean stress with fatigue limit diagram. Finally, calculate the cumulative damage of every load frequency using Miner's law.

2.3 Design space of fatigue reliability

Based on the numerical simulation results, the stress history of diaphragm in pressing process can be obtained. The fatigue reliability of diaphragm can be evaluated by evaluating the stress history using the fatigue evaluation process mentioned above. The flow chart of reliability evaluation of diaphragm is shown in Fig. 2.16. Example of fatigue evaluation of diaphragm is introduced in chapter 5.

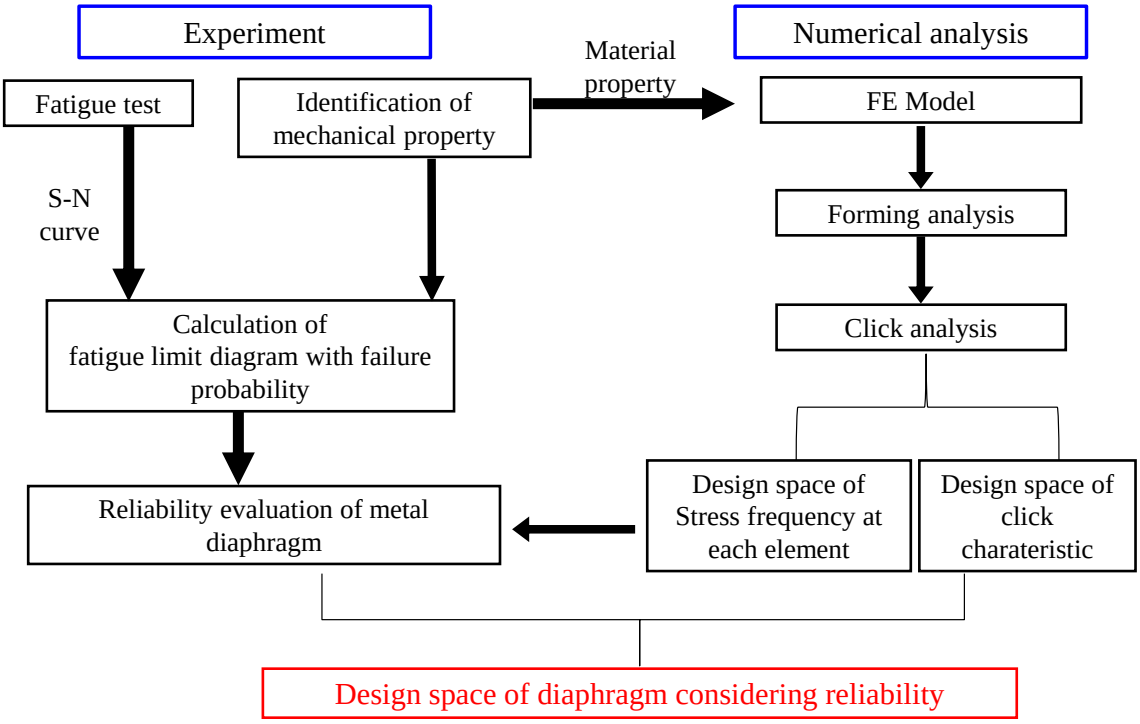

Fig. 2.16 Flowchart of reliability evaluation of diaphragm

2.4 Designable space method considering fatigue reliability

It is time consuming to design diaphragm by making prototypes. In this research a method of designable space is proposed, which makes it easy to design diaphragm. There are four steps to make a designable space considering fatigue reliability. Firstly, evaluate the design space of click characteristics of diaphragm, which can be found in chapter 3 and 4. Secondly, fix the designable space according to the click characteristics demanded, which can be found in chapter 3. Thirdly, evaluate the fatigue reliability of design space, which can be found in chapter 5. Last, designable space can be constructed by combining the designable space with the failure probability design space which also can be found in chapter 5. The scheme of designable space considering fatigue reliability is shown in Fig. 2.17. The Design space of fatigue reliability shows the failure probability of 10^4 cycles, and the designable space can be obtained according to the process in chapter 2.1. Designable space considering fatigue reliability can be obtained by combing the two design space. By using the designable space method, both fatigue reliability and click characteristics can be considered.

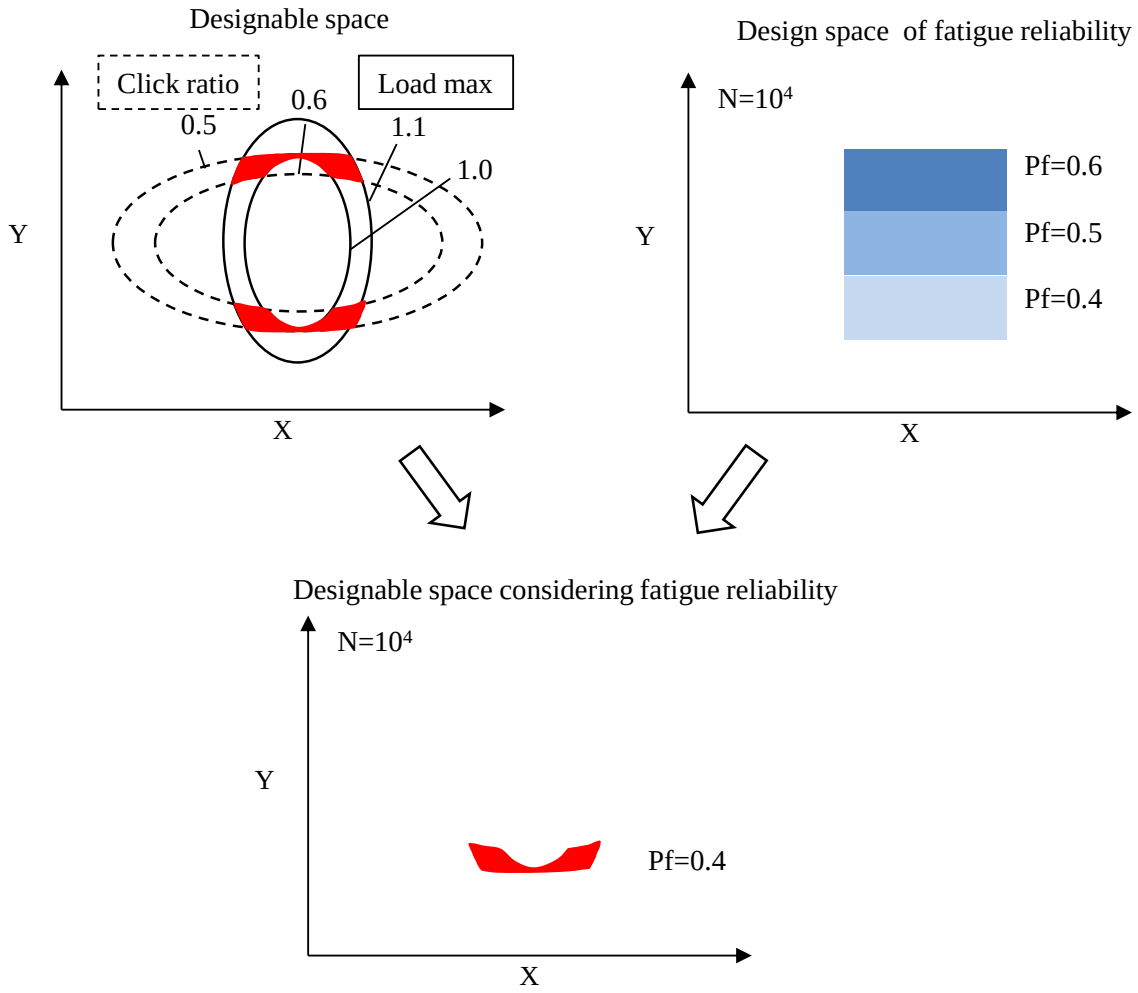

Fig. 2.17 Scheme of designable space considering fatigue reliability

2.5 Summary

In this chapter, time consuming is a major problem in designing diaphragm, in order to solve this problem, designable space method is proposed and procedure of making designable space is introduced. In addition, the fatigue evaluation method used in this research is introduced, and then the method of making designable space considering failure probability is presented. The outline of this chapter is shown as follows.

(1) The process of making diaphragm is introduced. There are many parameters in designing diaphragm, and it is time consuming to design diaphragm. The method of design space is introduced.

(2) In fatigue evaluation of structural and component, it is important to consider the mean stress effect and fatigue life scattering. Fatigue limit diagram considering failure probability is used in this research, which is capable of considering the mean stress effect and scatter of fatigue life.

(3) The fatigue reliability of diaphragm can be evaluated by the fatigue evaluation method mentioned in this paper, based on the stress history obtained from numerical results.

(4) Designable space considering fatigue reliability can be constructed by comparing the designable space with design space of fatigue reliability, which is considered to improve the efficiency of designing diaphragm.

Chapter 3 Functional design of round type diaphragm

Functional design of diaphragm is to design the click characteristics of diaphragm to fit certain requirement. In recent years, space saving switch is required, as electric devices are becoming more functional and smaller. Therefore, different kinds of diaphragms with smaller size and high function ability are required. In this chapter, the mechanical behavior of round type diaphragm during pressing process is discussed, and then the effect of diameter on functional design space is discussed. Functional design pace of space saving diaphragm are discussed in chapter 4 based on the method mentioned in chapter 2.1.

3.1 Finite element analysis

3.1.1 Finite element model of diaphragm

Finite element analysis is a powerful tool to predict the performance of any component or system in the design phase. Finite element analysis increases the accuracy of design, and provides better insight into critical design parameter. By building numerical model instead of virtual prototype, the design period and the cost can be dramatically decreased. There are many commercial FEM packages which are good at different fields. MSC MARC is advanced in nonlinear analysis, and gives a good performance in plastic and contact analysis. Hence, MARC is used in this analysis.

The Finite element model is shown in Fig. 3.1. The right part shows the image of diaphragm deformed after punching process. The punching process is considered having tiny effect on diaphragm, which can be neglect in simulation process. Considering the biaxial geometrical symmetry of diaphragm and biaxial loading symmetry in both manufacturing process and clicking process, 1/4 model is taken as the numerical model.

Eight-node, isoparametric, eight-point Gaussian integration, arbitrary hexahedral element (Type 7) is used in this analysis. For the sake of saving the analysis time, it is common to use shell element for thin structure analysis, the stress of which is considered to distribute in the plane. But it is not capable to present the stress and strain in thickness direction. Although eight-node, isoparameteric, arbitrary hexahedral element uses trilinear interpolation functions, the strains tend to be constant throughout the element. This results in a poor representation of shear behavior. In this research alternative interpolation functions are used to improve the shear characteristics. Three layers are divided in thickness direction. The material property of stainless steel used is

considered to be anisotropy, which is obtained from tensile test. The principle axis of the material is defined as L, T and Z. The rolling direction of stainless steel is L, which agrees with X, T and Z agree with Y and Z separately. The value of material property is shown as follows.

$E_L = 190.0$ (GPa), $E_T = 212.8$ (GPa), $E_Z = 212.8$ (GPa)
$G_{TZ} = 82.11$ (GPa), $G_{ZL} = 70.50$ (GPa), $G_{LT} = 70.50$ (GPa)
$\nu_{TZ} = 0.2900$, $\nu_{ZL} = 0.3040$, $\nu_{LT} = 0.2639$

The simulation process is divided into two processes, forming process and pressing process, which is the same with manufacturing process and pressing process.

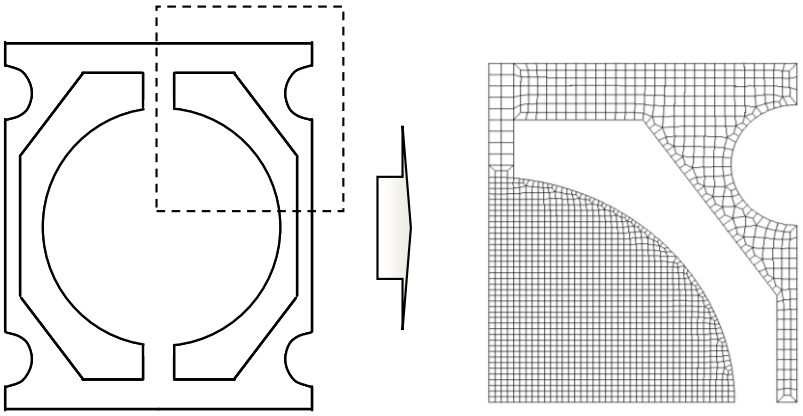

Fig. 3.1 Diaphragm with bridge and Finite element model

3.1.2 Evaluation of forming process

In the forming process of making a diaphragm, high stress distribution will be generated in the edge of diaphragm. It is considered to affect the clicking behavior and the fatigue life of diaphragm. In order to get the convincible result, both forming process and pressing process is carried out. The stress history of pressing process will be used in the future research to estimate the fatigue life of diaphragm.

Fig. 3.2 shows the forming analysis procedure of making diaphragm. The model of diaphragm is made as mentioned before. The mold consist two parts, punch and die. The geometrical shape of mold is defined as rigid body, which is different from the model of diaphragm, it is made of surface.

The stainless steel plane is placed right between punch and die at the beginning. Die is fixed and the load is exerted step by step to make punch moving to the die. In the former research the load is exerted by displacement. However, in factory, the mold is

moved by force. On the other hand, when using displacement control to simulate the forming process, we could not know how exactly should the displacement of punch will be, and at the moment when the diaphragm is almost completely compressed by die and punch, the stress in diaphragm are becoming very big, and sometimes the simulation couldn't go well. In order to make the simulation more similar to the real and more workable, the load control is used. The value of the load is obtained from the manufacturing process.

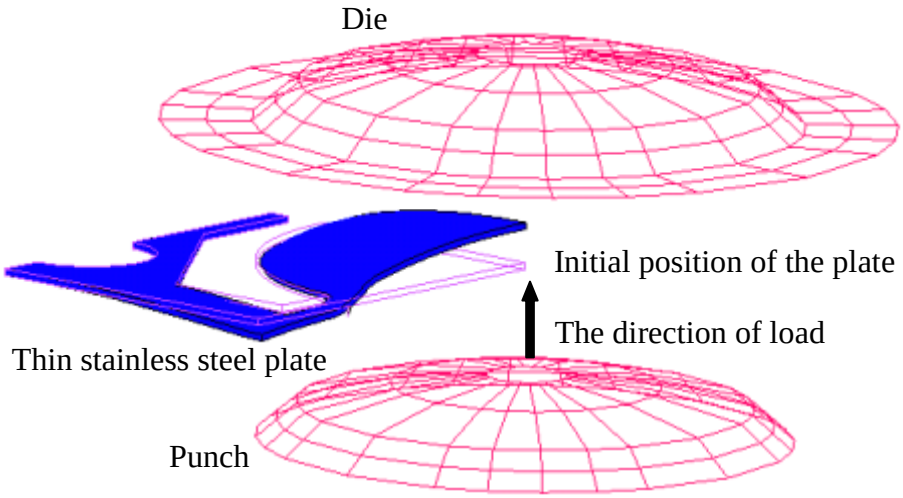

Fig. 3.2Forming analysis procedure

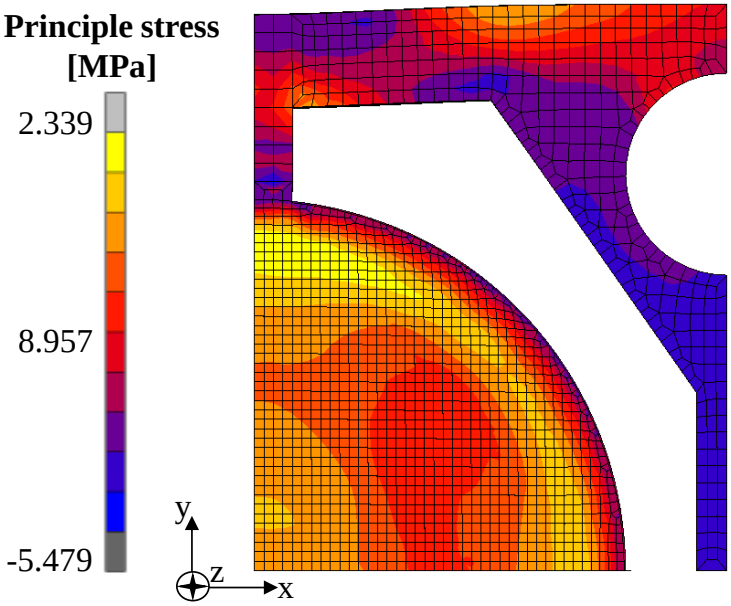

Fig. 3.3 Principle stress at the maximum point

Fig. 3.3 shows the stress distribution when diaphragm is almost completely compressed by die and punch, at that moment the nearest area between the die and the punch is the intersecting circle of mold. So the highest stress will be occurred in that area, which is also the highest stress area after the diaphragm is made, this is confirmed in the analysis.

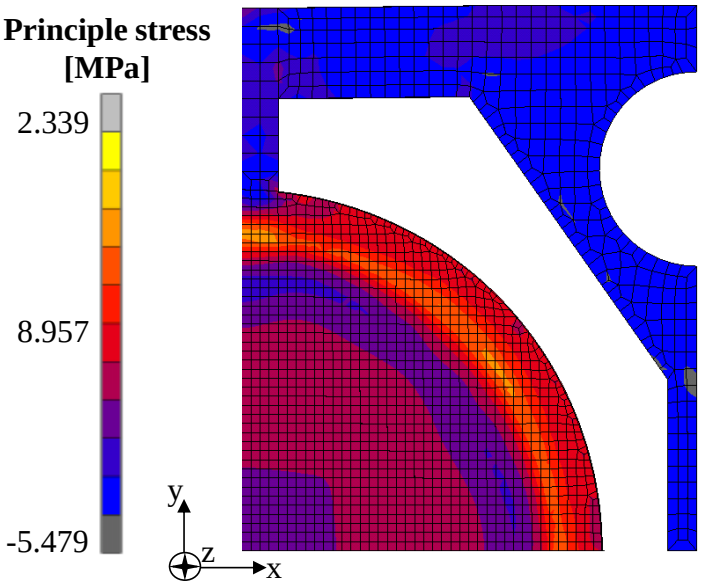

Fig. 3.4 Principle stress after press forming

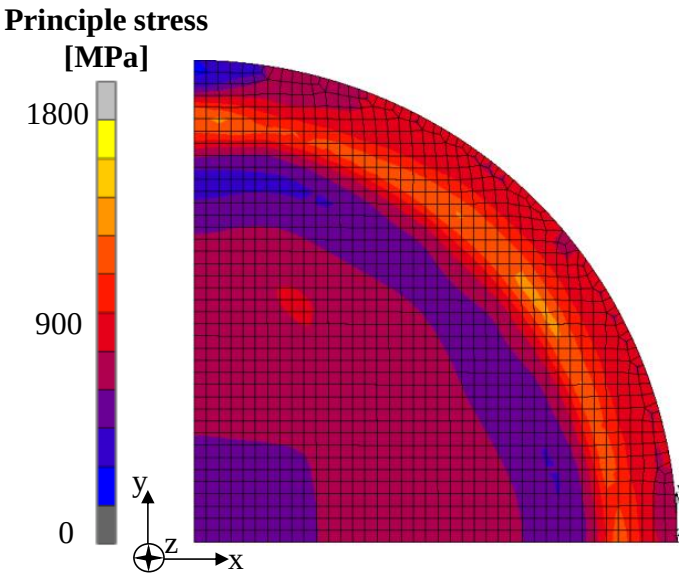

Fig. 3.5 Principle stress after cutting frame

Furthermore, the stress distribution that after the punch is released is shown in Fig. 3.4. Because the part of diaphragm which is connected with the frame has an additional constraint, so the stress of this area is higher than other places. The place of diaphragm which will break firstly is dependent on the stress distribution and the Material anisotropy. When the frame is released from the diaphragm after forming process, the constriction from the frame is released, the stress will be distributed and the high stress generated near the connecting part between diaphragm and frame will be decreased. The stress distribution after diaphragm is released from the frame part is shown in Fig. 3.5

3.1.3 Variation of residual stress in clicking process

In the clicking process the residual stress analysis and the deformation behavior of diaphragm will be carried out. After forming analysis, high residual stress was generated in diaphragm, which will change in the clicking process. It not only affects the clicking characteristic of diaphragm, also affects the fatigue life of diaphragm. In the Fig. 3.6, the actuator and the ground are defined as rigid body, the same as in the forming process. First, press the actuator onto the diaphragm until the diaphragm contact with the ground, then return the actuator to the original place. This is called one clicking process. The residual stress of diaphragm is considered to be redistributed after the first clicking process.

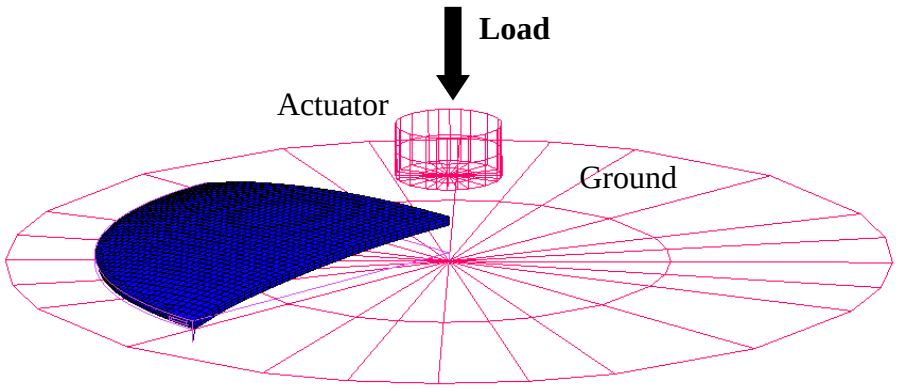

Fig. 3.6 Image of clicking process

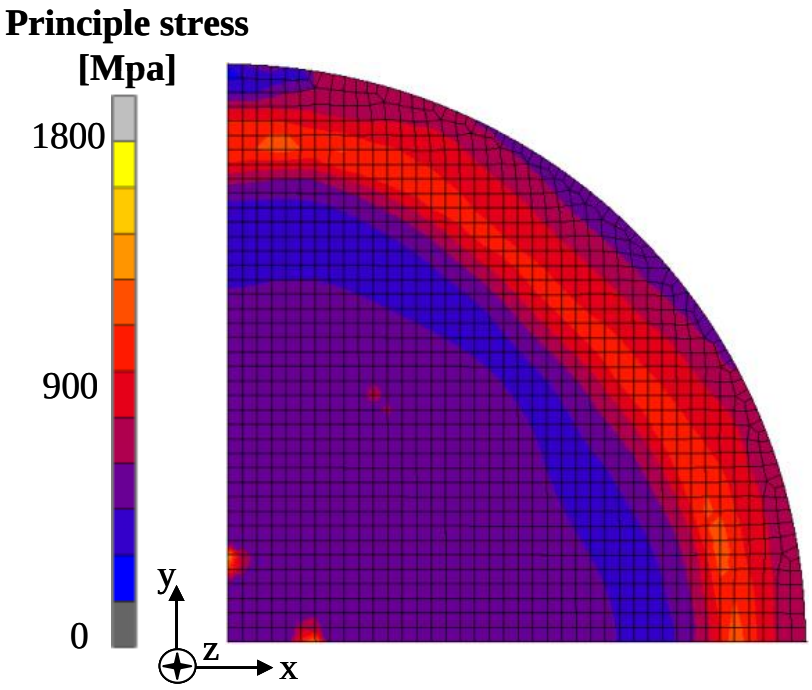

Fig. 3.7 Principle stress after first clicking

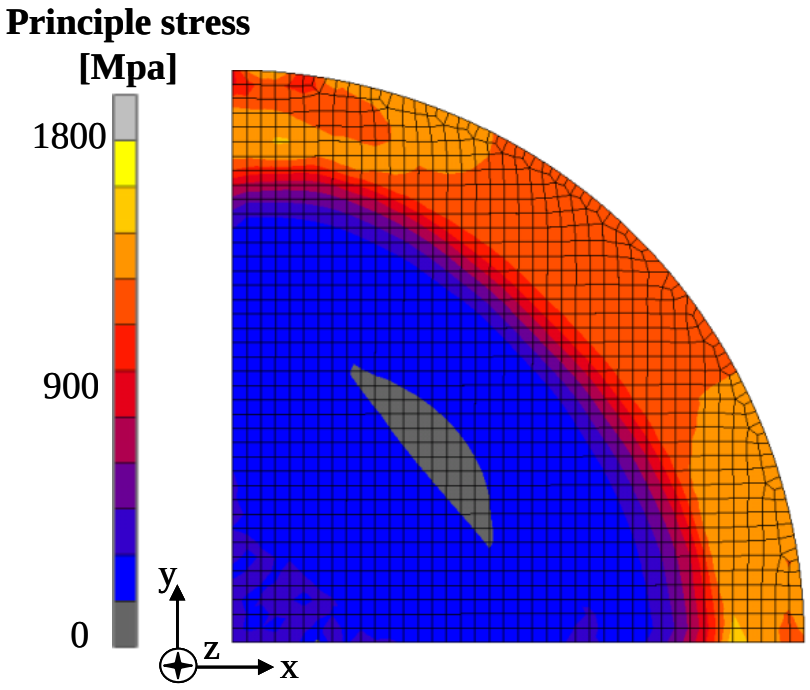

Fig. 3.8 Principle stress at grounding state

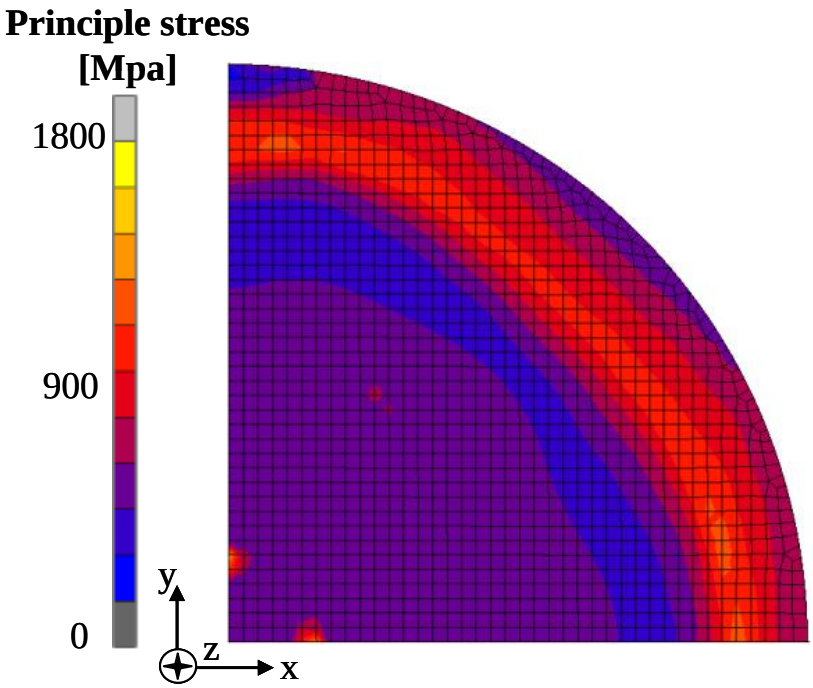

Fig. 3.9 Principle stress after second clicking

Fig. 3.7 shows the stress distribution when the first clicking process is finished. Comparing Fig. 3.7 with Fig. 3.5, both biggest stress and the stress distribution are different from each other. The residual stress redistribution phenomenon is confirmed. In each Figure, the edge of diaphragm has the biggest stress than other area. Next, proceed with the second clicking. Fig. 3.8 and Fig. 3.9 show the stress distribution when diaphragm is contacting with the ground and after second clicking respectively. The stress distribution of the final state of Fig. 3.7 and Fig. 3.9 are almost the same. The stress distribution is considered to be changing in the clicking process, but it didn't affect the stress distribution of final state. As a result, the residual stress is considered to be fully redistributed in first clicking process. From the second clicking, the residual stress is considered stable, which is confirmed in both simulation and experiment [47], [48]. Therefore, in this paper, the clicking simulation consists two clicking process, and the data from the second process is used to evaluate the characteristic of clicking process.

Fig. 3.10 shows the comparison of response curve obtained from numerical analysis and experiment. The vertical axis means the load normalized by maximum load of numerical results. The horizontal axis indicates the displacement divided by the height of a punch. It is recognized that the numerical results have a good agreement with the experiments.

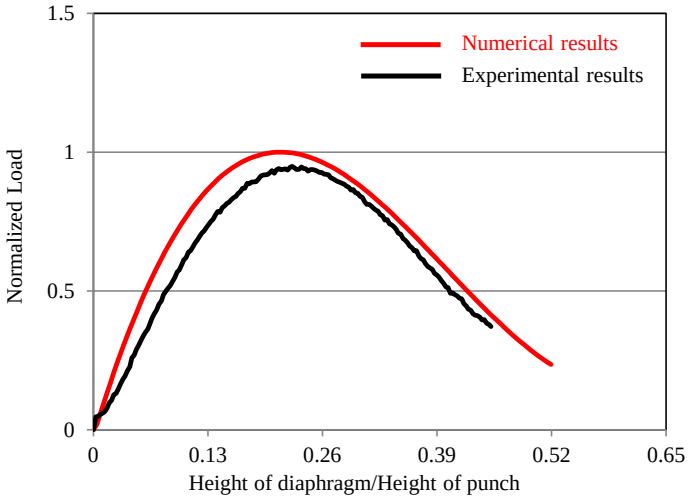

Fig.3.10 Comparison of feeling curve obtained from numerical analysis and experiment

3.2 Evaluation of Mechanical behavior of Round type diaphragm

3.2.1 Design parameters

In this chapter, effects of the geometry of mold on click characteristics are discussed, and the geometry of punch is taken as design parameter. Fig. 3.11 shows the cross-section of a punch. There are many parameters affecting the click characteristics of diaphragm. As the shape of diaphragm is mainly determined by the height and the cone angle at the edge, the height from the ground to the top of diaphragm and the diameter of the intersection of upper-sphere and lower-cone are taken as design parameters to evaluate the relationship between the design parameters and click characteristics of a diaphragm. In this study, the diaphragm of current size is defined as a standard model (S model). By increasing and decreasing parameter A (the height of a punch) based on S model, two models SA+ and SA- are generated. In the same way, models SB+ and SB- are generated by changing the diameter. The numerical analysis is carried out according to the forming and clicking process using these models.

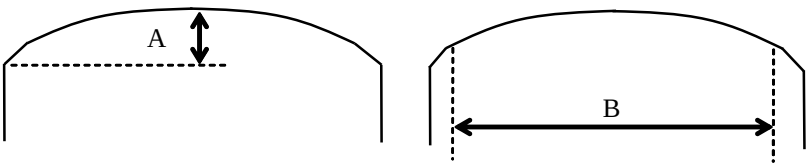

Fig. 3.11 Cross section of a punch and design parameters

3.2.2 Effect of design parameter A

3.2.2.1 Feeling curve

Fig. 3.12 shows the Feeling curve of the diaphragms of Group A molds, it indicates that the mold with the bigger cone has bigger Load Max and smaller clicking ratio.

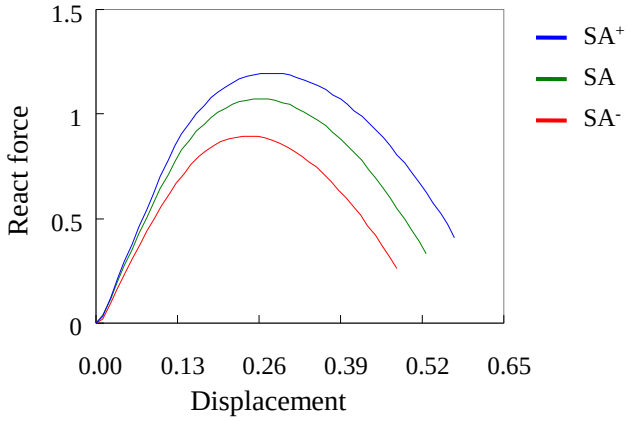

Fig. 3.12 Feeling curve of model group A

3.2.2.2 The stress distribution of model group A

Fig. 3.13, Fig. 3.14 and Fig. 3.15 are showing the stress distribution of diaphragm of SA mold group. Each figure contains two group stress distributions of outer surface and inner surface, and each group has three stress distribution states— Initial, Load Max and Final.

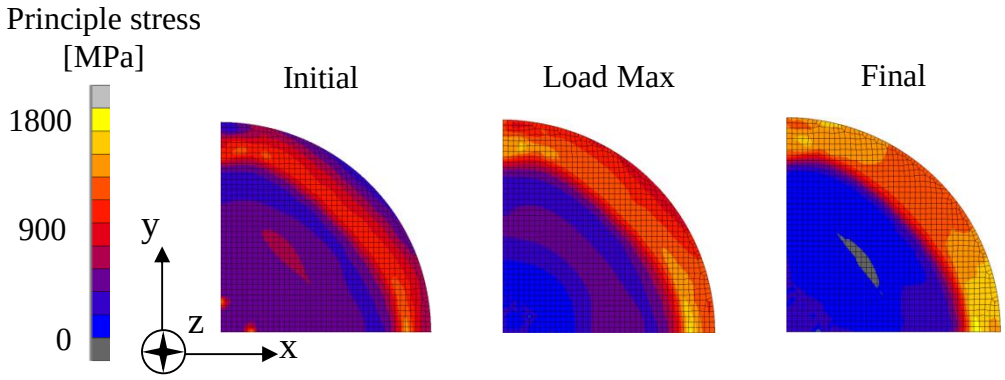

(a) Stress distributions of the surface of diaphragm

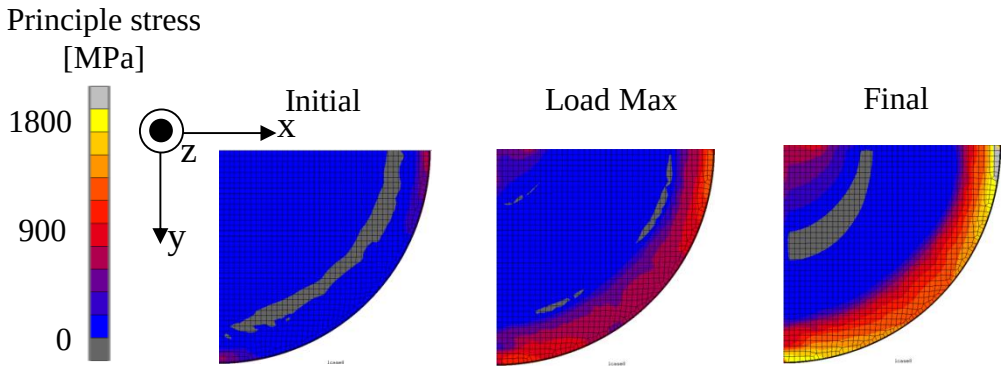

(b) Stress distributions of the inner surface of diaphragm

Fig. 3.13 Stress distribution of SA+

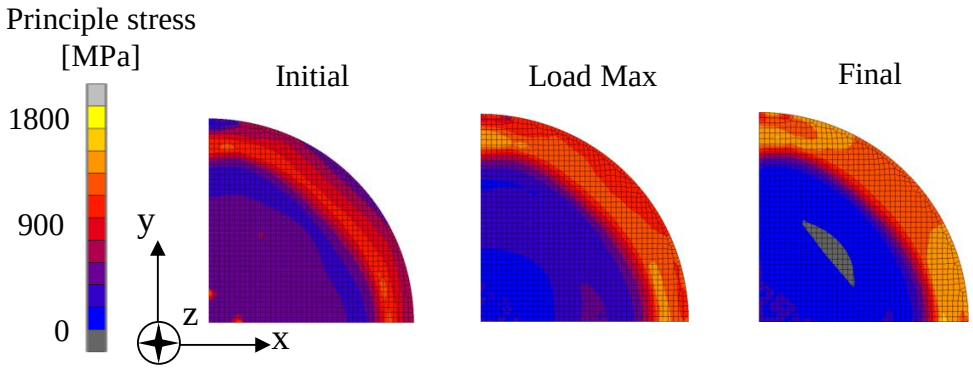

(a) Stress distributions of the surface of diaphragm

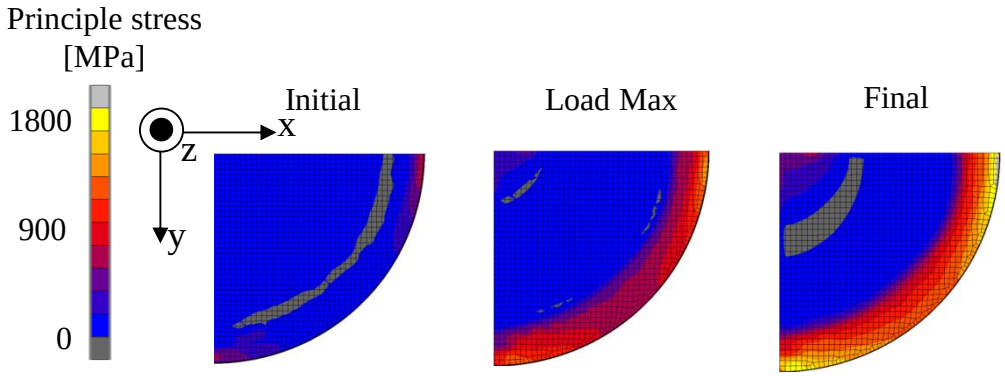

(b) Stress distributions of the inner surface of diaphragm

Fig. 3.14 Stress distribution of SA

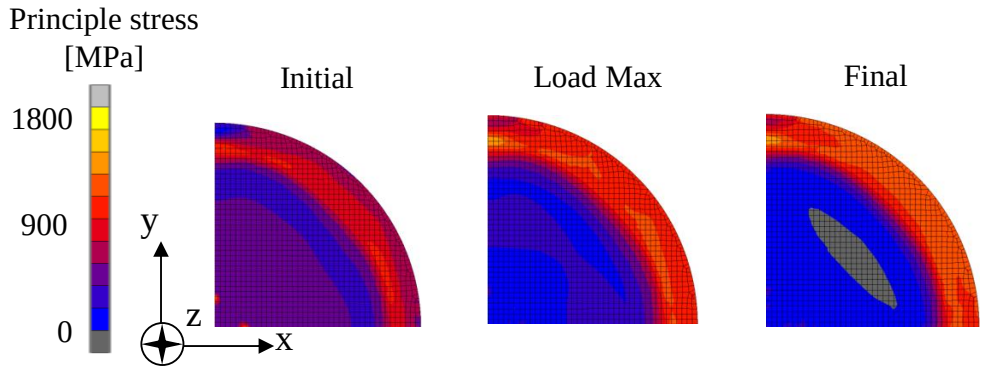

(a) Stress distributions of the surface of diaphragm

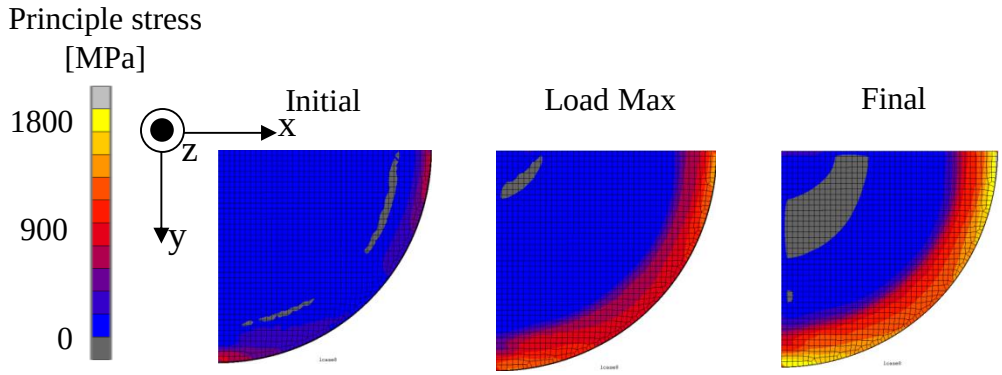

(b) Stress distributions of the inner surface of diaphragm

Fig 3.15 Stress distribution of SA-

At the surface of diaphragm, the area compressed by the spherical surface of mold present a stress around 500MPa, and the area contacted with the cone of mold, during the forming process of making diaphragm, show a stress higher than 600MPa. From the Initial state to the Final state, the stress of the area that compressed by the spherical surface of mold are becoming smaller, because the surface of diaphragm is compressed by the actuator, so the residual tension stress in the surface of diaphragm are becoming smaller. However, in the tangent direction to the circle a tensile force are exerted to the diaphragm, and the stress in the area contacted with the cone of mold are becoming bigger.

The stress in the center of the inner surface of diaphragm shows a low stress state around 145MPa. The center of the inner surface of diaphragm is under a tensile stress in the clicking process, so from the Initial state to the Final state the stress at the center of the inner surface is becoming bigger. The same as the area that compressed by the cone

of mold in the surface, the stress of inner part are also becoming bigger.

In SA group SA+ has a bigger cone, as a result length of the high stress area which is defined as bigger than 600 MPa near the edge of diaphragm, are bigger than others.

3.2.2.3 The deformation modes of model group A

The deformation mode is presented by using the variation of the coordinates of the node in clicking process. The nodes selected to present the shape deformation of diaphragm are on the surface of the X axis of symmetry, which are shown in Fig. 3.16. The deformations of SA group are shown in Fig. 3.17, Fig. 3.18, and Fig. 3.19. The SA+ model has the biggest Z coordinate value in SA group. It can be seen that the deformation mode of SA+, SA and SA- are different from each other. Relation between click characteristics and deformation mode will be discussed in the chapter 3.2.4.

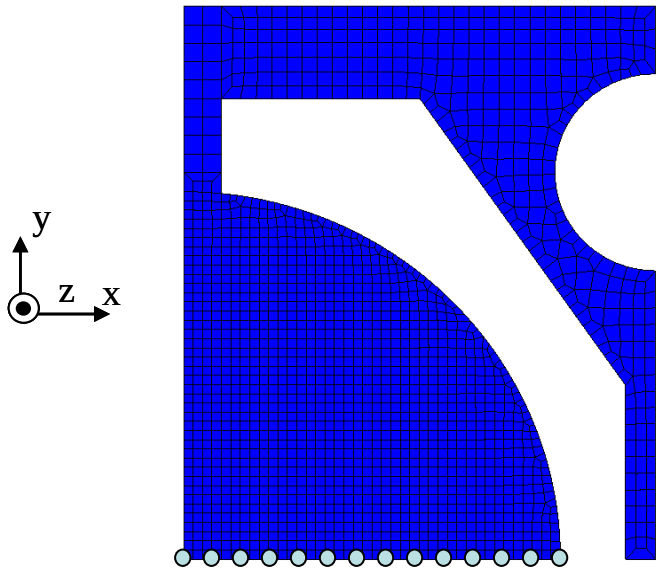

Fig. 3.16 Finite Element model of round type diaphragm

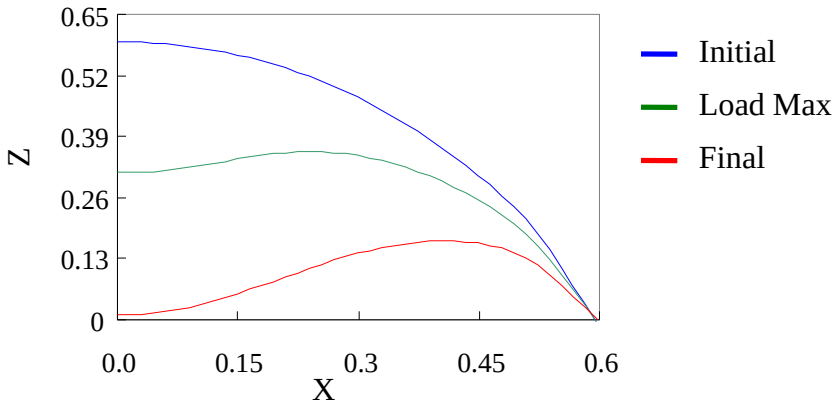

Fig. 3.17 Deformation mode of SA+

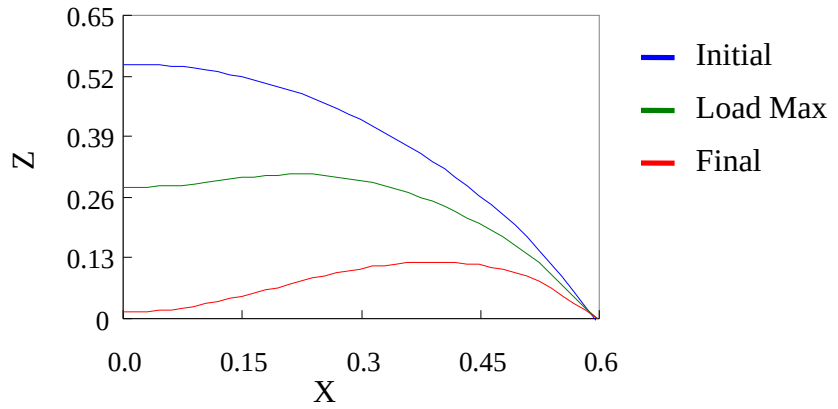

Fig. 3.18 Deformation mode of SA

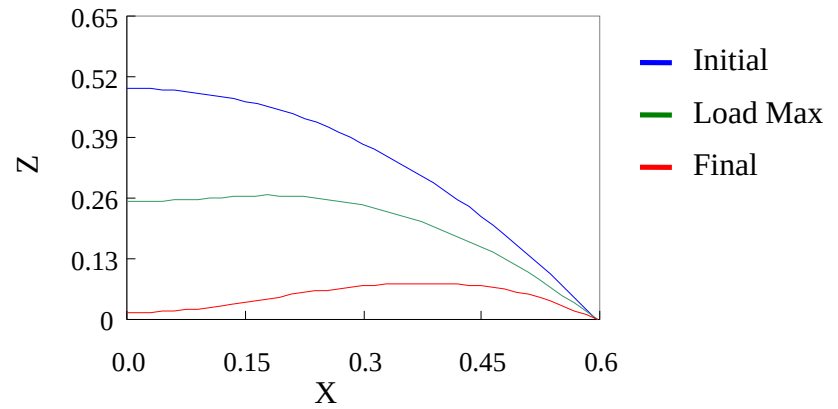

Fig. 3.19 Deformation mode of SA-

3.2.3 Effect of design parameter B

3.2.3.1 Feeling curve of model group B

Fig. 3.20 shows the Feeling curve of the diaphragm that made by Group B molds. It indicates that the mold with the bigger radius of the intersecting circle has bigger clicking ratio and small Load Max.

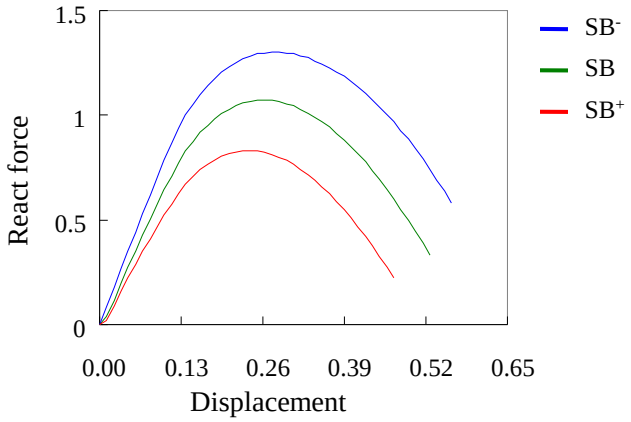

Fig. 3.20 Feeling curve of group B

3.2.3.2 The stress distribution of model group B

Fig. 3.21 and Fig. 3.22 are showing the stress distributions of diaphragms of SB+ and SB- mold. SB model is the same model as SA. Each figure contains two group stress distributions of outer surface and inner surface, and each group has three stress distribution states— Initial, Load Max and Final.

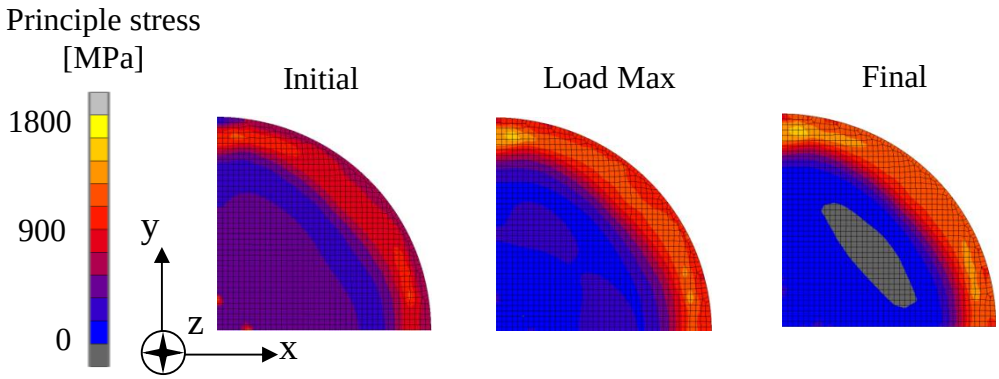

(a) Stress distributions of the surface of diaphragm

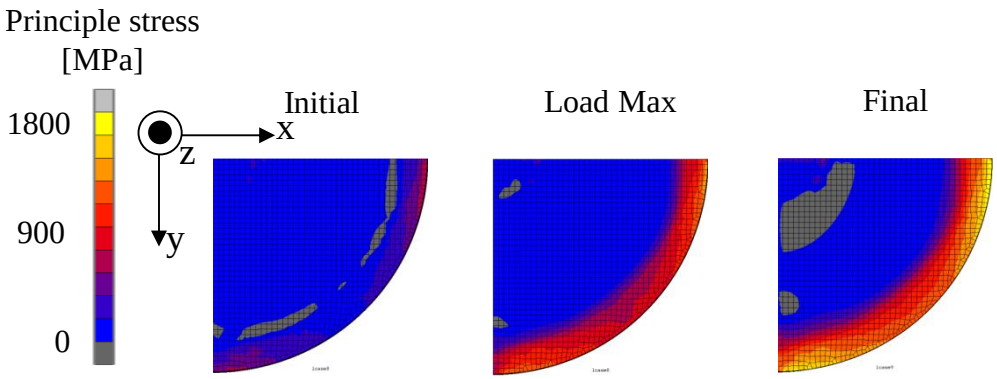

(b) Stress distributions of the inner surface of diaphragm

Fig. 3.21 Stress distribution of SB+

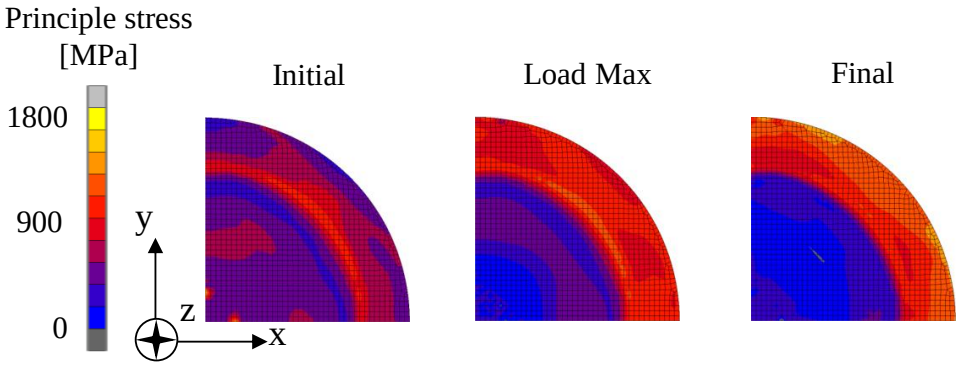

(a) Stress distributions of the surface of diaphragm

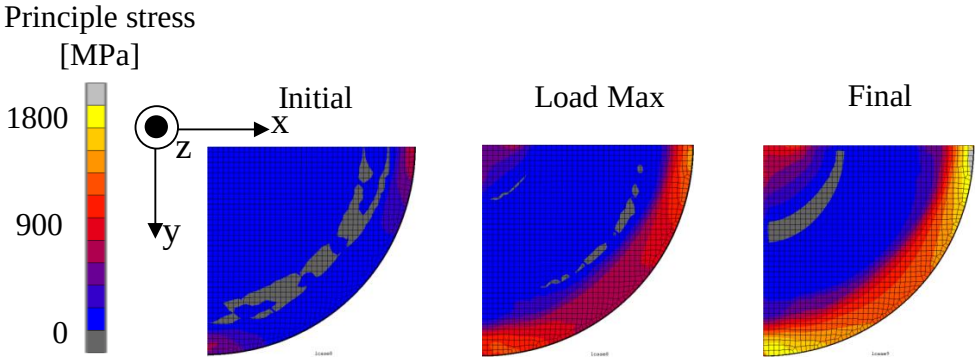

(b) Stress distributions of the inner surface of diaphragm

Fig. 3.22 Stress distribution of SB-

In the clicking process, from Initial state to Final state, the trends of the variation of stress distribution of group B are the same as group A. From the Initial state to the Final

state, the stress of the area that compressed by the spherical surface of mold are becoming smaller, the stress at the center of the inner surface is becoming bigger. The length of the stress area over 600 MPa near the edge of diaphragm of SB- model which has a bigger cone, are bigger than others in group B.

3.2.3.3 The deformation mode of model group B

The deformation modes of SB+ and SB- are shown in Fig. 3.23 and Fig. 3.24. The SB- model has the biggest Z coordinate value in SB group.

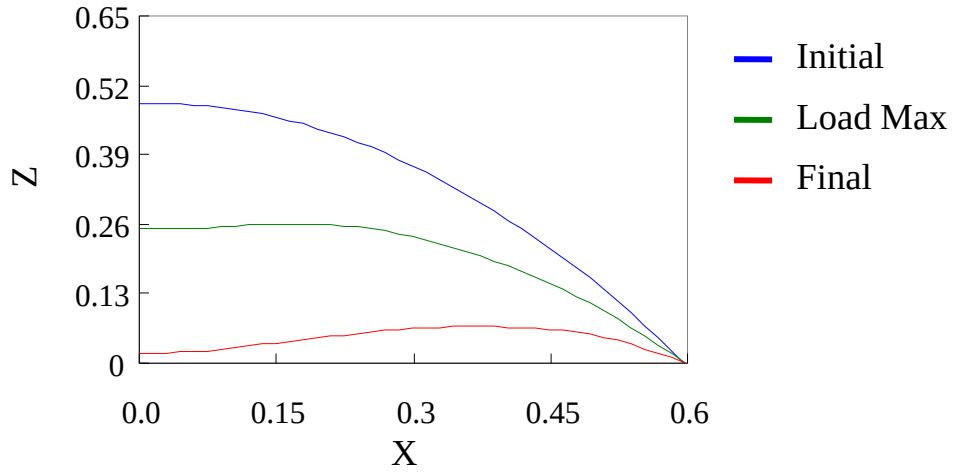

Fig. 3.23 Deformation mode of SB+

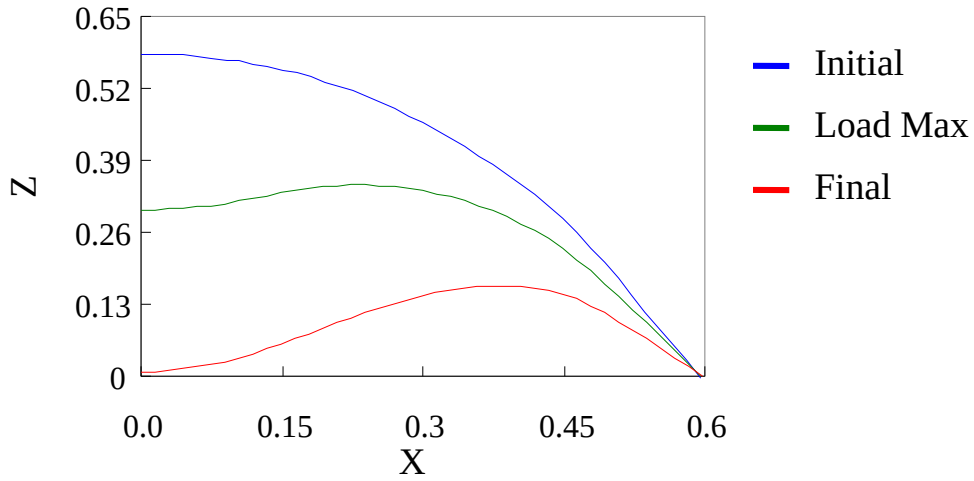

Fig. 3.24 Deformation mode of SB－

3.2.4 Mechanism of clicking process

3.2.4.1 Parameters affecting the clicking characteristic

In order to find out the relationship between the geometry of mold and the clicking characteristic, clicking ration and Load Max obtained from Group A and Group B are sorted out by the height of the mold and the radius of the intersecting circle are shown in Fig. 3.25 and Fig. 3.26 separately. The clicking ratio increases with the radius of the intersecting circle, and decreases with the increase of the height of mold can be seen in Fig. 3.25. The Load Max increases with the height of mold, and decreases with the increase of the radius of the intersecting circle. Clicking ratio and Load Max are showing an opposite trend of the relation with the shape of mold.

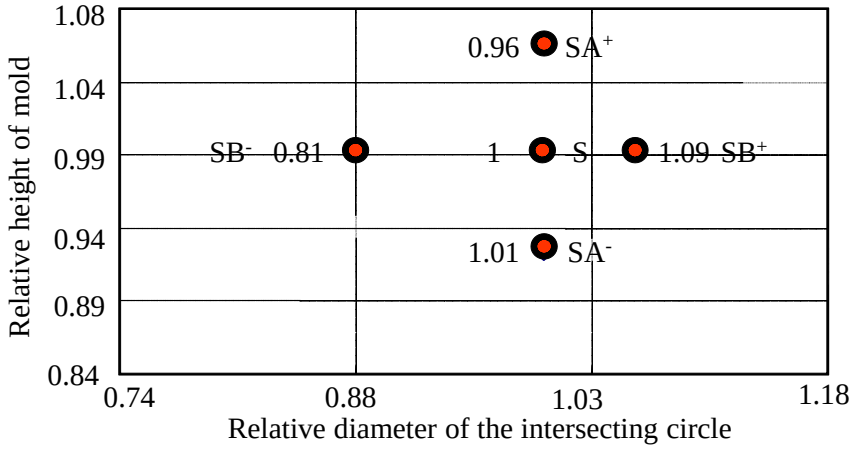

Fig. 3.25 The relation between clicking ratio and the shape of mold

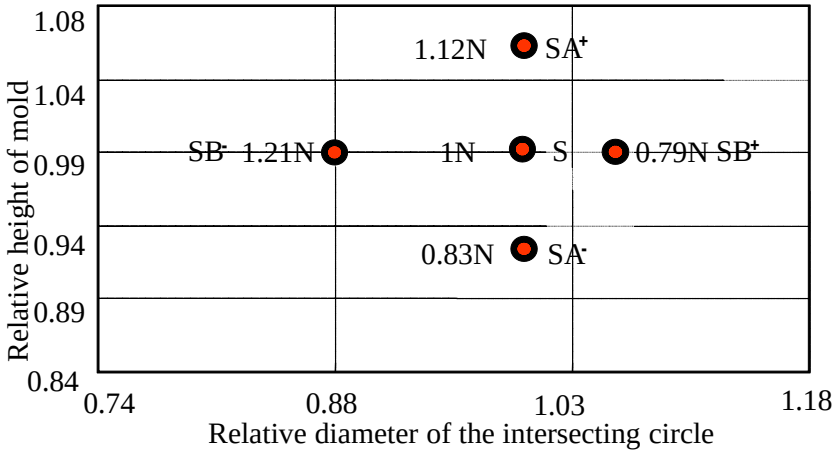

Fig. 3.26 The relation between Load Max and the shape of mold

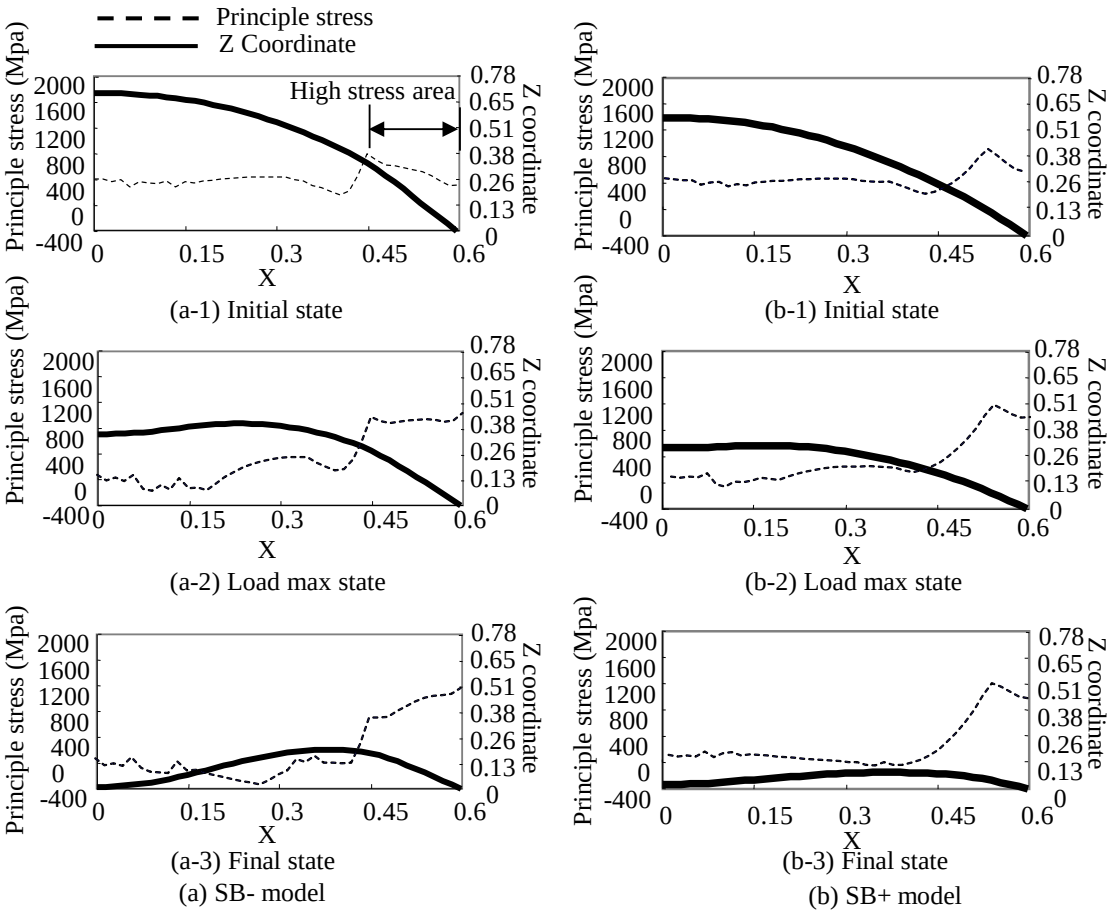

Fig. 3.27 Deformation and stress distribution comparison of SB- and SB+

As the SB- and SB+ are showing a relatively bigger Load Max and bigger clicking ratio separately, SB- and SB+ model are taken as an example to expound the mechanism of clicking process. Fig. 3.27 shows the comparison of deformation and stress distribution of SB- and SB+.

The area that has a stress distribution over 600MPa of SB- is larger than that of SB+, so the edge of SB- diaphragm is difficult to be deformed than SB+. We define the deformation mode like SB- as global deformation and deformation mode like SB+ as regional deformation. It is considered that in the clicking process, diaphragm with the uniform deformation mode has a bigger react force and the diaphragm with the regional deformation mode has a smaller react force. Fig. 3.28 shows the image of regional deformation mode and uniform deformation mode.

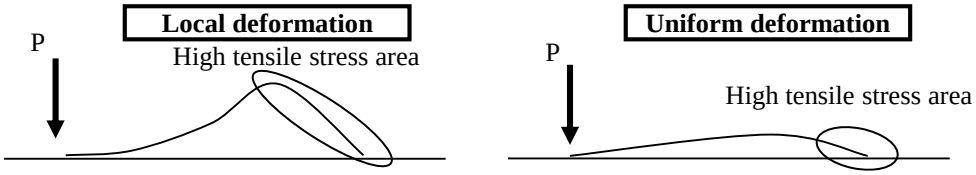

Fig. 3.28 Deformation image of diaphragm

We can conclude that the diaphragm with the global deformation mode has a smaller reaction force, and the diaphragm with the global deformation mode has a bigger reaction force.

3.2.4.2 Clicking analysis without residual stress

In order to evaluate how the residual stress affects the clicking characteristic, the Finite Element model that are made by removing the residual stress of S model are used in clicking analysis. The feeling curves of diaphragm with residual stress and without residual stress are shown in Fig. 3.29.

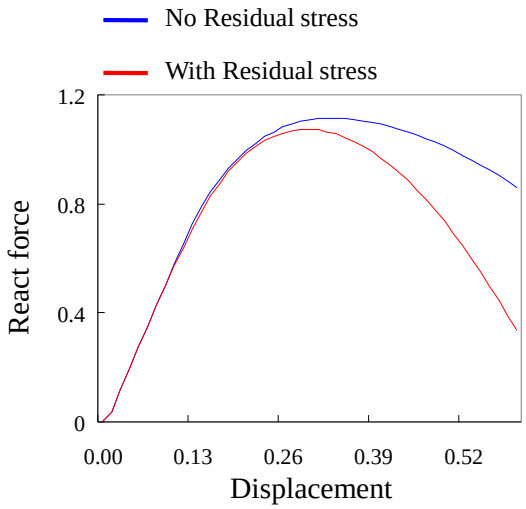

Fig. 3.29 Comparison of model with residual stress and without residual stress

The Load Max of the model without residual stress is a little bigger than that of model with residual stress. The react force of model with residual stress and without residual stress between Initial state and Load Max are generally the same. From the Load Max state to Final state the react force of the model without residual stress are bigger than the model with residual stress.

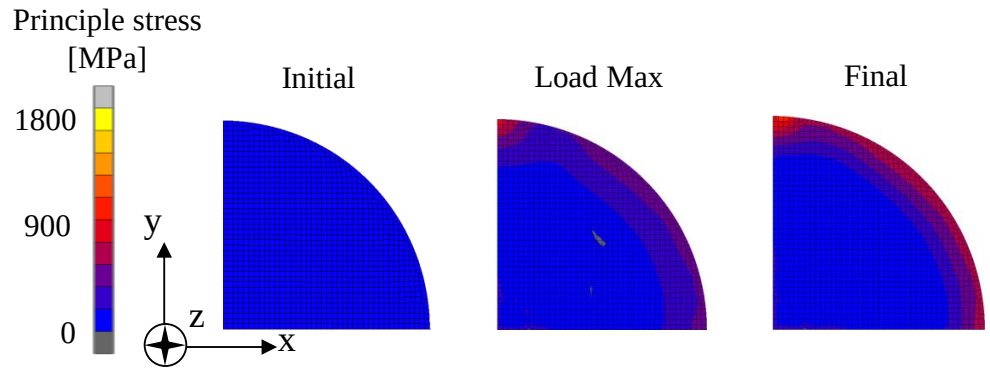

(a) Stress distributions of the surface of diaphragm

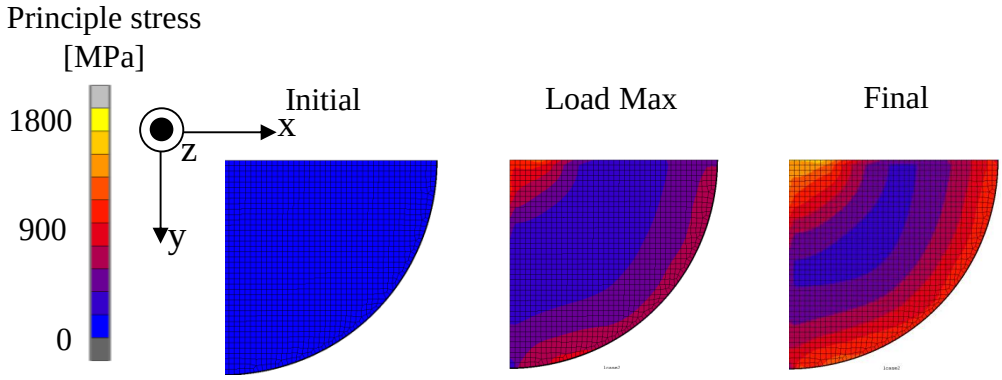

(b) Stress distributions of the inner surface of diaphragm

Fig. 3.30 Stress distribution of the model without residual stress

Fig. 3.30 shows the stress distribution of the model without residual stress. In the case of without residual stress, the stress generated in the clicking process can be seen at the center of diaphragm are very low (about 200MPa), the stress generated in the edge of diaphragm are bigger than the stress in the center of the surface of the diaphragm. The inner surface has a much bigger stress distribution than that of surface. We conclude that the residual stress generated in the forming process have a great effect on clicking characteristic.

3.2.5 Estimation of design space

3.2.5.1 Numerical results of load and click ratio with various parameters A and B

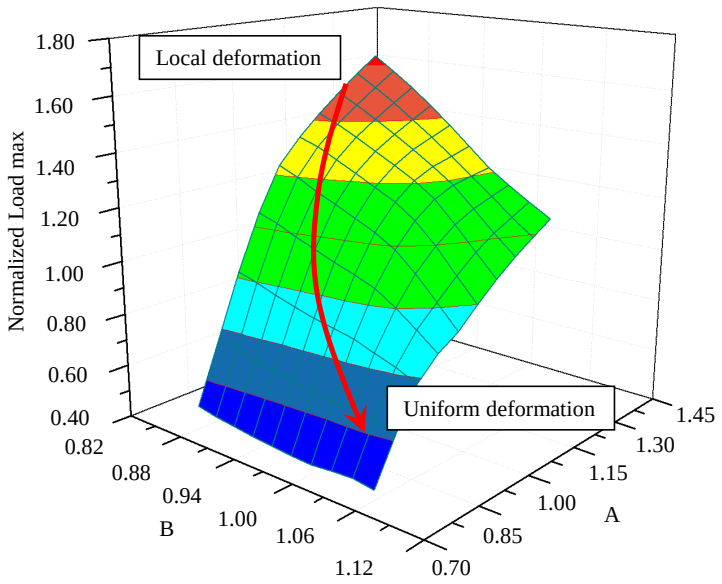

Fig. 3.31 Change of normalized load with various value of A and B

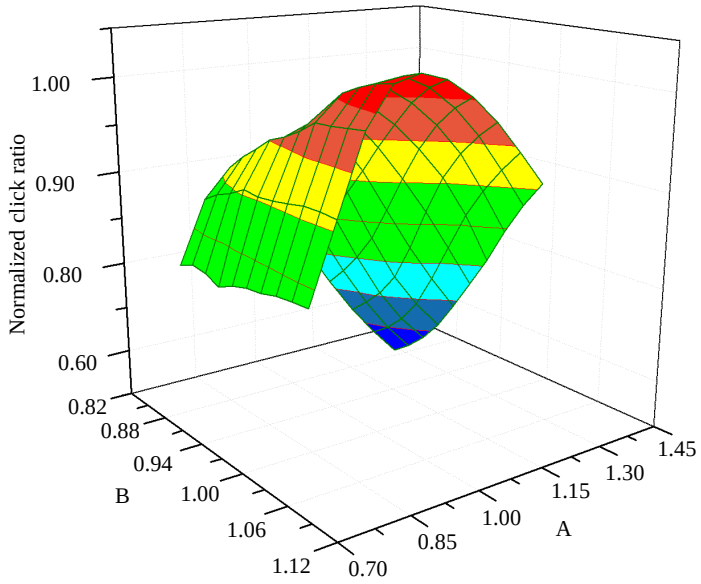

Fig. 3.32 Change of click ratio with various value of A and B

Numerical simulations with various value of A and B have been carried out to evaluate the relationship between the design parameter and click characteristics. Fig.

3.31 shows the relationship between design parameter (A, B) and load max. The load is normalized by the value of S model. The relationship between design parameter (A, B) and click ratio are also shown in Fig. 3.32. When the load is high, the deformation shows ‘local deformation’ type. In case that the diameter (design parameter B) increases and the height (design parameter A) decreases, the load max is reduced and the deformation is shifted to ‘Uniform deformation’ type.

3.2.5.2 Estimation of design space

When certain levels of load max and click ratio are given, the designable area is estimated by considering the effects of parameters (A, B) on clicking characteristics. Fig. 3.33 and 3.34 show the contour plots of load max and click ratio based on Figs. 3.31, 3.32. If a user requires a diaphragm with the click characteristics that load max exceeds 1.00 and click ratio exceeds 1.00, the designable area can be obtained by overlapping two contour plots. Fig. 3.35 shows the overlapped results of the two contour maps. The designable area is III region as shown in Fig. 3.35. From these results, we can obtain the designable area by controlling the parameter A and B if the certain levels of load max and click ratio are given.

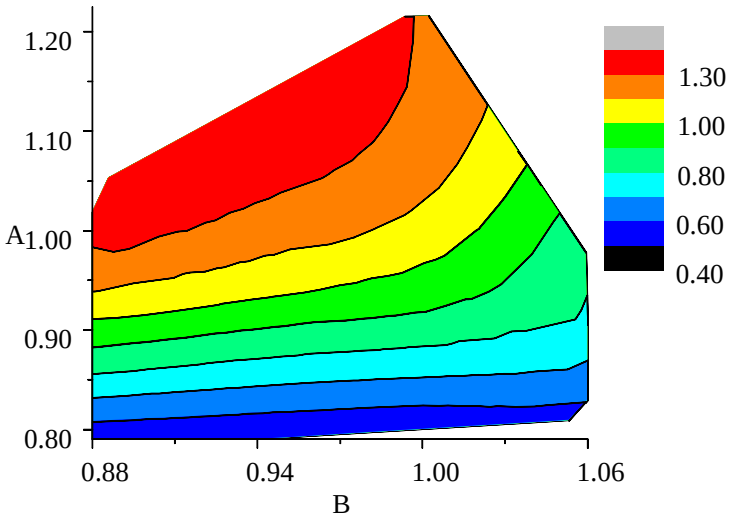

Fig. 3.33 Design space of Load max

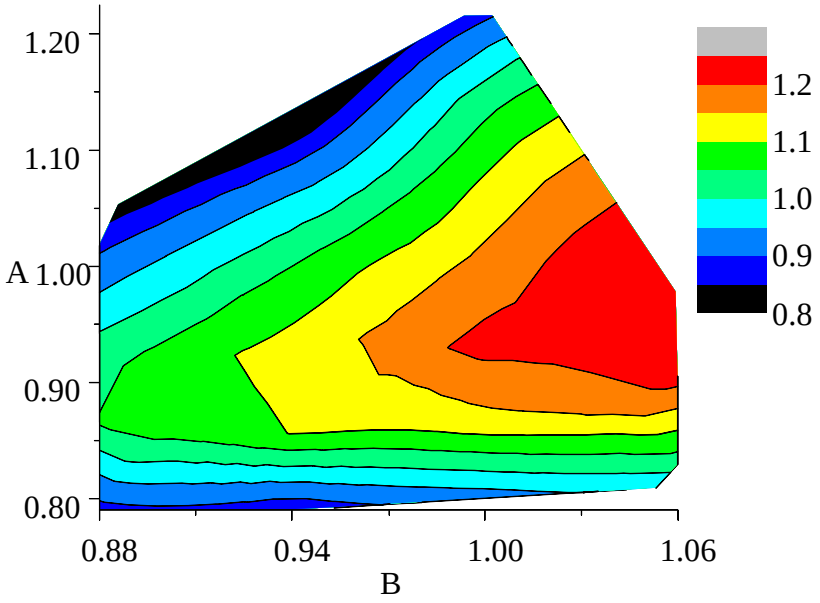

Fig. 3.34 Design space of Click ratio

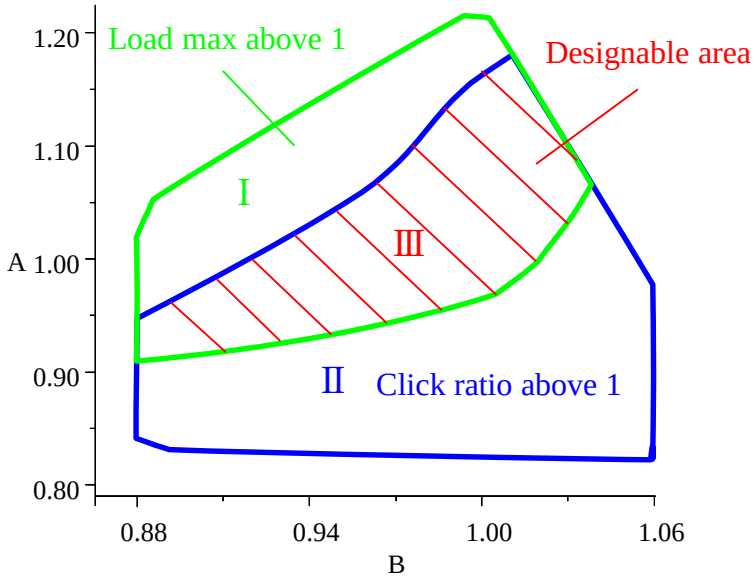

Fig. 3.35 Designable area satisfied region I and II

3.2.5.3 Application of design space to diaphragm with smaller diameter

In order to investigate the design space when the diameter of a diaphragm is changed, additional numerical analysis is carried out with smaller diaphragm model (diameter of 90% of current diaphragm). The numerical results of load max and click ratio by changing the parameters A and B are shown in Fig. 3.36, 3.37 respectively. The value of

parameters A and B is normalized based on S model (current model).

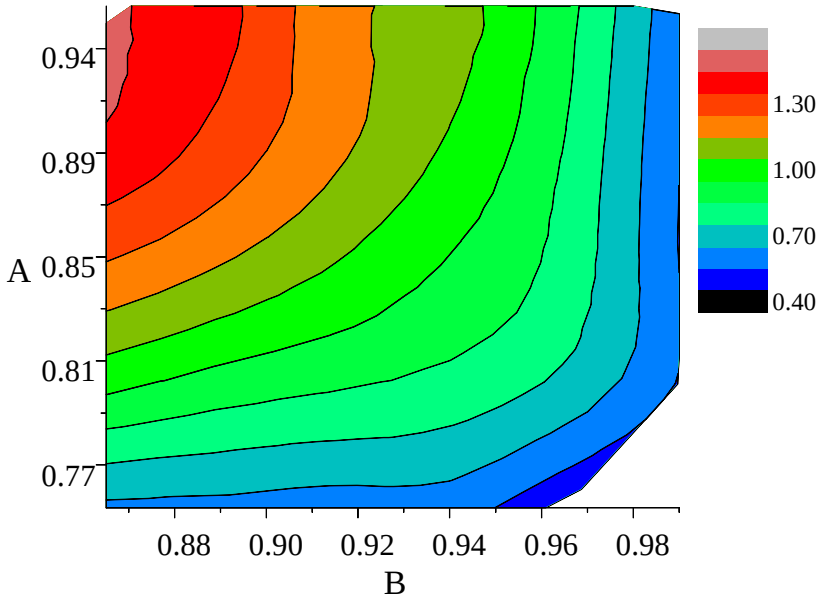

Fig. 3.36 Design space of load max in case of smaller diaphragm

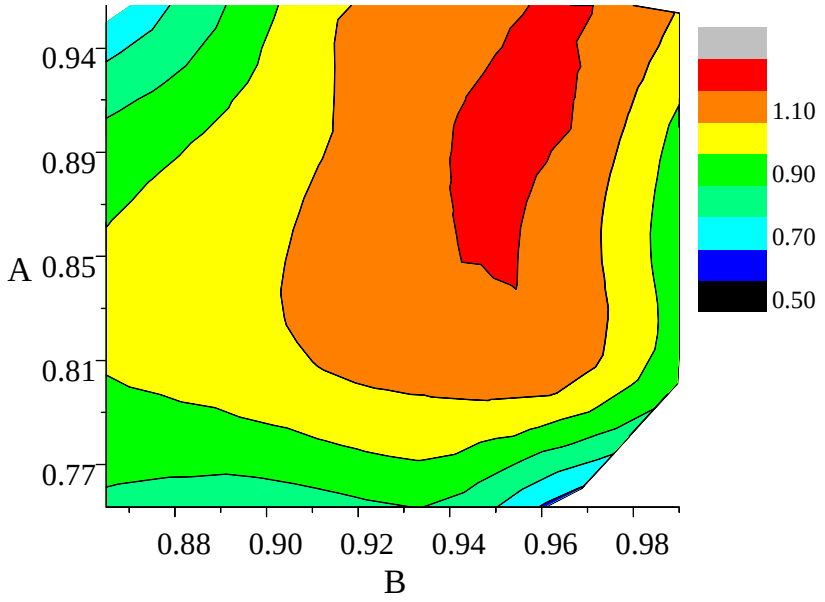

Fig. 3.37 Design space of click ratio in case of smaller diaphragm

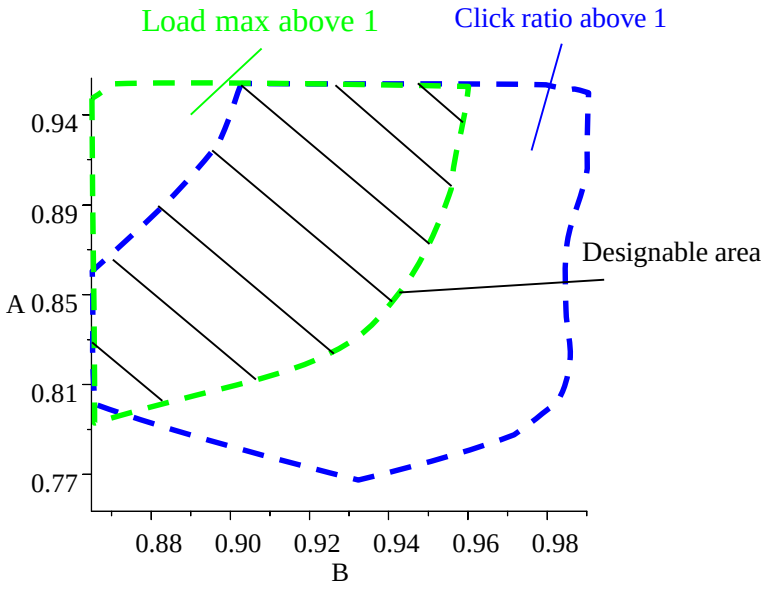

Fig. 3.38 Design space of smaller diaphragm

The relationship between design parameter and click characteristics of smaller diaphragm shows the same trend with current size diaphragm. The load max increases with the increase of parameter A, and the click ratio decreases with the increase of parameter A. It is possible to estimate click characteristics of diaphragm with different diameter using design space.

Fig. 3.38 shows the designable area of smaller diaphragm that load max exceeds 1.00 and click ratio exceeds 1.00. Fig. 3.39 shows the comparison of designable area for current size diaphragm, smaller diaphragm based on Figs. 3.35 and 3.38. Designable area (VI) of smaller diaphragm is shifted to a lower range compared with designable area (III) of current model, and the designable area of smaller diaphragm is narrower than that of current diaphragm. From these results, if the diameter of a diaphragm is changed, we can choose the diaphragm that satisfies requirements by controlling the design parameters based on the proposed designable area.

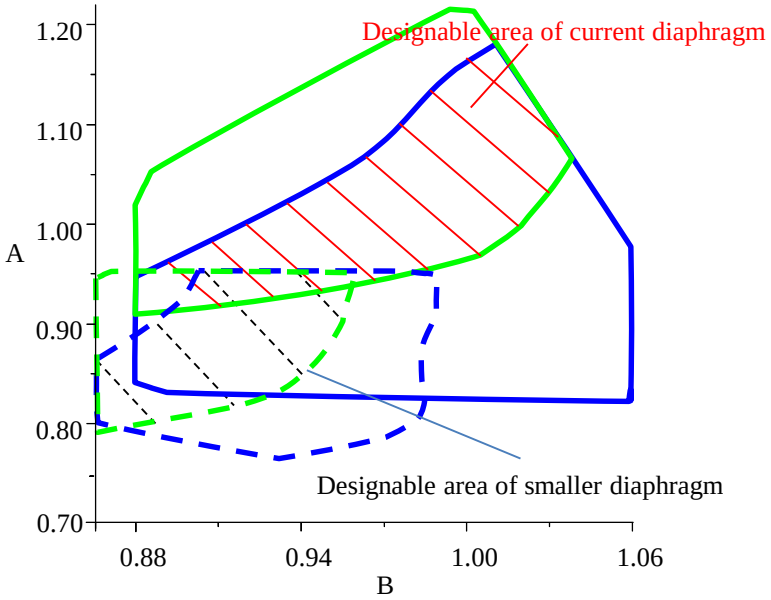

Fig. 3.39 Comparison of designable area for two diaphragm model (current, smaller diaphragm)

3.3 Summary

In this chapter, process of manufacturing and clicking diaphragm is simulated based on finite element method. The mechanical behavior of clicking process is evaluated according to the deformation mode and residual stress generated in forming process. Moreover, the relationship between design parameter and click characteristic is defined as design space, and the designable region of a diaphragm considering the clicking characteristics certain requirements is estimated. The concluding remarks are as follows.

(1) The effect of design parameter of the height and the diameter of a punch on click characteristics is evaluated under forming and clicking process. The load max increases with increasing of the height and decreasing of the diameter. The click ratio shows a trade-off relationship with load max. Especially, the diameter of a punch has big effect on click characteristics.

(2) The residual stress generated in forming process has big influence on the click characteristics of diaphragm. The diaphragm with high residual stress at the edge parts has a high reaction force, and shows local deformation mode. The diaphragm with smaller residual stress at the edge parts has low reaction force and shows uniform deformation mode.

(3) The relationship between the design parameter and click characteristics is defined as ‘design space’, and the designable area of a diaphragm is estimated by using the

design space. We can get the designable area by controlling the design parameter if certain levels of clicking characteristics (load, click ratio) are given.

(4) Furthermore, if the diameter of a diaphragm becomes small, both design space and designable space become narrow.

Chapter 4 Functional design of oval type diaphragm

4.1 Conventional type

4.1.1 Finite element model

Electric devises are becoming more functional and small. Space saving diaphragm, oval type diaphragm is becoming popular. As the manufacturing process and loading process of oval type diaphragm is similar to round type diaphragm, 1/4 model is also used for oval type diaphragm. The finite element model is shown in Fig. 4.1. In order to find out the relationship between the shapes of mold and the clicking characteristic of diaphragm, two groups of models as round type diaphragm have been made based on standard model: group SA is obtained by changing parameter A, group SB is obtained by changing parameter B. The process of making oval type diaphragm is the same as round type diaphragm. The image of design parameter A and B are similar as Fig. 3.11. The numerical analysis is carried out according to the forming and clicking process using these models.

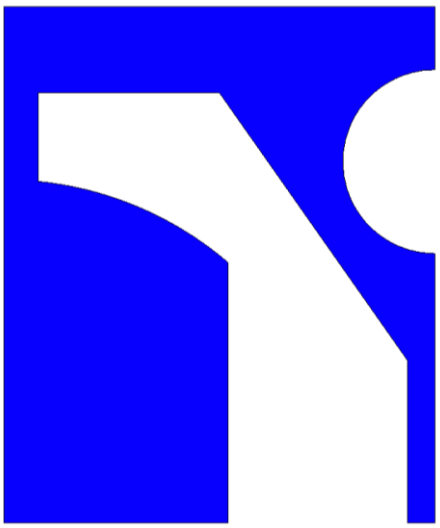

Fig. 4.1 FE model of oval type diaphragm

4.1.2 Effect of design parameter A

The clicking ratio and the Load Max sorted out by the height of the mold and the radius of the intersecting circle are shown in Fig. 4.2. From Fig. 4.2 it can be seen that

the clicking ratio of oval type diaphragm decrease with the increase of the height of mold, the model SA- that has the biggest angle of cone has the smallest clicking ratio. The Load max of oval type diaphragm increase with the increase of the height of mold. In group SA the model SA+ has the biggest Load max.

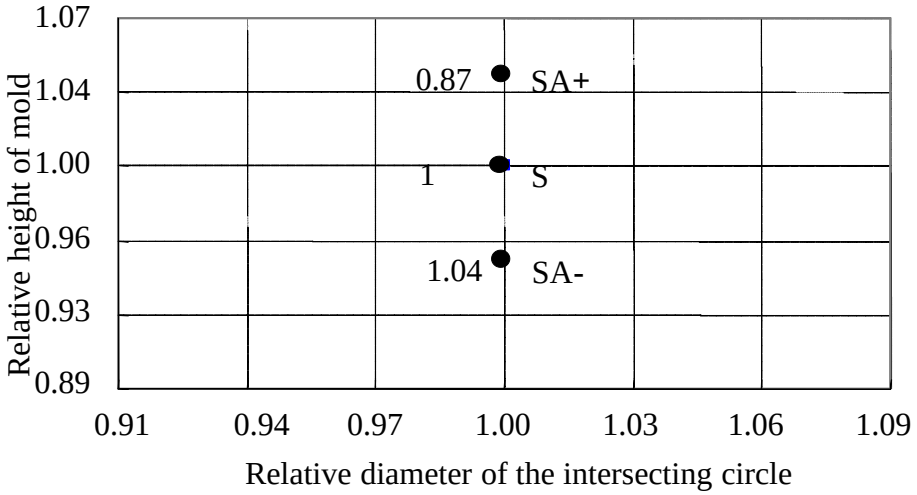

(a) Clicking ratio of SA group

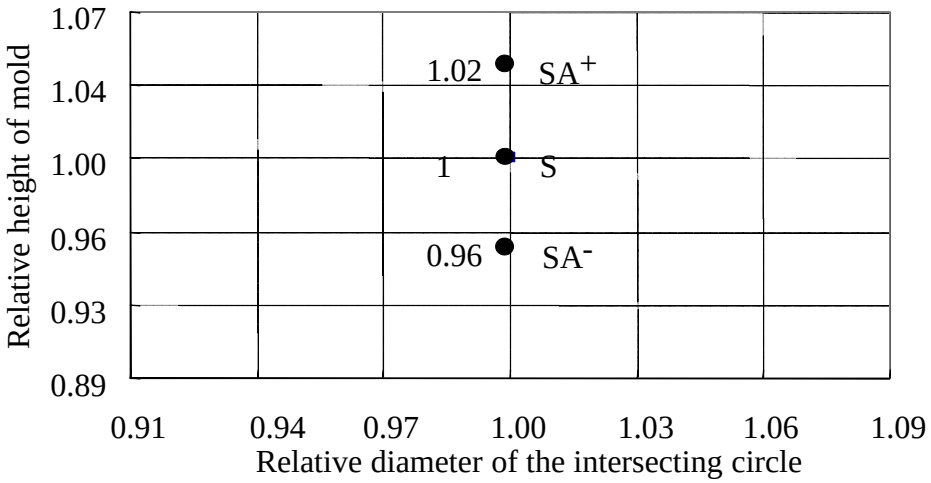

(b) Load max of SA group

Fig. 4.2 Clicking characteristic of SA group

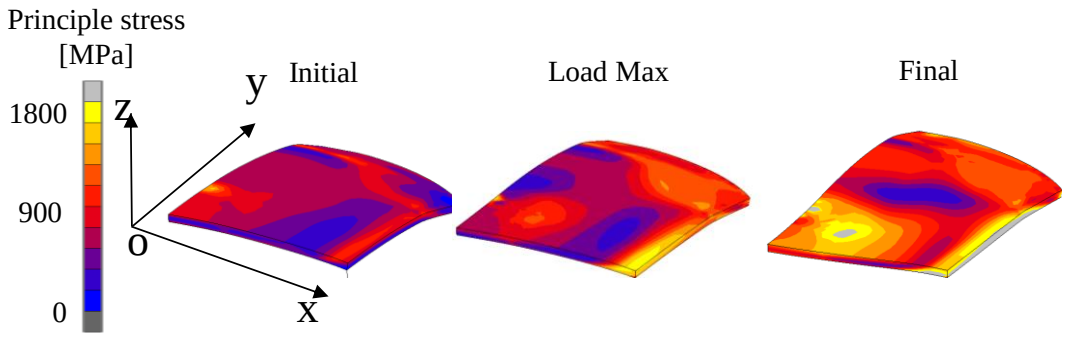

(a) Stress distribution of SA+ model

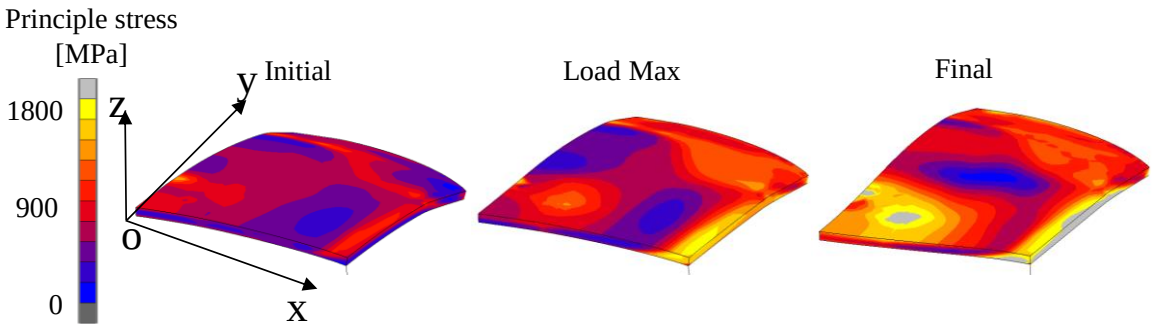

(b) Stress distribution of S model

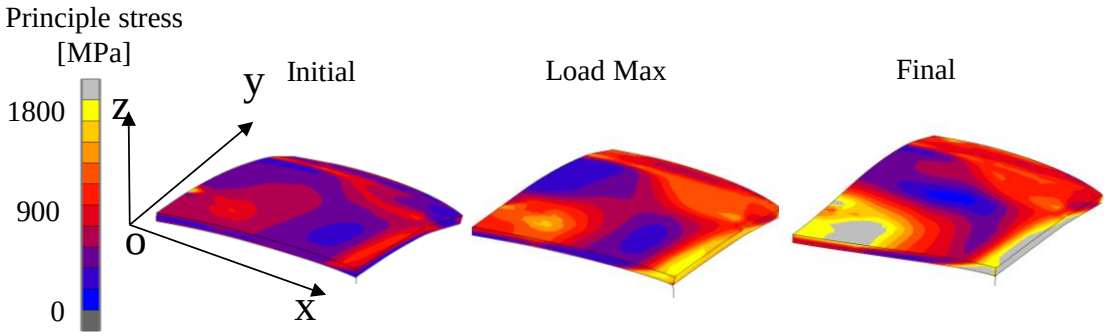

(c) Stress distribution of SA- model

Fig. 4.3 Stress distribution of SA group

The stress distribution of diaphragm of SA group in the clicking process is showed in Fig. 4.3, the stress distribution of every model contents three stress states. The stress distributions of oval type diaphragm are showing the same tendency as round type diaphragm. A high stress distribution is shown in the center of diaphragm and near the area that contact with the intersecting circle of mold. The only difference is the stresses

in the round edge of oval type diaphragm are small then the round type diaphragm, because the strength in the circumference direction of oval type diaphragm is weaker than that of the round type diaphragm. The stress distribution in the straight edge is bigger than the round edge area.

In the clicking process, the stress variation shows a same tendency as the round type diaphragm. From the Initial state to the Final state, the stress in the center of oval type diaphragm are becoming small, and the stress in both round edge and straight are becoming bigger. The model which has the bigger angle of cone has a larger stress distribution.

Since the oval type diaphragm is axial symmetry, it is necessary to evaluate the deformation mode at two axes. The nodes shown in Fig. 4.4 are used to present the deformation mode of oval type diaphragm.

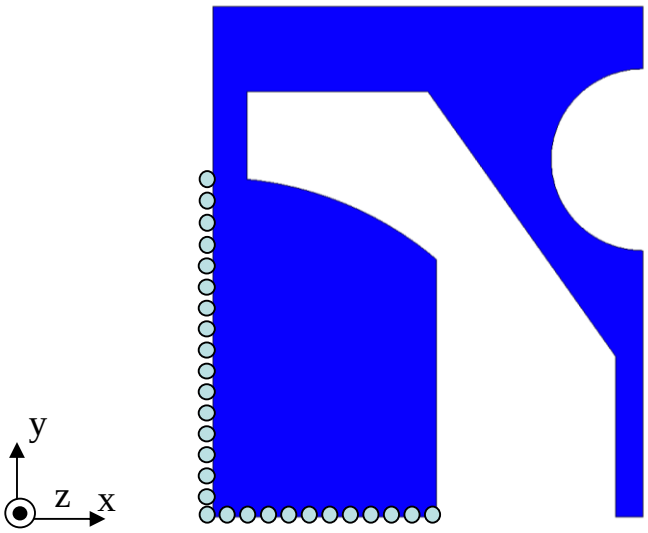

Fig. 4.4 Finite Element of oval type diaphragm

Fig. 4.5 shows the deformation mode of the Y axis symmetry of group SA, Fig. 4.6 shows the deformation mode of the X axis symmetry. The deformation shown in Fig. 4.5 is similar as round type diaphragm, the height of the model which has a bigger angle of cone is bigger.

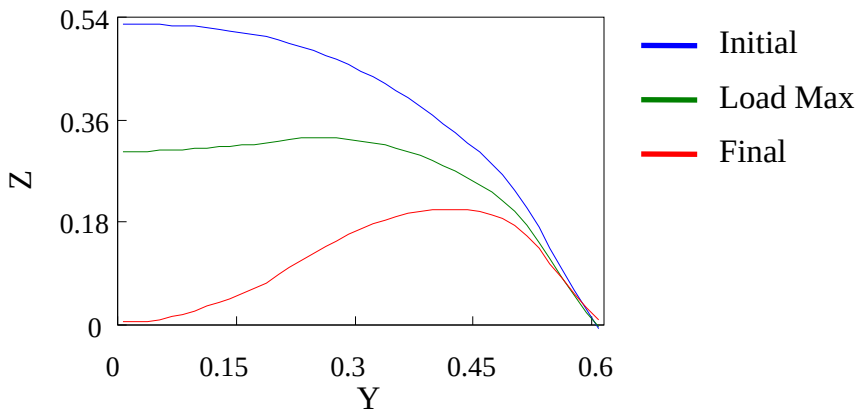

(a) Deformation mode of SA+ model

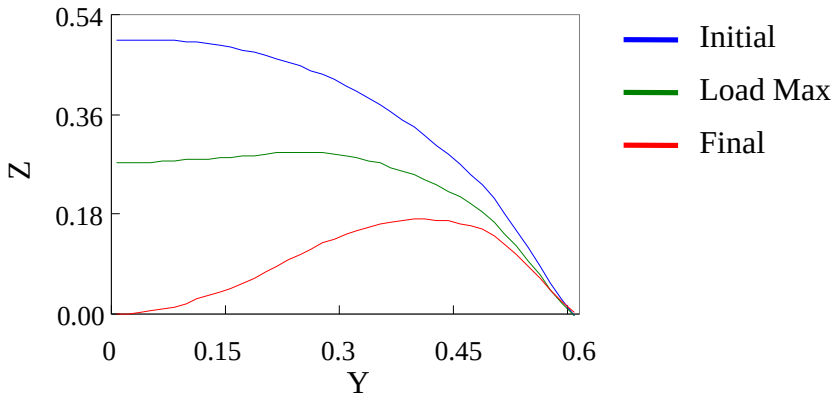

(b) Deformation mode of S model

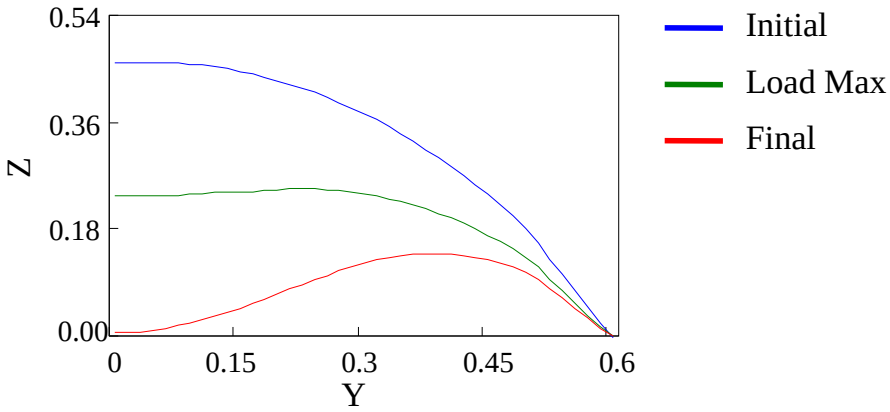

(c) Deformation mode of SA- model

Fig. 4.5 Deformation mode of SA model in Y axis

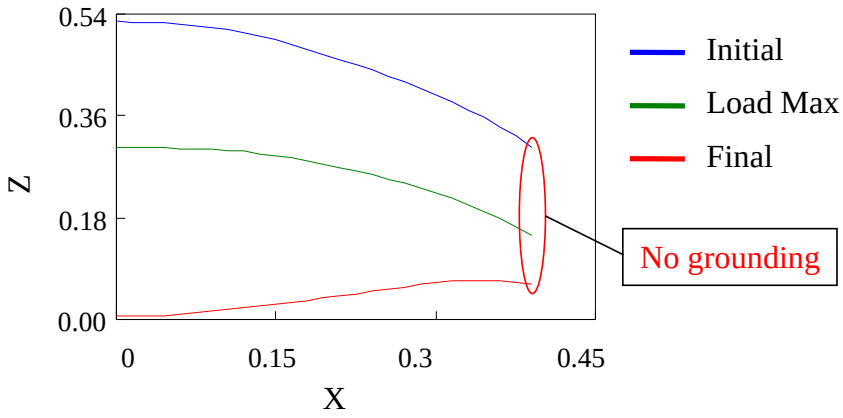

(a) Deformation mode of SA+ model

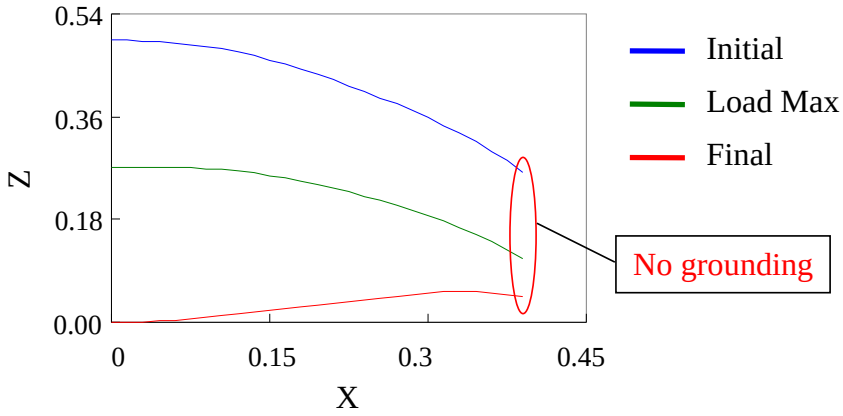

(b) Deformation mode of S model

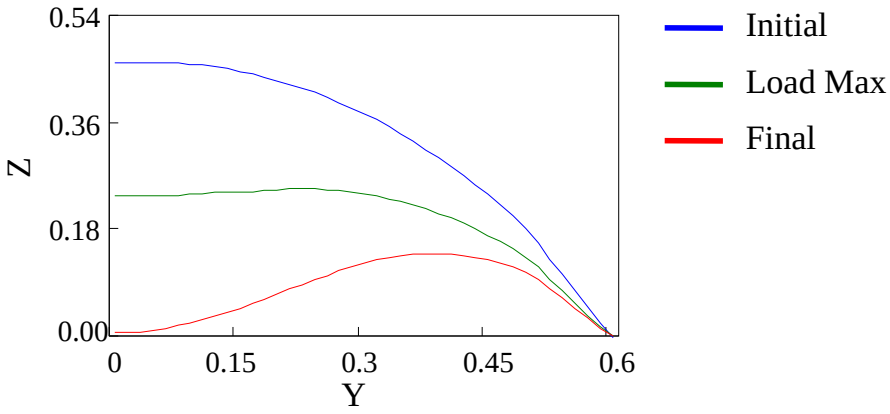

(c) Deformation mode of SA- model

Fig. 4.6 Deformation mode of SA model in Y axis

From Fig. 4.6 it can be seen that the deformation mode in the Y axis and X axis are much different from each other that the edge of in the X direction are not contacting with the ground, which is considered to be the reason why the height is much higher than the round type diaphragm, but the variation of Load max is almost the same as round type diaphragm.

4.1.3 Effect of design parameter B

The clicking ratio and the Load Max sorted out by the height of the mold and the radius of the intersecting circle are shown in Fig. 4.7. The clicking ratio increases with the radius of the intersecting circle, the Load max decreases with the increase of the radius of the intersecting circle.

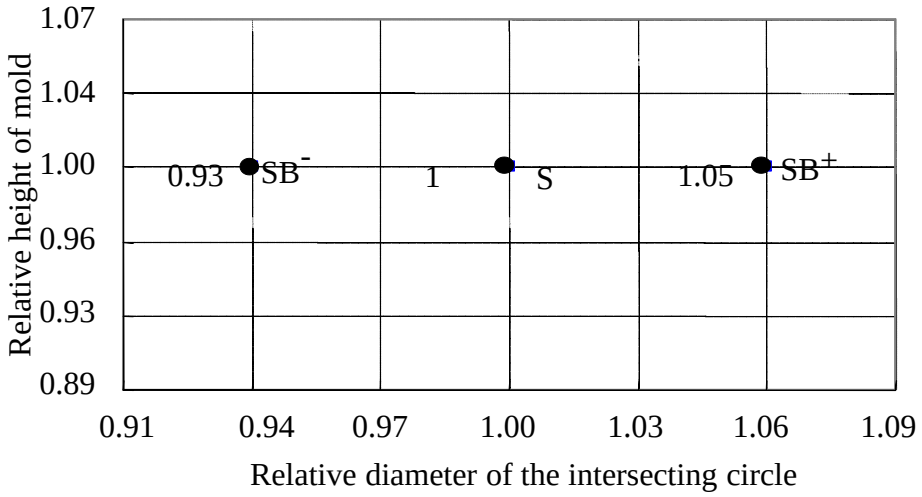

(a) Clicking ratio of SB group

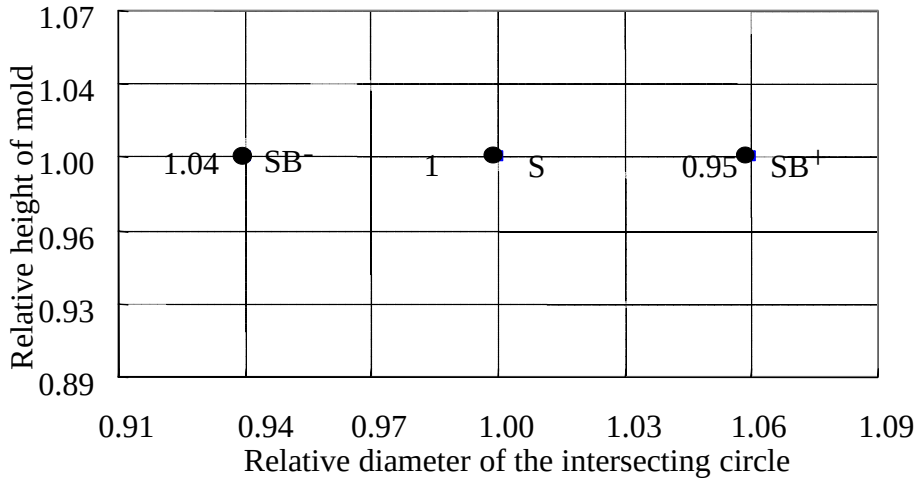

(b) Load max of SB group

Fig. 4.7 Clicking characteristic of SA group

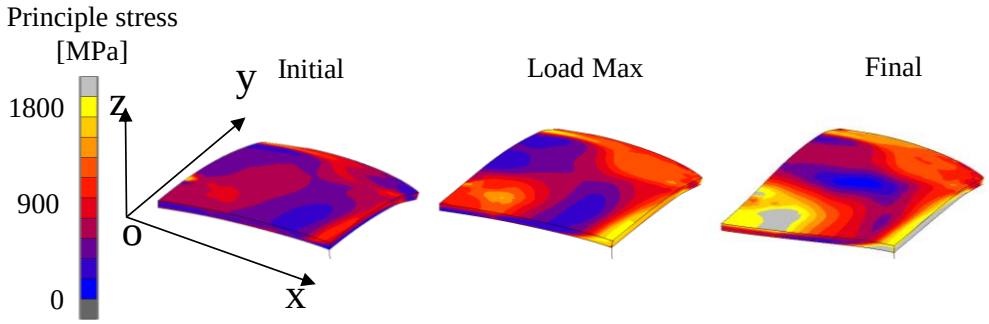

(a) Stress distribution of SB+ model

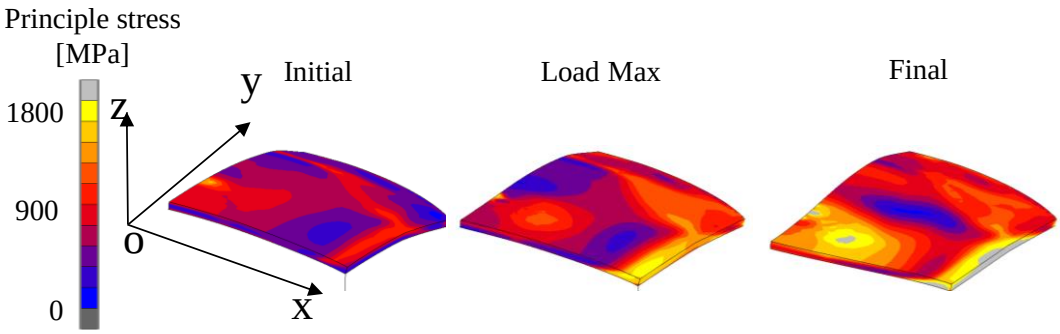

(b) Stress distribution of SB- model

Fig. 4.8 Stress distribution of SB group

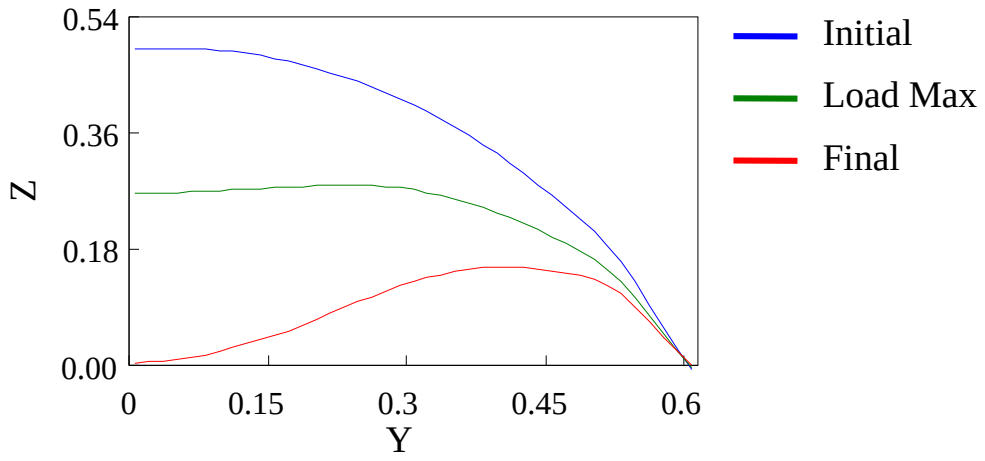

(a) Deformation mode of SB+ model

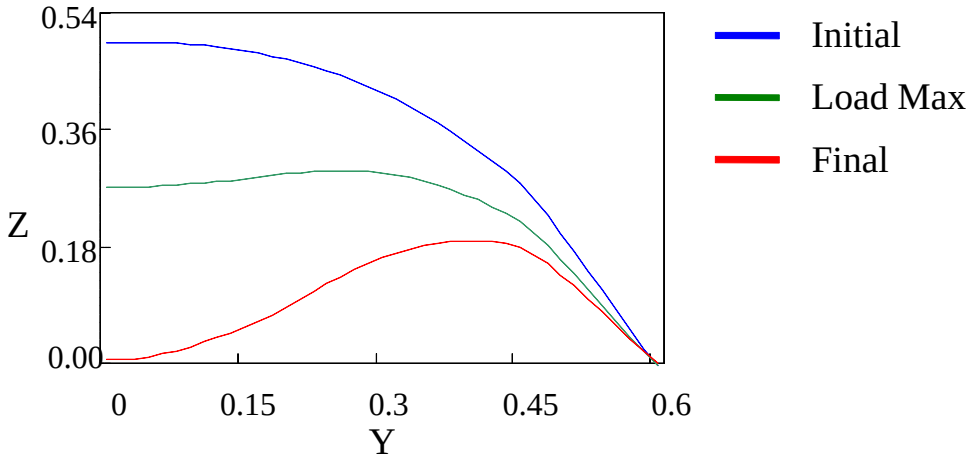

(b) Deformation mode of SB- model

Fig. 4.9 Deformation mode of SB model in Y axis

The stress distribution of oval type diaphragm of SB group is showed in Fig. 4.8. The stress distribution of SB group shows the same tendency as group SA. A high stress distribution is shown in the center of diaphragm and near the area that contacts with the intersecting circle of mold.

Fig. 4.9 shows the deformation mode of group SB along the Y axis, Fig 4.10 shows the deformation mode along the X axis. Comparing the clicking characteristic of round type diaphragm with oval type diaphragm, both Load max and clicking ratio of oval type diaphragm are smaller than that of round type diaphragm. From the deformation mode of oval type diaphragm, we can find that the edge in the X axis direction is not

contacting with the ground, which has been seen in both SA model and SB model. There are two reasons considerable that result in the low Load Max and Low clicking ratio of oval type diaphragm. One is the strength in the circumference direction of oval type diaphragm is weaker than that of the round type diaphragm, the other is the straight edge cannot contact with the ground.

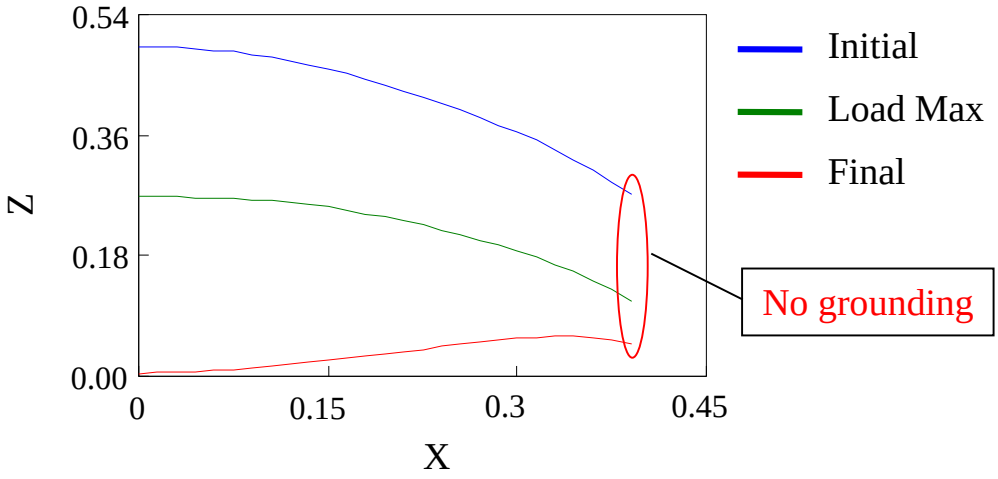

(a) Deformation mode of SB+ model

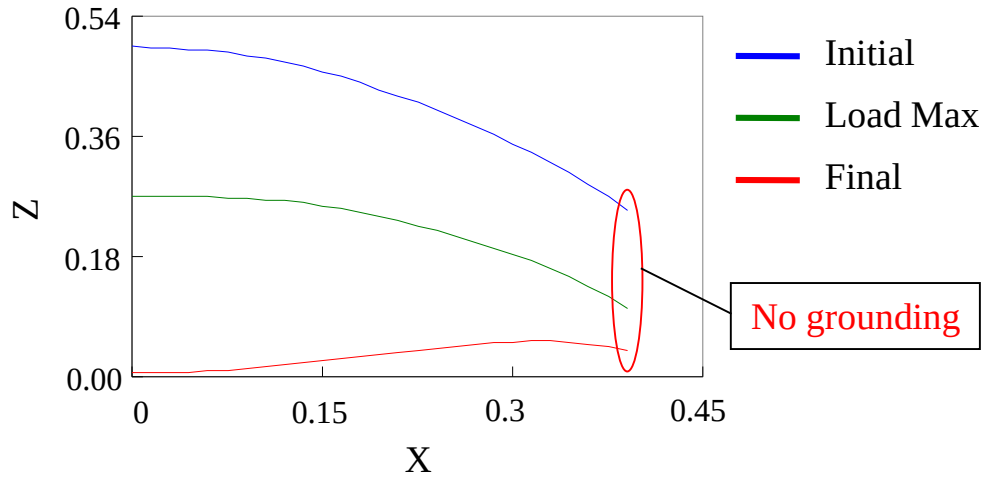

(b) Deformation mode of SB- model

Fig. 4.10 Deformation mode of SB model in X axis

4.2 Proposed Oval type diaphragm

4.2.1 New pattern of mold

Considering the two aspects affect the characteristic of oval type diaphragm, a new shape of mode is proposed to make up the shortage of conventional oval type diaphragm. The image of the mode is shown in Fig. 4.11.

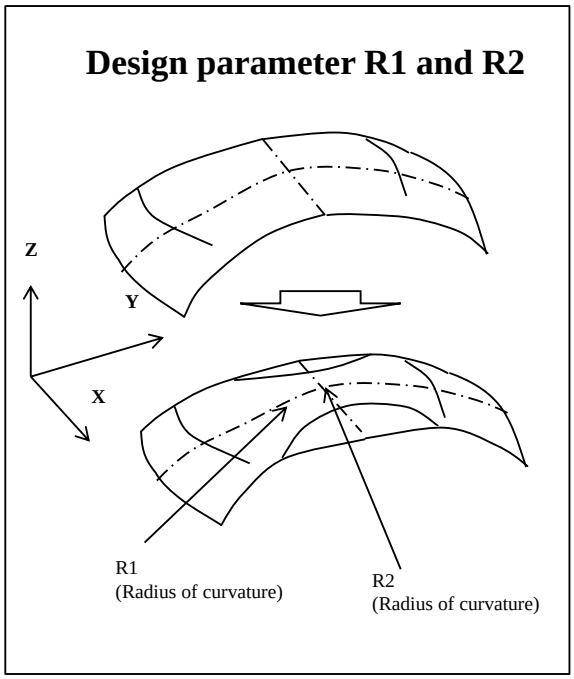

Fig. 4.11 The proposed mold for making oval type diaphragm

The conventional mold used to make the oval type diaphragm can be considered to be consisted of a spherical surface and cone. In order to strengthen the strength of diaphragm in the circumference direction, an incline is set onto the die, at the area corresponds to the straight edge of diaphragm. Punch is replaced by a surface made of two curvatures as Fig. 4.11 shows. The curvature R1 is kept bigger than R2, both of which are supposed to be smaller than the original curvature.

4.2.2 The numerical results of proposed oval type diaphragm

The two curvatures of the surface are varied based on the curvature of conventional standard model. In Fig. 4.12 the combination of design parameter R1 and R2 can be divided into three parts No grounding, center grounding and straight edge grounding by the deformation mode. The straight edge grounding part is defined as design space.

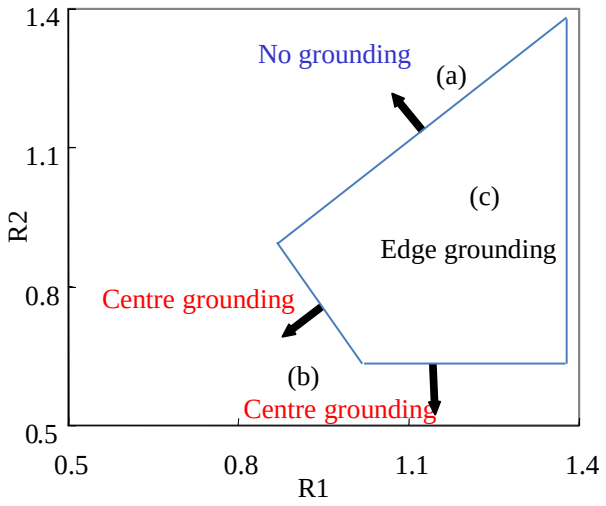

Fig. 4.12 The division of design space

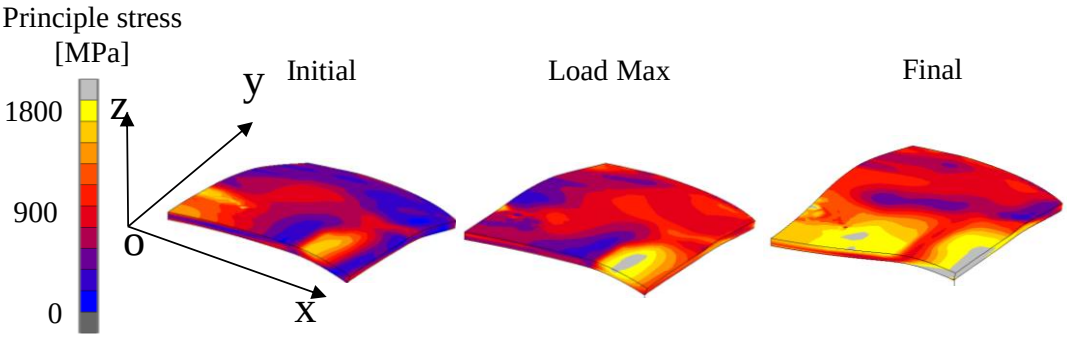

(a) Stress distribution

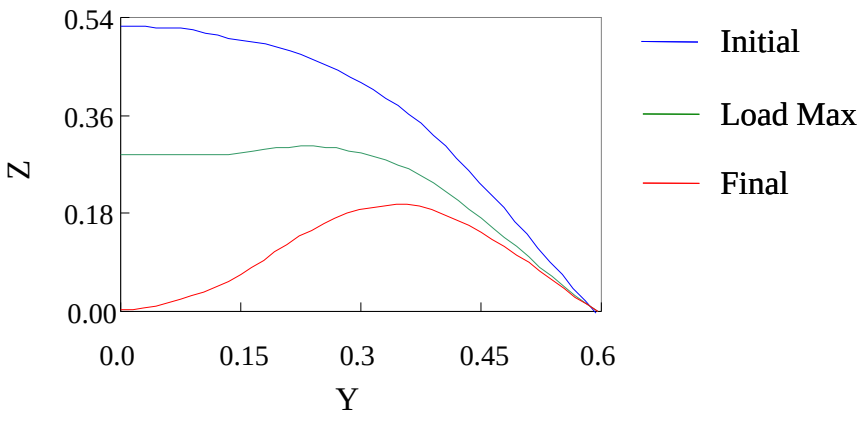

(b) Deformation mode in Y direction

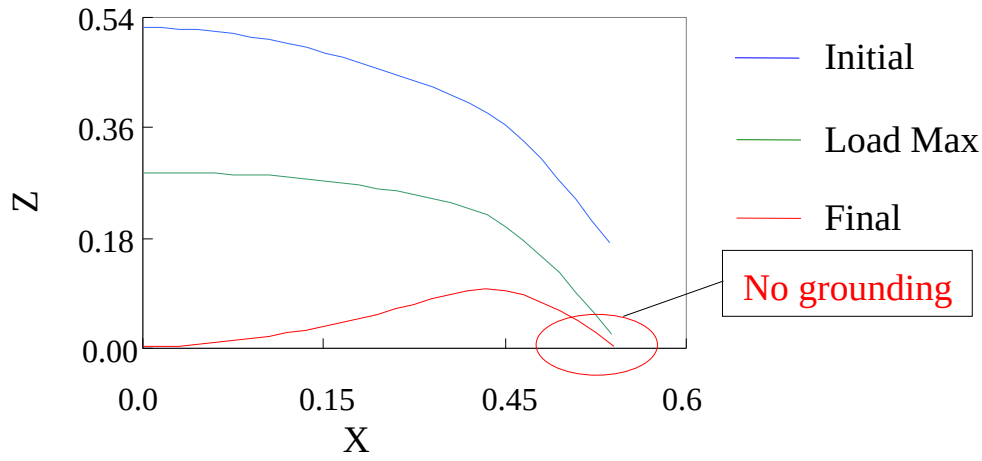

(c) Deformation mode in X direction

Fig. 4.13 The stress distribution and deformation mode of no grounding diaphragm

When the curvature R1 is smaller than or equal to R2, the straight edge will certainly not contact with the ground. This area is defined as No grounding as shown in Fig. 4.12. The model with the curvature of R1=R2=1.19 is illustrated as an example as shown in Fig. 4.13. In Fig. 4.13 (c) it can be seen that the straight edge is not contacting with the ground.

When the curvature of punch becomes too different from the curvature of die, the deformation mode of diaphragm will change. The model with the curvature of R1=0.94, R2=0.63 is taken as an example of Centre grounding mode area to show the characteristic of center grounding diaphragm in Fig. 4.14. It can be seen that in Fig. 4.14 (b), the deformation mode is different from the model of design space, the center of the diaphragm is contacting with the ground in Y direction. As diaphragm is used as a connection of electricity, the diaphragm with center grounding mode doesn't fits the job.

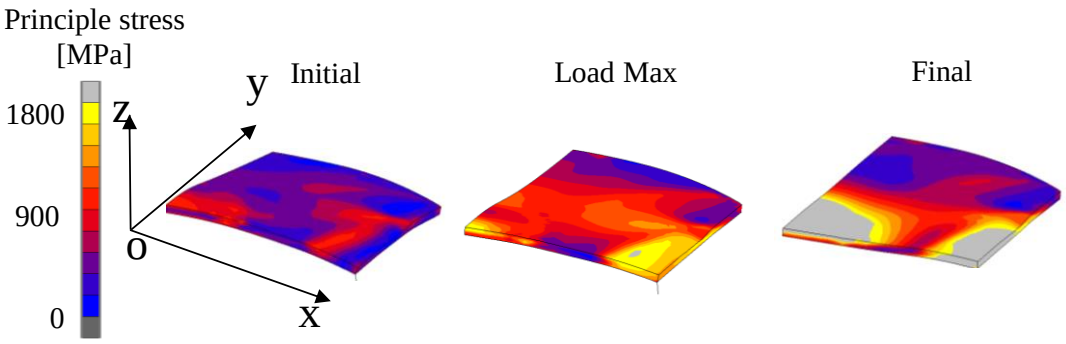

(a) Stress distribution

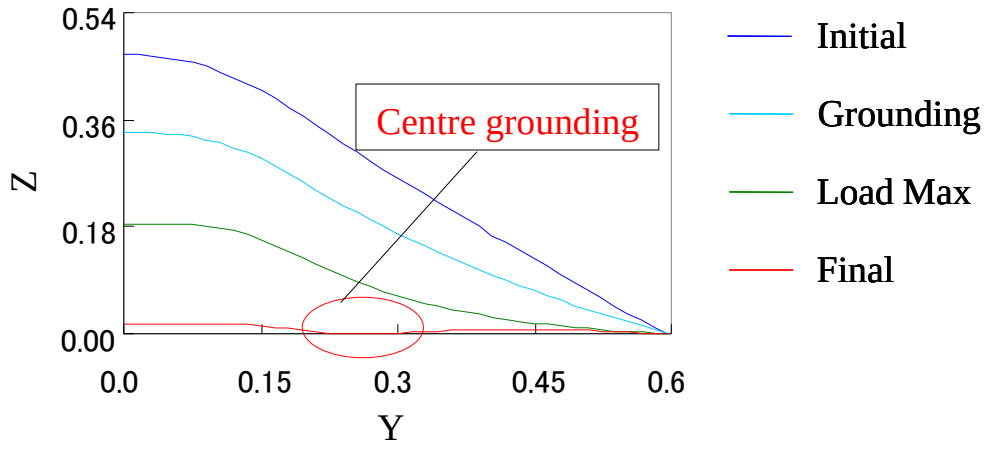

(b) Deformation mode in Y direction

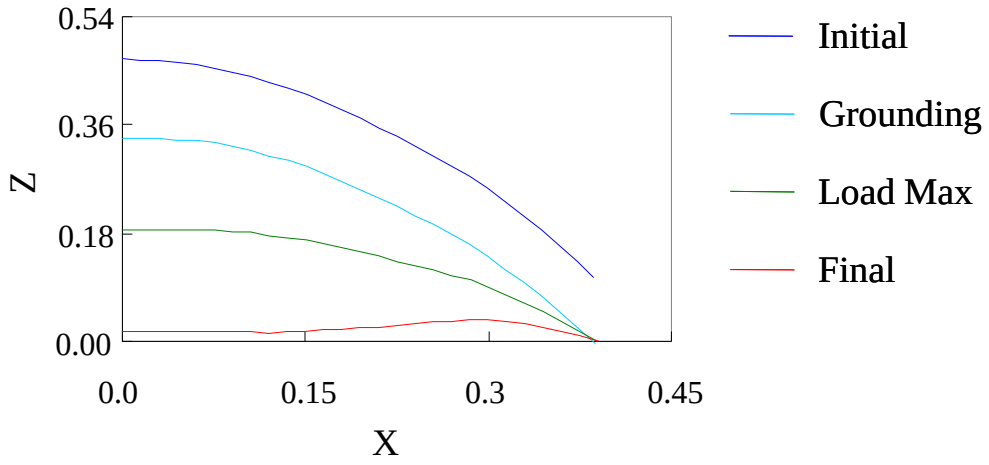

(c) Deformation mode in X direction

Fig. 4.14 The stress distribution and deformation mode of center grounding diaphragm

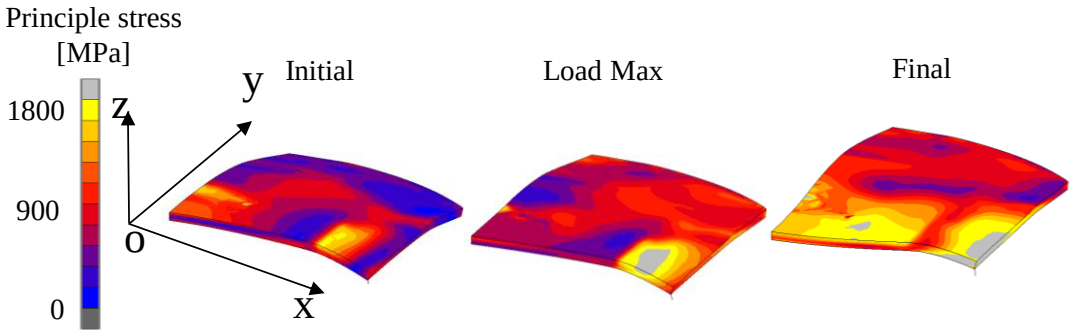

(a) Stress distribution of R2+ model

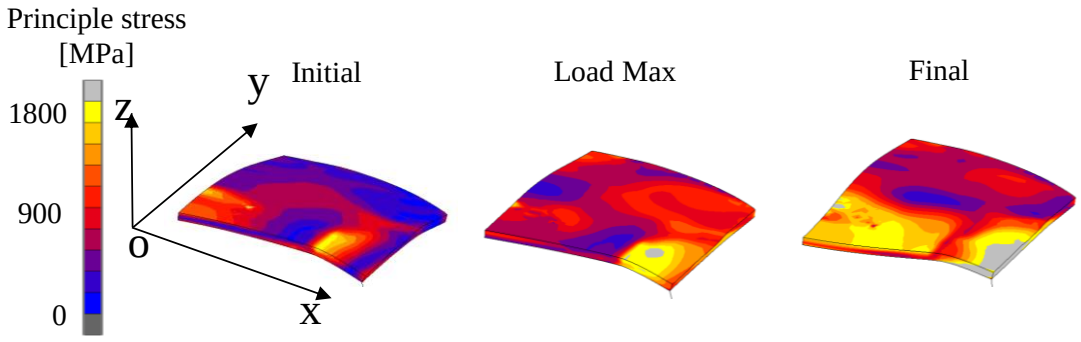

.

(b) Stress distributions of RS model

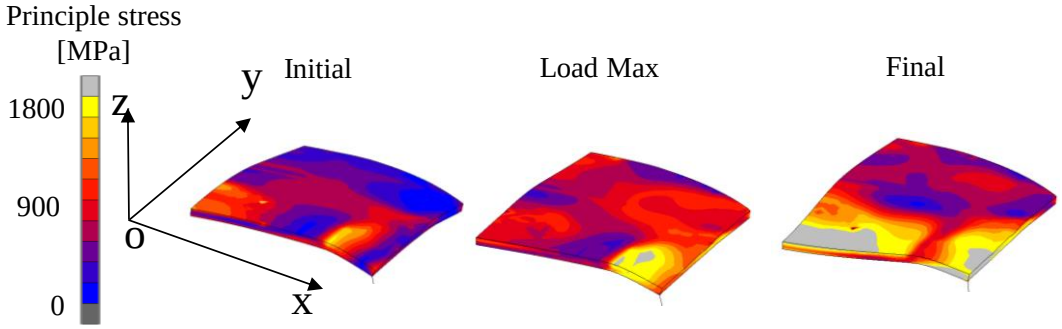

(c) Stress distribution of R2- model

Fig. 4.15 Stress distribution of R2 model group

When the combination of R1 and R2 is in a certain scope, the edge grounding will appear. R2 model group with three models: R2- (R1=1.25, R2=1.03), RS (R1=1.25, R2=1.09), R2+ (R1=1.25, R2=1.19) which were chosen as an example to illustrate the clicking characteristic of the model in the design space. The stress distributions of which were shown in Fig. 4.15, the deformation mode in Y axis in Fig. 4.16, the deformation mode in X axis in Fig. 4.17

As Fig. 4.15 shows, the stress distribution of every model in R2 group contains three stress states. The figure shows a significant difference in stress distribution comparing with conventional oval type diaphragm. Although the variation of the stress distribution at the center of the diaphragm showing a same tendency as the conventional oval type diaphragm, at the round edge area, a relatively bigger high stress distribution area is seen in the conventional oval type diaphragm, while the corresponding areas in the proposed diaphragm are showing a lower stress distribution.

The curvature of the renovated punch is smaller than that of the die; as a result the area of the circumference of diaphragm cannot be completely compressed by the mold

as the conventional diaphragm, while the center of the renovated diaphragm can be fully compressed. So the residual stress in the edge of diaphragm is smaller than the conventional one, but the stress distribution in the center of the diaphragm is showing the same tendency as conventional one.

Comparing the R2 group, the R2- model is found to have the smallest stress distribution in R2 model group and the R2+ model has the highest stress distribution in R2 model group. It is because when R1 is close to R2, the diaphragm is close to perfectly contact with the mold.

The variation of the stress distribution of R2 group shows the same tendency as conventional oval type diaphragm. The stress at the center of diaphragm shows a relatively higher stress distribution, and the round edge of diaphragm shows a small stress distribution, while the stress at the straight edge are bigger.

Fig. 4.16 and Fig. 4.17 show the deformation mode of model group R2, in the Y direction and X direction separately. Comparing with the conventional oval type diaphragm shown in Fig. 4.6 and Fig. 4.10, the light blue line express the state that the renovated diaphragm is contacting with the ground is shown in Fig. 4.17. By adding the new parameter to the mold, we succeed to make the straight edge of diaphragm contacting with the ground, as a result the Load max improved tremendously.

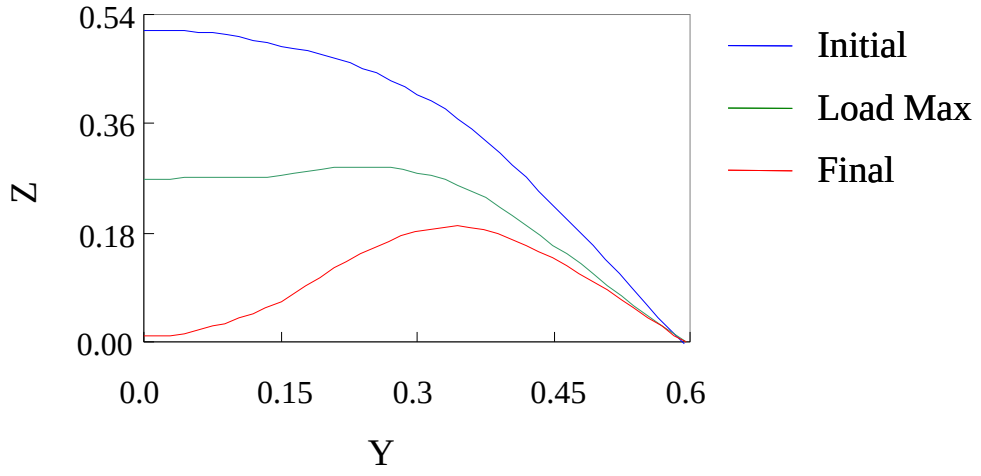

(a) Deformation of R2+ model

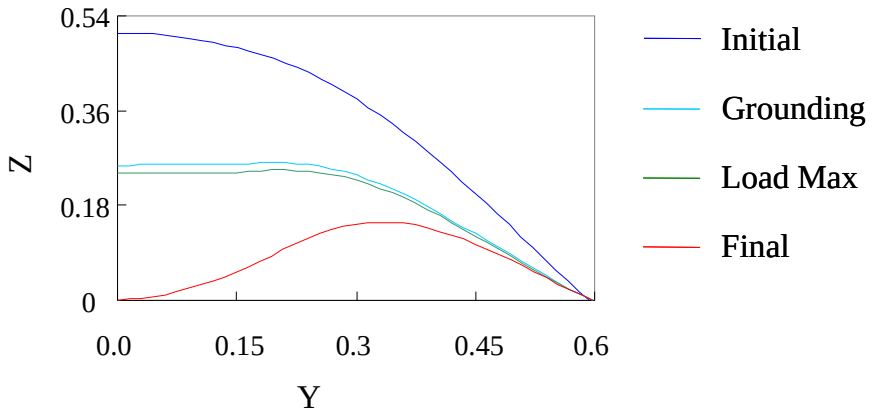

(b) Deformation mode of RS model

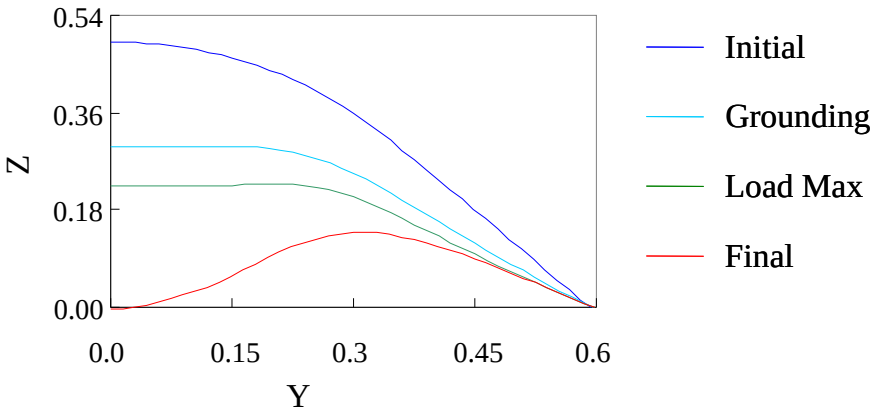

(c) Deformation of R2- model

Fig. 4.16 Deformation mode of R2 model in Y axis

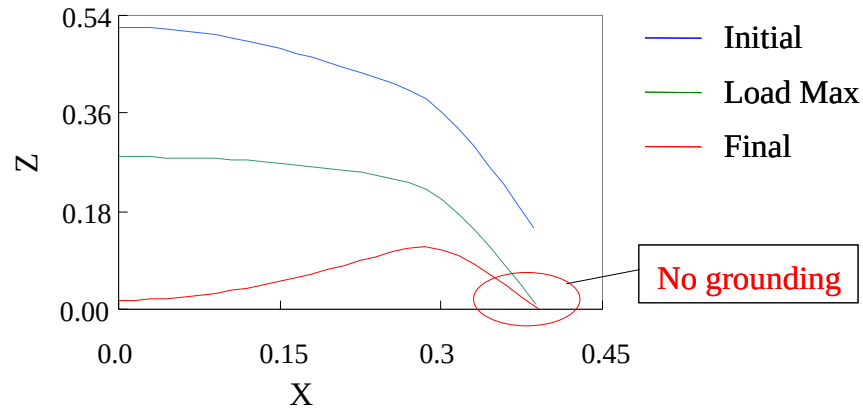

(a) Deformation of R2+ model

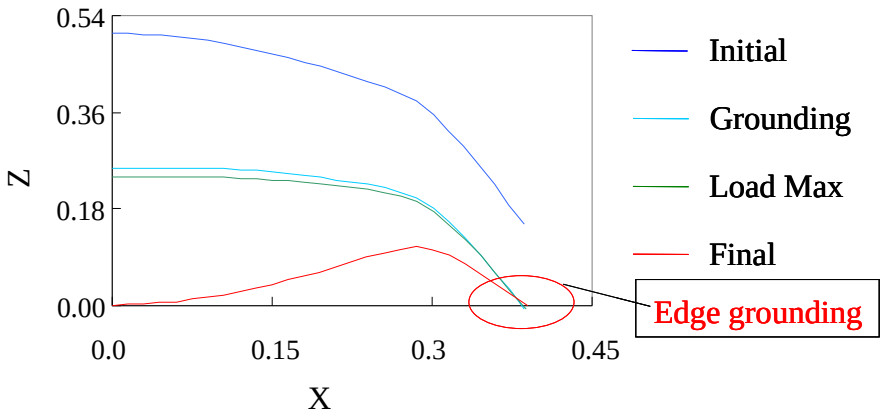

(b) Deformation mode of RS model

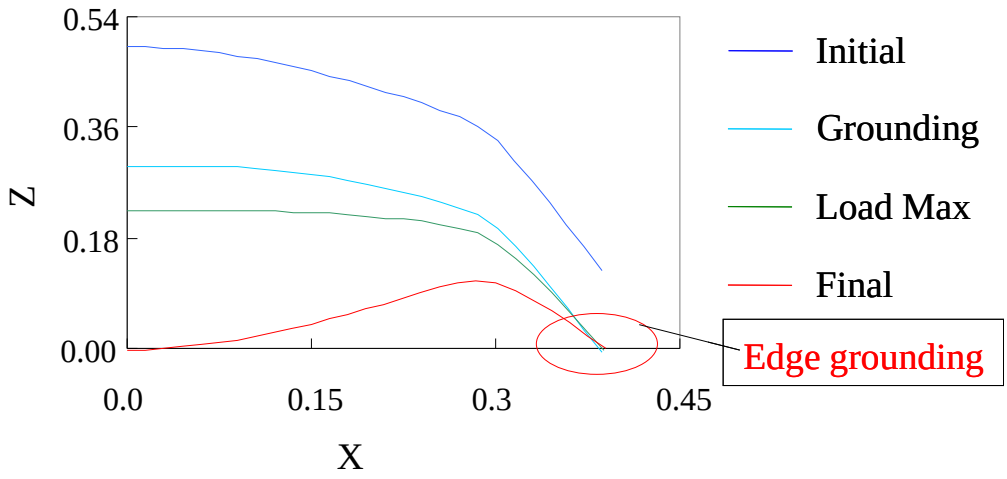

(c) Deformation mode of R2- model

Fig. 4.17 Deformation mode of R2 model in X axis

When R1 is close to R2, the diaphragm is close to a state of perfectly contacting with the mold in deforming of diaphragm, the residual stress in the center will be bigger as shown in Fig. 4.15. As a result, the center of R2+ is difficult to be deformed, load max is appeared the same time straight edge is contact with ground. For RS and R2- model load max appears after straight edge is contact with ground, which is shown in Fig. 4.17.

4.3 Design space of oval type diaphragm

Based on the numerical results, the functional design spaces are constructed as Fig. 4.18 and Fig. 4.19. The value in Fig. 4.18 and Fig. 4.19 are normalized based on old oval type diaphragm. The click characteristics are all over 1, which means they are all bigger than old type diaphragm. When certain levels of load max and click ratio are given, the designable area that satisfying the requirement can be estimated by considering the effects of parameters (R1, R2) on clicking characteristics. For example, if there is a requirement of a diaphragm with the click characteristics that load max is between 1.40 and 1.50, and click ratio is between 1.10 and 1.20, which can be found in Fig. 4.18 and Fig. 4.19. Then the designable area can be obtained by overlapping two contour plots as shown in Fig. 4.20. The area I that surrounded by the dot line is the area satisfying the requirement of click ratio. The area Ⅱ that surrounded by the solid line is the area satisfying the requirement of load max. The shadow area Ⅲ is the designable area satisfying this requirement. From these results, we can obtain the designable area by controlling the parameter R1 and R2 if the certain levels of load max and click ratio are given.

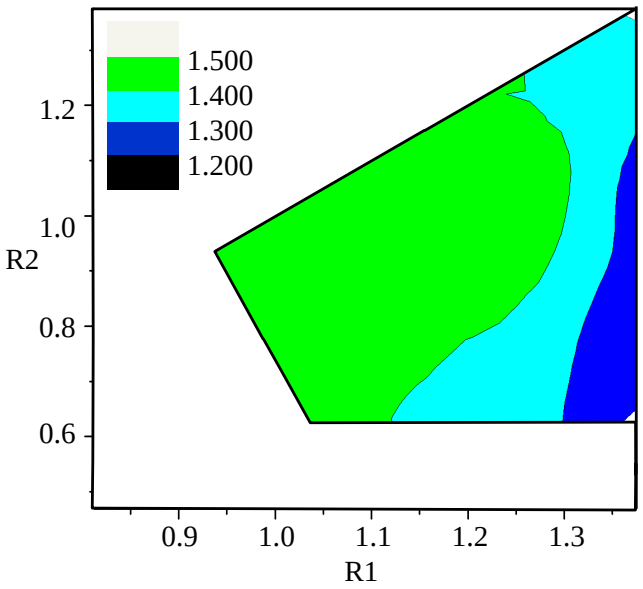

Fig. 4.18 Design space of Load max

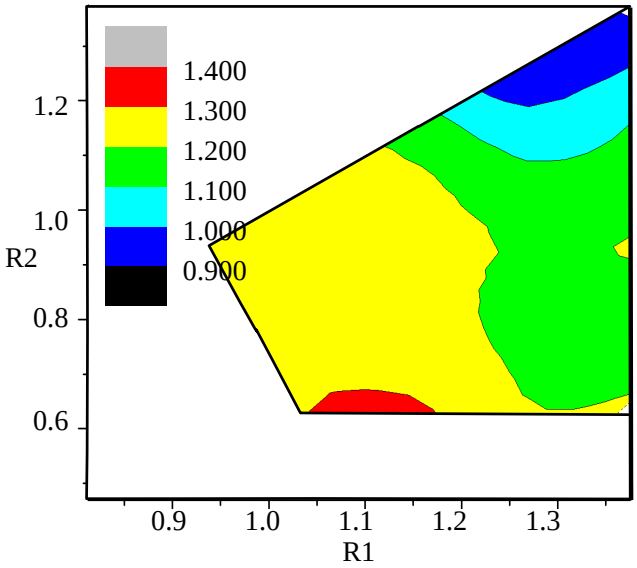

Fig. 4.19 Design space of click ratio

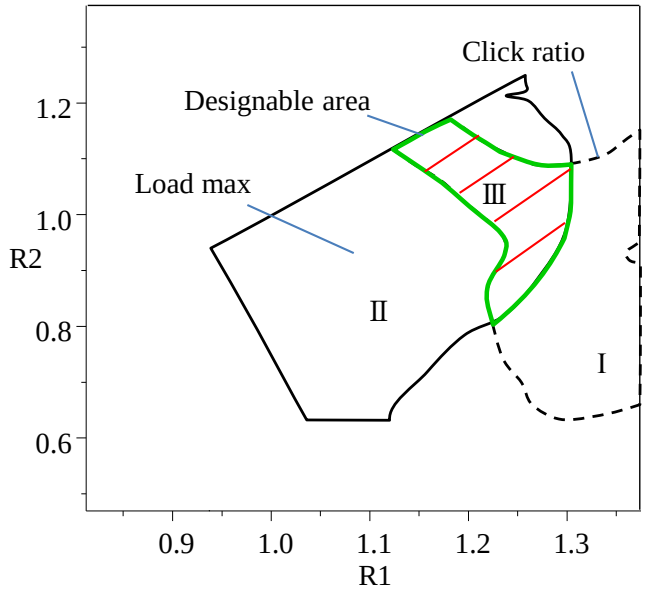

Fig. 4.20 Designable space of click characteristics

4.4 Summary

In this chapter, numerical simulation of oval type diaphragm is carried out. The click characteristics of oval type diaphragm are smaller than that of round type diaphragm. There are two reasons for this: One is the strength in the circumference direction of oval type diaphragm is weaker than that of the round type diaphragm, the other is the straight

edge cannot contact with the ground. In order to strengthen the strength of diaphragm in the circumference direction, an incline is set onto the die at the area corresponds to the straight edge of diaphragm. Punch is replaced by a surface made of two curvatures.

From simulation results, the combination of design parameter R1 and R2 can be divided into three parts No grounding, Centre grounding and Straight edge grounding by the deformation mode. The Straight edge grounding part is defined as design space. Based on the numerical results, the functional design spaces are constructed. The click characteristics of proposed oval type diaphragm are all bigger than old type diaphragm. Designable space under the condition of load max between 1.40 and 1.50, and click ratio between 1.10 and 1.20 has been constructed.

Chapter 5 Evaluation of fatigue reliability of diaphragm

5.1 Evaluation of stress history on diaphragm

Stress distribution of diaphragm various during click process, which will contribute to the fatigue of diaphragm. Examples of stress distribution's variation of model M (R1=1.38, R2=1.38) during the clicking process of the initial state and the state of contacting with ground are shown in Fig. 5.1 In general, point A is considered to be the dangerous point in old diaphragm, which has the highest residual stress, but for new type diaphragm, as the largest deformation occurs at point B in forming process,

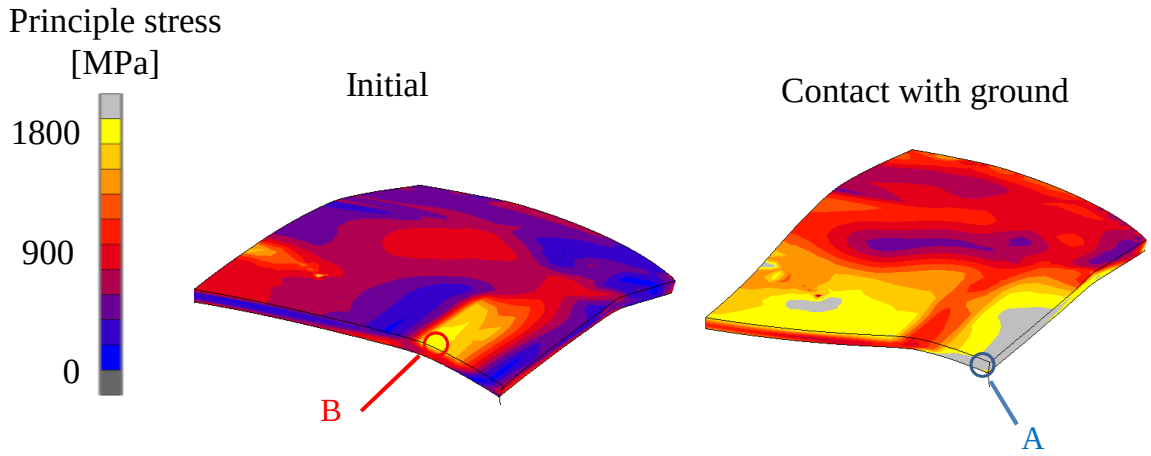

Fig. 5.1 Stress variation of model M (R1=1.38, R2=1.38)

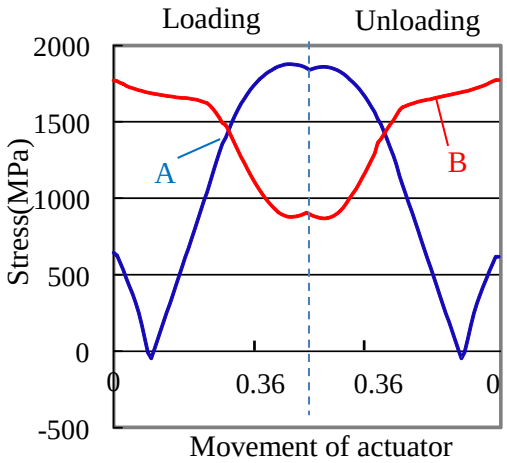

Fig. 5.2 Stress history of point A and point B of model M (R1=1.38, R2=1.38)

point B shows the highest residual stress at initial state. Point A has the biggest stress distribution when diaphragm is contact with ground. It is difficult to determine which the dangerous point is. When diaphragm is pressed, the stress history of point A and point B of model M are changing as shown in Fig. 5.2, which will be used in fatigue life evaluation.

5.2 Fatigue reliability evaluation of diaphragm

5.2.1 Drawing S-N curve

The fatigue tests of the stainless steel sheet in several directions against the rolling direction had been carried out. The S-N curve with a design margin considering the failure probabilities has been estimated with the computational system based on fatigue life at each stress level. The S-N curve considering failure probability in case of Θ=0 deg. is obtained as the experimental database in Fig. 5.3 based on the method mentioned in chapter 2.

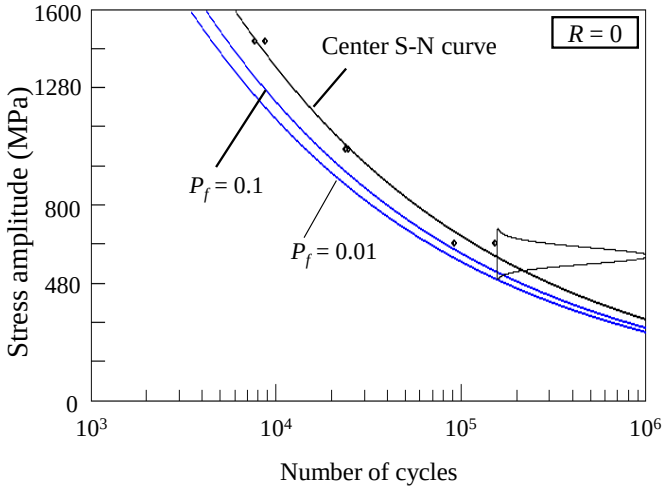

Fig. 5.3 S-N curve for each failure probability in case of Θ=0 deg.

5.2.2 Life estimation with Goodman diagram

From the numerical results, the stress history of every point on diaphragm can be obtained as shown in Fig. 5.2. The mean stress σ_m and the stress amplitude σ_a are calculated from Eq.2.6 and Eq.2.7. The point on diaphragm can be judged whether safe or not by plotting the couples of the stress amplitude and mean stress on the Goodman diagram comparing with the fatigue limit line, when the point plotted is under the

fatigue limit line, it is judged that the life is satisfied as safety. Fatigue limit diagram considering strength probability is obtained according to the process introduced in chapter 2. The couples of mean stress and stress amplitude of point A and point B of model M which is shown in Fig. 5.2, is taken as an example, to demonstrate the life estimation using Goodman diagram which is shown in Fig. 5.4.

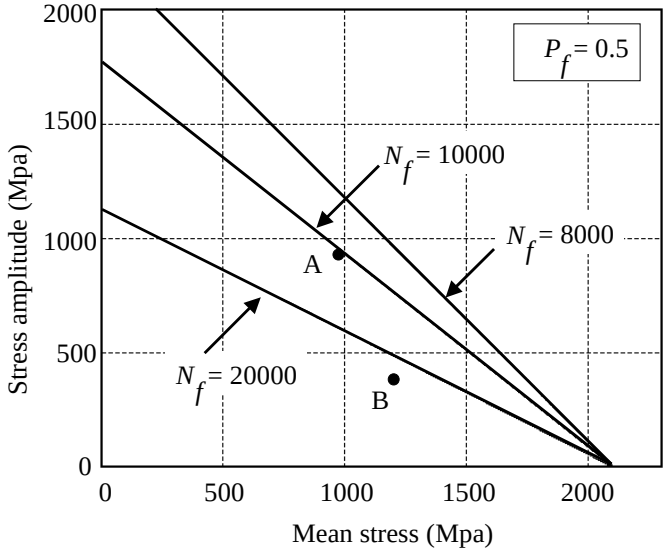

Fig.5.4 Goodman diagram for each number of cycles to failure in case of Θ=0 deg.

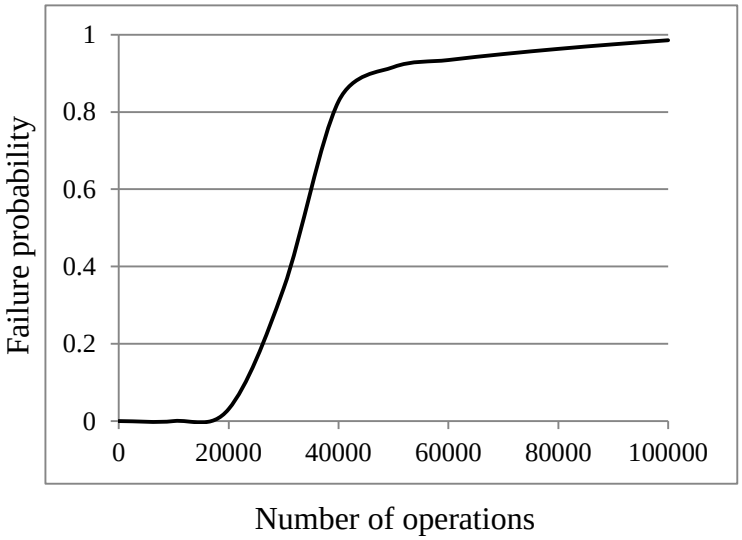

Fig. 5.5 Failure probability at point B

From Fig. 5.4, we can see point A is between the 20000Cycles line and 10000Cycles line, and point B is under the 20000Cycles line. As a result, point B is safer than point A

in the case of model M. Furthermore, fatigue life under certain probability also can be evaluated. Fig.5.5 shows the failure probability of point B under various fatigue life. It can be see that point B is distributed from 20000 to 100000 cycles.

5.3 Design space evaluation of failure probability

The fatigue reliability of the design space is evaluated using the method mentioned above. The results of the design space of probability of fatigue life under 10000Cycles of point A and point B are shown in Fig. 5.6 and 5.7.

In the case of point A, 80% of the design space's failure probability is over 0.1. The bigger failure probability is taken when R1 is between 1.1 and 1.3. The model of R1=1.03, R2= 0.81 has the smallest failure probability at point A under 10000 Cycles. In the case of point B, the failure probability of design space is under 0.08. The failure probability decreases when R1 or R2 is increasing. By comparing the failure probability of point A to point B, it is clear that the failure probability of point A is bigger than that of point B in a quite big area. But the failure probability of point B is bigger than point A at the area around the combination of R1=1.03 and R2=0.81. As a result, it is not possible to decide the fatigue life of which point is longer just from the initial residual stress or the stress state when diaphragm is contact with ground, and the dangerous point on every diaphragm is not the same area. It is necessary to evaluate the failure probability of every point on diaphragm to find out the most dangerous point. All the point on every diaphragm is evaluated using the same procedure. Fig. 5.8shows an example of failure probability under 10000 cycles of model M (R1=1.38, R2=1.38). The failure reliability of dangerous point all diaphragms are shown in Fig. 5.9. The failure probability of the dangerous point increases with the increase of R1, and changes very little when R2 is changed.

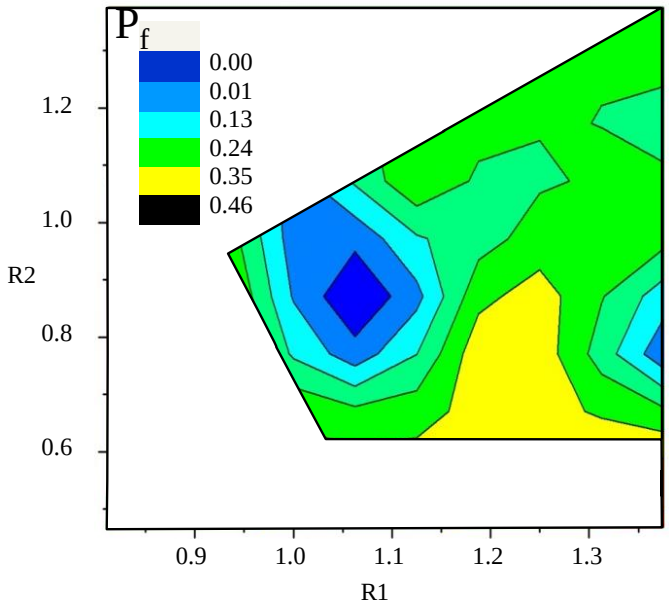

Fig. 5.6 Probability evaluation of design space on point A in case of $N_f=10^4$

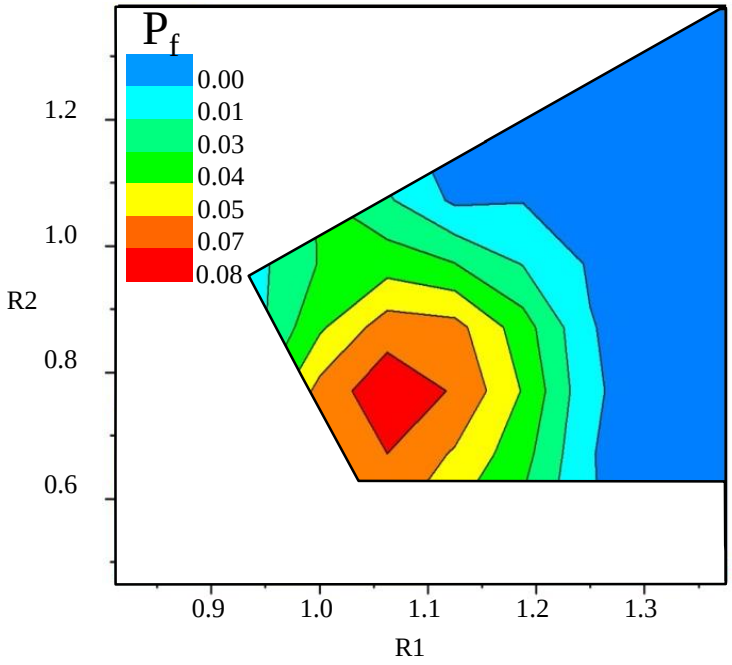

Fig. 5.7 Probability evaluation of design space on point B in case of $N_f=10^4$.

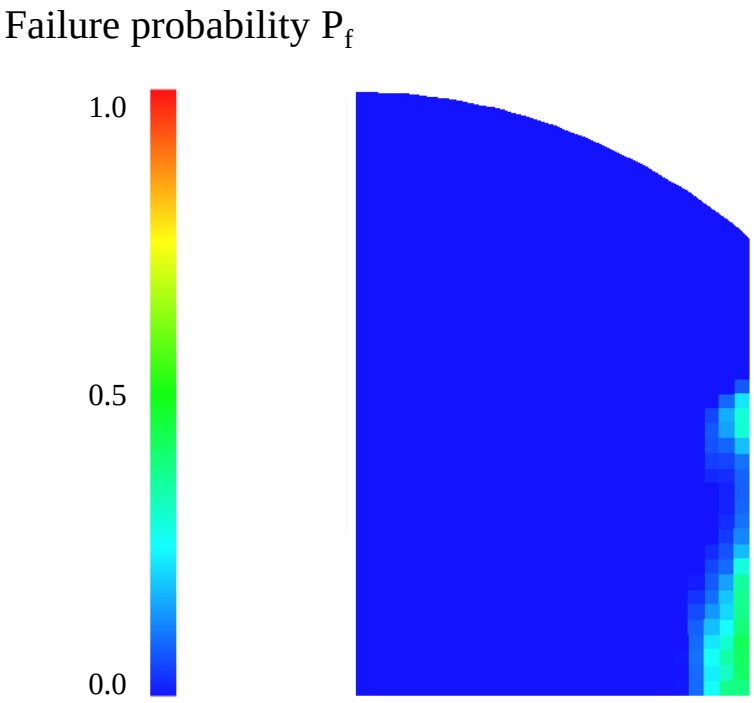

Fig. 5.8 Distribution of failure probability of model M (R1=1.38, R2=1.38)

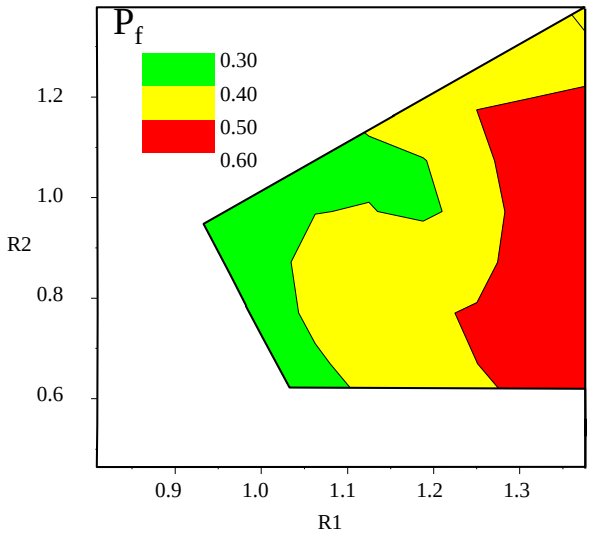

Fig. 5.9 Probability evaluation of design space on the dangerous point in case of $N_f=10^4$

5.4 Designable space considering clicking behavior and fatigue life

The designable space of diaphragm with click characteristics of load max between 1.10 and 1.20, click ratio between 1.40 and 1.50, has already been constructed as Fig.

4.20 in chapter 4. And the probability evaluation of the dangerous point in design space under 10000cycles is shown in Fig. 5.8. By combining these two data, designable space considering clicking behavior and fatigue life can be obtained. The designable space of failure probability under 0.4, 0.5, and 0.6 are shown in Fig. 5.9, 5.10 and 5.11, separately.

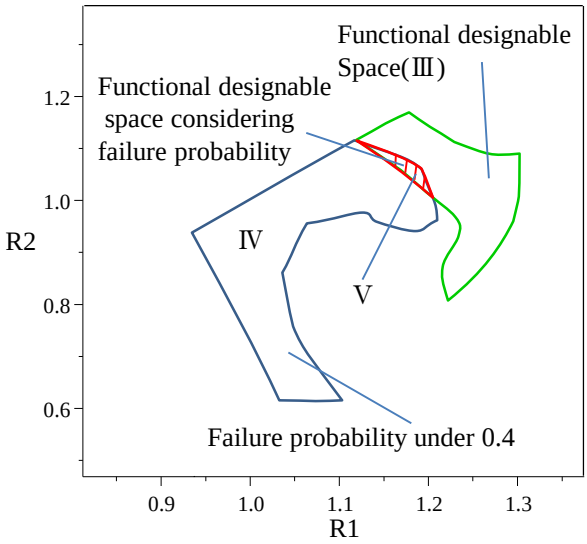

Fig. 5.9 Designable space (load max between 1.10 and 1.20, click ratio between 1.40 and 1.50) with failure probability under 0.4 in the case of $N_f=10^4$

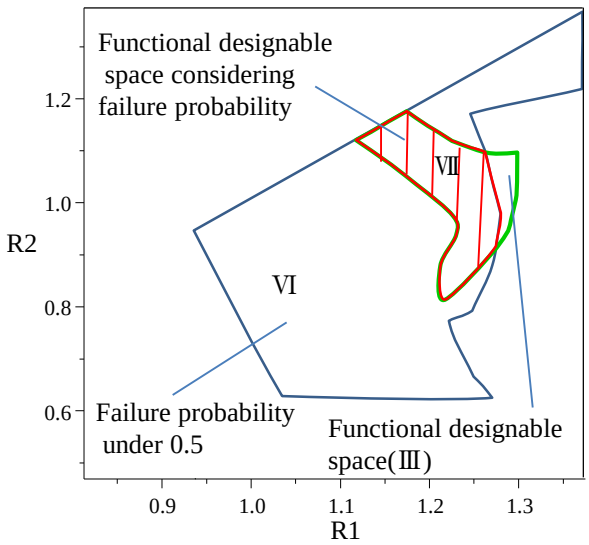

Fig. 5.10 Designable space (load max between 1.10 and 1.20, click ratio between 1.40 and 1.50) with failure probability under 0.5 in the case of $N_f=10^4$

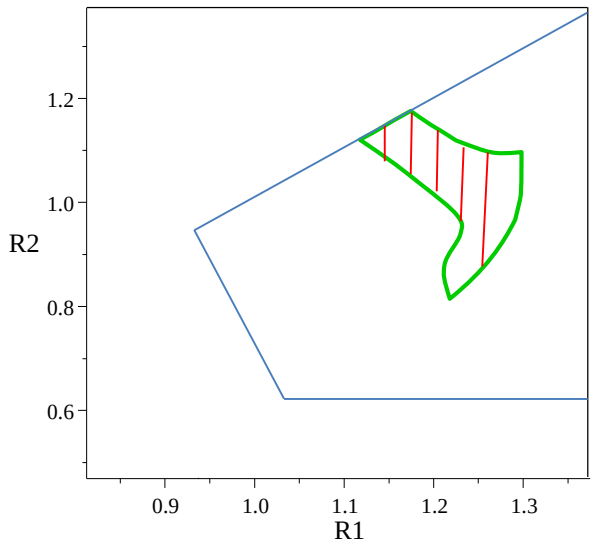

Fig. 5.11 Designable space (load max between 1.10 and 1.20, click ratio between 1.40 and 1.50) with failure probability under 0.6 in the case of $N_f=10^4$

In Fig. 5.9, the shadow area Ⅴ is the designable space of failure probability under 0.4 which is obtained by comparing the area Ⅲ (functional designable space) and the area Ⅳ (failure probability under 0.4). In the same way, the designable space with failure probability under 0.5 of the area Ⅶ is obtained by comparing Ⅲ (the functional design space) and the area Ⅵ (the failure probability under 0.5). As the failure probability of diaphragm in functional designable space is all under 0.6, the designable space of failure probability under 0.6 is the area Ⅲ. When both click characteristics and fatigue life of diaphragm is required, the designable space with different failure probability can be obtained. And then diaphragms satisfy the requirement can be designed using the design parameters corresponding to the designable space. If only click characteristics is required, the most optimum diaphragm can be obtained by comparing with fatigue reliability design space. By using the designable space, the design process can be automatically can effectively.

5.5 Conclusion

Evaluation of the fatigue reliability of oval type diaphragm is carried out based on the stress history obtained from numerical result of click process. The point with maximum stress was able to be obtained from numerical analysis, but evaluation of fatigue life only considering the maximum stress is not possible. In this study, both mean stress effect and failure probability is evaluated based on fatigue limit diagram considering

failure probability. Furthermore, the relationship between design parameter and fatigue reliability is evaluated, based on which designable space considering failure probability has been constructed. It is considered that design period and cost can be cut down by using designable space method considering failure probability.

Chapter 6 Summary

In this paper, in order to provide a convenient approach for designing diaphragm, designable space method is proposed which considers both click characteristics and fatigue reliability of diaphragm.

Electric component as diaphragm values less alone, but the correct operation of it is the basic requirement for the overall operation of electric devices. In designing diaphragm, prototypes are usually used for testing the click characteristics and fatigue life. However, this costs much and the time period for design is long, which are the problem facing in reduce design costs. It is badly needed to reduce design period especially for electric component as diaphragm. A new design method that can reduce the design period is needed.

The purpose of this paper is to propose a method of designable space considering failure probability for designing diaphragm. The mechanical behavior of click process is also discussed. And then the application of designable space considering failure probability is presented. The summary of this paper is as follows.

Chapter 1 introduces the application of momentary push button switch and diaphragm used in it is introduced. Then, two important parameters in designing diaphragm, click characteristics and fatigue life, are introduced. And then, the current situation of designing switch and the problem in designing switch are introduced. Finally, the purpose of this study and the introduction of each chapter are introduced.

In chapter 2, manufacturing process of making diaphragm is introduced, and then design parameter for designing diaphragm is discussed. In designing diaphragm that satisfies certain requirement, the geometry of punch and die are usually determined based on experience, which is usually take many times to get to the required click characteristics. Therefore, making prototypes based on experience to design diaphragm are very time consuming and costly. Regarding to this problems, designable space considering fatigue reliability is proposed. For fatigue evaluation, S-N curve and fatigue strength distribution is very important, the method of determinate S-N proposed by Zako et al. is used. The process of making designable space is as follows.

Firstly, make designable space of diaphragm. Finite element analysis is used to evaluate the click characteristics of diaphragm according to the forming process and click process. By changing the design parameters, the relationship between design parameters and click characteristics are obtained, which is defined as design space. When certain click characteristics is requirement, the area satisfy the requirements is

called designable space.

Secondly, evaluate the fatigue reliability of diaphragm. P-S-N curve and fatigue limit diagram considering fatigue strength probability can be obtained based on experimental data. Comparing stress status of every point on diaphragm to fatigue limit diagram, the fatigue reliability of all the point on diaphragm can be obtained.

Thirdly, construct designable space considering failure probability. The failure probability of design space under various fatigue cycles can be evaluated according to the evaluation results of fatigue reliability of diaphragm in design space. The designable space considering failure probability can be obtained by comparing the failure probability design space with designable space of click characteristics.

Chapter 3 introduces the process of making functional design space of round diaphragm. Numerical analysis is carried out according to the manufacturing and pressing process. From the numerical results of round type diaphragm, it is clear that the residual stress and deformation mode affects click characteristics of diaphragm. Diaphragm with local deformation mode shows small load max and big click ratio. Global deformation is contrary to local deformation mode. Based on the numerical analysis, the relationship between design parameter and click characteristics is evaluated, and then the functional design space is constructed.

Chapter 4 introduces the functional design space of oval type diaphragm. Simulation of oval type diaphragm is carried out the same as round type diaphragm. The click characteristics of oval type diaphragm turned out to be smaller than round type diaphragm, due to the weak strength in the circumference direction. In order to improve the click characteristics, new oval type diaphragm is proposed. From simulation results, the combination of design parameter R1 and R2 can be divided into three parts No grounding, Centre grounding and Straight edge grounding by the deformation mode. The straight edge grounding part is defined as design space. Functional design space of new oval type diaphragm is constructed based on the results of numerical analysis. The click characteristics of new oval type diaphragm are bigger than conventional oval diaphragm.

Chapter 5 introduces the evaluation of fatigue reliability of diaphragm. Stress history of every point on diaphragm has been evaluated based on rain flow counting method. The fatigue reliability of the highest stress of A (when diaphragm is contacting with ground) and B (at initial state) on diaphragm are evaluated, from which it is clear that the point with highest stress is not surely the most dangerous point. Therefore, the fatigue reliability of all the point on diaphragm is evaluated. The failure probability design space is constructed based on the failure probability of most dangerous point on

diaphragm. Comparing the designable space under certain requirement with the failure probability design space, designable space considering failure probability is obtained. When both click characteristics and fatigue life of diaphragm is required, the designable space with different failure probability can be obtained. And then diaphragms satisfy the requirement can be designed using the design parameters corresponding to the designable space. If only click characteristics is required, the most optimum diaphragm can be obtained by comparing with fatigue reliability design space. It is considered that design period and cost can be cut down by using designable space method considering failure probability.

Chapter 6 summarizes the five chapters above.

Reference

1. Home page of Panasonic Industrial Devices, http://industrial.panasonic.com/ww/index_e.html

2. Jon H. L. and Albert H. J., Nonlinear Analysis of Elastomeric Keyboard Domes, Transaction of American Society of Mechanical Engineers Series E Journal of Applied Mechanics, vol.56, (1989), pp.751-755.

3. Hirashima, T. and Zako, M., Development of Design System for Keyboard Rubber Diaphragm, Journal of the Society of Materials Science, Japan 51(10)(2002), pp. 1141-1146.

4. Hirashima, T. and Zako, M., Analysis and Design of Keyboard Rubber Diaphragms, the Japan Society of Mechanical Engineers, vol. 77, No.3 (2002), pp.61-62.

5. Suzuki, H., Takahashi, S., Sagawa, D., Nishino, S., Nakamura, M., and Tomitsuka, T., Influences of residual stress on click characteristic of Metal Dome for Mobile Phones, Ibaraki district conference 2002, (2002-08), pp.167-168.

6. Tomitsuka, T., Ajimura, S., Kawahira, T. and Noguchi, Y., Metal Dome for a Mobile, Communication Terminal Equipment, Fujikura Technical Journal, No.104 (2003), pp.42-46.

7. Ralph I. Stephens, Ali Fatemi, Robert R. Stephens, Henry O., Fuchs Metal Fatigue in Engineering second edition, Wiley-Interscience, (Oct. 2000).

8. Murray, JAH (Ed), A New English Dictionary on Historical Principles. Vol. 4. Clarendon Press, Oxford, (1901).

9. Pook, L.P, The Role of Crack Growth in Metal Fatigue. Metals Society, London, (1983).

10. 'Wöhler`s Experiments on the Strength of Metals', Engineering, (August 23, 1967), pp.160.

11. Ewing, J.A., Humphrey, J.C., The fracture of metals under rapid alternations of stress. Phil. Trans. Roy. Soc. London, A200: (1903), pp. 241–250.

12. Pook, L.P., Microscopic examination of fatigue fracture surfaces. Laboratory Test Note LTN 135. Hawker Siddeley Aviation, Coventry, (1960).

13. Pook, L.P., Quantitative fractography. Examples showing information derived from aircraft components after fatigue testing. Laboratory Test Note LTN 212. Hawker Siddeley Aviation, Coventry,(1962).

14. Pook, LP., Brittle fracture of structural materials having a high strength weight ratio, PhD thesis, University of Strathclyde, (1968).

15. Bathias, C., There is no infinite fatigue life in metallic materials, Fatigue & Fracture of Engineering Materials & Structures, 22 (1999), pp .559-565.

16. Miller, K. J., O'dnnell, W. J., The fatigue limit and its elimination, Fatigue & Fracture of Engineering Materials & Structures, 22 (1999), pp. 545-557.

17. Nishijima, S., Kanazawa, K., Stepwise S-N curve and fish-eye failure in gigacycle fatigue, Fatigue & Fracture of Engineering Materials & Structures, 22 (1999), pp. 601-607.

18. Bathias, C, An understanding of the gigacycle fatigue of metals. In: Materials Science for the 21st Century. The Society of Materials Science, Kyoto, Japan, Vol. A, (2001), pp. 12–18.

19. Stanzl-Tschegg, S (Ed), Fatigue in the very high cycle regime (Vienna Conference). Fatigue Fract. Engng. Mater. Struct. 25: (. 2002), pp. 725–896.

20. Tatsuo, S., Atsushi, S., Publication of the Second Edition of"Standard Evaluation Method of Fatigue Reliability for Materials" [Standard Regression Method of S-N Curves], The Society of Materials Science, Japan, (Vol. 54), No. 1, (2005), pp. 37-43.

21. Satoshi, N., Statistical Analysis of Small Sample Fatigue Data, Transactions of the Japan Society of Mechanical Engineers, (Vol.A), No. 46, (1980), pp. 1303-1313.

22. Shinsuke, S., Hiroyuki, O., Koji, S., Reliability Analysis On S-N Evaluation Model', The Society of Materials Science, Japan, (Vol. 42), No.483, (Dec. 1993), pp.1394-1399.

23. JSME Standard Method of Statistical Fatigue Testing S 002.

24. Bastenaire F, A study of the scatter of fatigue test results by statistical and physical methods. In: Barrois W, Ripley EL (Eds) Fatigue of Aircraft Structures. Pergamon Press, Oxford, (1963), pp. 53–85.

25. Frost NE, Marsh KJ, Pook LP (1974) Metal Fatigue. Clarendon Press, Oxford. Reprinted with minor corrections (1999), Dover Publications, Mineola, NY.

26. Murakami Y, Metal Fatigue: Effects of Small Defects and Nonmetallic Inclusions. Elsevier Science, Oxford. (2002).

27. Schijve J, Statistical distribution functions and fatigue of structures. Int. J. Fatigue, 27: (2005), pp.1031–1039.

28. Zako, M., Kurashiki, T., Hanaki, S., Nakai, H., Ito, A. and Fukuda, M., 'Evaluation on Fatigue Characteristic of Thin Plates for Diaphragms', Materials Science Research International, Vol.8, No.3 (2002), pp.122-127.

29. Zako, M., Kurashiki, T., Hanaki, S., Nakai, H., Ito, A. and Fukuda, M., On Reliability Evaluation of a Diaphragm in a Light Touch Switch, Materials Science Research International, Vol.8, No.3 (2002), pp.128-133.

30. Nakai, H., Zako, M., Kurashiki, T. and Fukuda, M., A new approach of reliability evaluation of a diaphragm in switch module made of thin plate, Proceedings ICOSSAR 2005, Safety and Reliability of Engineering Systems and Structures, pp.2435－2439.

31. Nakai, H., A proposal of fatigue reliability evaluation based on fatigue limit diagram considering failure probability and application on metallic diaphragm used in switch. Univ. of Osaka, (2004).

32. Nihei, M., Heuler, P., Boller, Ch., Seeger, T., Evaluation of mean stress effect on

fatigue life by use of damage parameters, International Journal of Fatigue, Vol.8, Issue 3, (1986), pp. 119–126.

33. McClaflin, D., Fatemi, A., Torsional deformation and fatigue of hardened steel including mean stress and stress gradient effects, International Journal of Fatigue, Vol. 26, Issue 7, (2004), pp. 773–784.

34. Susmel, L., Tovo, R., Lazzarin, P., The mean stress effect on the high-cycle fatigue strength from a multiaxial fatigue point of view, International Journal of Fatigue, Vol. 27, Issue 8, (2005), pp. 928–943.

35. William N. F., A theory for the effect of mean stress on fatigue of metals under combined torsion and axial load or bending, Division of Engineering, Brown University, (1958).

36. Soderberg, C.R., Fatigue of safety and working stress, Transactions of the American Society of Mechanical Engineers Vol. 52 (Part APM-52-2), (1930), pp.13-28.

37. Goodman, J., Journal of Mechanics Applied to Engineering, 1st ed., Longmans, Green, New York, (1899).

38. Gerber, W. Z., Calculation of the allowable stresses in iron structures, Green, Ney York, (1899).

39. Morrow, J., Fatigue Design Handbook, Advances in Engineering, Vol. 4, SAE, Warrendale, PA, (1968), ppp.21-29.

40. Potter, JM, Watanabe, RT , Development of Fatigue Loading Spectra, ASTM special technical publication; 1006.

41. Murakami, Y., The Rainflow Method in Fatigue. Butterworth-Heinemann, Oxford. (1992).

42. Anzai, H., Algorithm of the rainflow method. In:Murakami, Y., The Rainflow Method in Fatigue. Butterworth-Heinemann, Oxford, (1992), pp. 11–20.

43. Etube LS, Fatigue and Fracture Mechanics of Offshore Structures. Professional

Engineering Publishing, London. (2001).

44. Pook LP, The Role of Crack Growth in Metal Fatigue. Metals Society, London, (1983).

45. Langer BF, Fatigue failure from stress cycles of varying amplitude. J. Appl. Mech., 59: A160–A162. (1937).

46. Miner MA , Cumulative damage in fatigue. J. Appl. Mech., 12: (1945), A159–A164.

47. Toshio, T., Tetsuya, A., Kouji, W. and Taro, O., Effect of Welding Residual Stress on Fatigue Strength of Welded Joint, the society of Materials Science, Japan. Material 36(410), (1987), pp. 1246-1252.

48. Shotaro, K., Residual stress and fatigue, Material Science, 19, 3(1982), pp.151-156.

Acknowledgement

Foremost, I would like to express my sincere gratitude to my advisor Ass.Prof. Tetsusei KURASHIKI for the continuous support of my Ph.D study and research, for his patience, motivation, and inspiration. From academic knowledge to solve problems, from presentation skills to Japanese language, my progress of all these are inseparable with his afford. His advice is not only on this research, which also shapes my thinking. His enthusiastic and energetic attitude towards life and research inspires me to move forward.

Special thanks to Pro. Zako who has given many constructive suggestions, encouragement and personal attention for my Ph.D and the future.

This research was a co-work by Osaka University and Panasonic, and I like to thank those who from Panasonic Co. Ltd., for their resources and advice. I also want to sincerely acknowledge the Japanese government for providing financial assistance for my research and life in Japan.

A special thanks to my family. Words cannot express how grateful I am to my family. It is impossible for me to study in Japan without their sacrifice.

To my dear comrades in Kurashiki. Lab, thank you for your advices and supports in daily life. From whom I learned not only academic knowledge, but also Japanese and Japanese cultures.

List of Scientific Publications

A. First authorship:

1. Xingsheng LI, Tetsusei KURASHIKI, Study on Clicking Characteristics and Designable Region of Oval-type Diaphragm for Electrical Assembles. **Japanese Journal of Structural Safety and Reliability (A). Vol.7 (2011) 530-535.**

2. Xingsheng LI, Tetsusei KURASHIKI, Masao FUKUDA, Effects of Design Parameters on Click Characteristics of A Round-type Diaphragm for Push Momentary Switch. **Journal of Advanced Mechanical Design, Systems, and Manufacturing Vol. 7 (2013) No.2. 268-281.**

3. Xingsheng LI, Tetsusei KURASHIKI, Masao FUKUDA, Proposal of Designable Space of Diaphragm Made of Thin Stainless Steel for Electrical Assemblies Considering Clicking Behavior and Fatigue Life. **International Journal of Structural Safety and Reliability Vol.11 (2013) (Review accepted).**

B. Third authorship:

4. Tetsusei KURASHIKI, Baiyu LIU, Xingsheng LI, Yasumasa NAKANISHI, Mechanical Characterization of Filaments Based on Rotary Bending Test. **Journal of Textile Engineering, Vol.59 No.2 (2013) 37-42.**

CONFERENCE/PRESENTATIONS

Outside Japan

1. Xingsheng LI, Tetsusei KURASHIKI, Masao FUKUDA. Proposal of Designable Space of Diaphragm Made of Thin Stainless Steel for Electrical Assemblies Considering Clicking Behavior and Fatigue Life. **11th International Conference on Structural Safety & Reliability.** Columbia University New York. June 16-20, 2013.

Inside Japan

1. Xingsheng LI, Tetsusei KURASHIKI. Study on Click Characteristics of Diaphragm Based on FEM. **E-square Entrepreneurship ×Education 2010.** Hyogo. November 21-22, 2010.

2. Xingsheng LI, Tetsusei KURASHIKI, Yuzo FUJITA , Masaru ZAKO. Mechanism of metalic diaphragm under clicking load. Mechanism of Metallic Diaphragm under Clicking Load, **JSME Kansai Annual Meeting, 86th 2011**. Kyoto. March 18-20, 2011.

3. Xingsheng LI, Tetsusei KURASHIKI, Yuzo FUJIDA, Masaru ZAKO, Masao FUKUDA. **The Seventh Japan Conference on Structural Safety and Reliability.** Tokyo. October 12-14, 2011.

4. XingSheng LI, Tetsusei KURASHIKI, Yuzo FUJITA. A Study on Designable Space of Structural Made of Stainless Based on FEM. **JSME Kansai symposiums for young researcher 6th 2011.** Osaka. December 9-10, 2011.

5. XingSheng LI, Tetsusei KURASHIKI . Designable space method of metallic diaphragm considering fatigue reliability based on FEM**. JSME Material and Mechanics Conference.** G